1983

Acoustic Transients in Ultrasonic Pulse-Echo Sytstems

Glenn A. Andrew
University of Rhode Island

ACOUSTIC TRANSIENTS IN ULTRASONIC PULSE-ECHO SYSTEMS

Thesis by

Glenn A. Andrew

In Partial Fulfillment of the Requirements

For the Degree of

Master of Science

in

Ocean Engineering

University of Rhode Island

Kingston, Rhode Island

1983

MASTER OF SCIENCE THESIS

OF

GLENN A. ANDREW

APPROVED:

Thesis Committee

Major Professor

Dean of Graduate School

UNIVERSITY OF RHODE ISLAND

1983

ABSTRACT

The transient behavior of an ultrasonic transducer operating in a pulse-echo system is studied both analytically and experimentally. Mathematically, the acoustic field is described using an impulse response approach, while a distributed parameter model is used to represent the transducer dynamics. The harmonic pressure field from a circular piston is first presented using a Fourier integral representation of the impulse response. A pulse-echo model for an ultrasonic system is then developed and used to evaluate the pulsed acoustic field response from a transducer for a variety of field points and electrical excitations. A multipulse structure is clearly observed in both the field pressures and the receive voltages. A set of transducers having various matching conditions are fabricated and used to obtain pulse-echo responses from a spherical target placed at different points throughout the acoustic nearfield. Again a multiple pulse structure is noted. To minimize the effect of these acoustic transients, various focusing schemes are experimentally studied. Spherical, conical and toroidal apertures are examined for both shaped-element and lens systems. Transducers of identical diameters, frequencies and focal distances have been designed and fabricated for each case. Measurements of the pulsed acoustic field from these transducers indicate that where sharply focused fields are employed, acoustic transient effects can be effectively eliminated from the focal zone.

ACKNOWLEDGEMENTS

I wish to thank my major professor, Dr. Peter Stepanishen, for his suggestion of the research topic and for his continued support and guidance throughout the conduct of work.

In addition, I acknowledge Mr. Charles W. Lamprey of General Dynamics, Electric Boat Division for his helpful insights and assistance in the design and fabricaton of the ultrasonic transducers and also Mr. R. H. Grills for his encouragement.

TABLE OF CONTENTS

Chapter	Title	Page
	ACKNOWLEDGEMENTS	ii
	ABSTRACT	iii
	TABLE OF CONTENTS	iv
	LIST OF TABLES	vi
	LIST OF ILLUSTRATIONS	vii
	INTRODUCTION	1
I	THE NORMALIZED HARMONIC PRESSURE FIELD OF A CIRCULAR PISTON	3
	The Impulse Response Approach	3
	Fourier Integral Representation of the Impulse Response	10
	Normalized Harmonic Pressure Field Responses	11
II	PULSE-ECHO MODEL OF A CIRCULAR ULTRASONIC TRANSDUCER	23
	The Model of a Piezoelectric Transducer	23
	The Pulse-Echo Model	29
III	ULTRASONIC TRANSDUCER CONSTRUCTION	60
	Review of Methods	60
	General Construction Procedure	63
	Special Fabrication Considerations	66
IV	EXPERIMENTAL RESULTS OF TRANSDUCERS	69
	Transducer Responses	69
	Pulsed Acoustic Field Measurements	80
V	PULSED ACOUSTIC FIELD FROM FOCUSED TRANSDUCERS	97
	Characteristics of Focused Transducers	97
	Beam Profiles of Focused Transducers	100
	Pulsed Acoustic Field Measurements	110

TABLE OF CONTENTS (continued)

Chapter	Title	Page
	SUMMARY AND CONCLUSIONS	118
	LIST OF REFERENCES	120
	BIBLIOGRAPHY	123

LIST OF TABLES

Table	Title	Page
I	Impedance Formulas for Matching Layers	28
II	Effect of Various Matching Schemes on Transducer Response	31
III	Matching Conditions of Test Transducers	64
IV	Comparison of Analytical and Experimental Transducer Responses	72

LIST OF ILLUSTRATIONS

Figure	Title	Page
1	Circular Piston Mounted In an Infinite Rigid Planar Baffle	4
2	Impulse Responses for R/A = 0.	6
3	Impulse Responses for R/A = 0.5	7
4	Impulse Responses for R/A = 1.	8
5	Impulse Repsonses for R/A = 2.	10
6	Spatial Points of Interest	12
7	Normalized Harmonic Pressure Response, R/A = 0.0, Z/A = 1.0	13
8	Normalized Harmonic Pressure Response, R/A = 0.0, Z/A = 4.0	14
9	Normalized Harmonic Pressure Response, R/A = 0.5, Z/A = 1.0	16
10	Normalized Harmonic Pressure Response, R/A = 0.5, Z/A = 4.0	17
11	Normalized Harmonic Pressure Response, R/A = 1.0, Z/A = 1.0	18
12	Normalized Harmonic Pressure Response, R/A = 1.0, Z/A = 4.0	19
13	Normalized Harmonic Pressure Response, R/A = 2.0, Z/A = 1.0	20
14	Normalized Harmonic Pressure Response, R/A = 2.0, Z/A = 4.0	23
15	Transducer Equivalent Circuit	24
16	Transducer Transmit and Receive Responses	26
17	Comparison of Matching Schemes	30
18	Ultrasonic Pulse-Echo Model	32
19	Velocity Response For Broadband Excitation	34
20	Velocity Response For Broadband Excitation Without Negative Capacitance	35
21	Velocity Response For Narrowband Excitation	36
22	Pulse-Echo Response,No Dynamics,Broadband Input,R/A=0.,Z/A=1	38
23	Pulse-Echo Response,No Dynamics,Broadband Input,R/A=.5,Z/A=1	39

LIST OF ILLUSTRATIONS (continued)

Figure	Title	Page
24	Pulse-Echo Response,No Dynamics, Broadband Input,R/A=1.,Z/A=1	40
25	Pulse-Echo Response,No Dynamics, Broadband Input,R/A=2.,Z/A=1	41
26	Pulse-Echo Response,No Dynamics, Broadband Input,R/A=0.,Z/A=4	43
27	Pulse-Echo Response,No Dynamics, Broadband Input,R/A=.5,Z/A=4	44
28	Pulse-Echo Response,No Dynamics, Broadband Input,R/A=1.,Z/A=4	45
29	Pulse-Echo Response,No Dynamics, Broadband Input,R/A=2.,Z/A=4	46
30	Pulse-Echo Response,No Dynamics,Narrowband Input,R/A=0.,Z/A=1	47
31	Pulse-Echo Response,No Dynamics,Narrowband Input,R/A=.5,Z/A=1	49
32	Pulse-Echo Response,No Dynamics,Narrowband Input,R/A=1.,Z/A=1	50
33	Pulse-Echo Response,No Dynamics,Narrowband Input,R/A=2.,Z/A=1	51
34	Pulse-Echo Response, Dynamics, Broadband Input, R/A=0.,Z/A=1	52
35	Pulse-Echo Response, Dynamics, Broadband Input, R/A=.5,Z/A=1	53
36	Pulse-Echo Response, Dynamics, Broadband Input, R/A=1.,Z/A=1	54
37	Pulse-Echo Response, Dynamics, Broadband Input, R/A=2.,Z/A=1	55
38	Pulse-Echo Response, Dynamics, Narrowband Input, R/A=0.,Z/A=4	56
39	Pulse-Echo Response, Dynamics, Narrowband Input, R/A=1.,Z/A=4	58
40	Pulse-Echo Response, Dynamics, Narrowband Input, R/A=2.,Z/A=4	59
41	Physical Configuration of Transducers.	61
42	Experiment Test Equipment.	71
43	Experimental Test Setup.	71
44	Transducer #1 Analytical Response	73
45	Transducer #1 Experimental Response	73
46	Transducer #2 Analytical Response	75
47	Transducer #2 Experimental Response	75

LIST OF ILLUSTRATIONS (continued)

Figure	Title	Page
48	Transducer #3 Analytical Response	76
49	Transducer #3 Experimental Response	76
50	Transducer #4 Analytical Response	78
51	Transducer #4 Experimental Response	78
52	Time Domain Artifacts of Transducers	79
53	Acoustic Transients From Transducer #1 for R/A = 0.	82
54	Acoustic Transients From Transducer #1 for R/A = .5	83
55	Acoustic Transients From Transducer #1 for R/A = 1.	84
56	Acoustic Transients From Transducer #2 for R/A = 0.	86
57	Acoustic Transients From Transducer #2 for R/A = .5	87
58	Acoustic Transients From Transducer #2 for R/A = 1.	88
59	Acoustic Transients From Transducer #3 for R/A = 0.	89
60	Acoustic Transients From Transducer #3 for R/A = .5	91
61	Acoustic Transients From Transducer #3 for R/A = 1.	92
62	Acoustic Transients From Transducer #4 for R/A = 0.	93
63	Acoustic Transients From Transducer #4 for R/A = .5	94
64	Acoustic Transients From Transducer #4 for R/A = 1.	95
65	Aperture Geometries For Transducer Focusing.	99
66	Configuration For Focusing Design.	101
67	Sound Beam Profiling Test Bed.	103
68	Beam Profile For Spherical Lens	105
69	Beam Profile For Conical Lens	106
70	Beam Profile For Toroidal Lens	107
71	Beam Profile For Spherical Element	108

LIST OF ILLUSTRATIONS (continued)

Figure	Title	Page
72	Beam Profile For Conical Element	109
73	Axial Pressure Response From Spherical Lens Transducer	111
74	Axial Pressure Response From Conical Lens Transducer	112
75	Axial Pressure Response From Toroidal Lens Transducer	114
76	Axial Pressure Response From Spherical Element Transducer	115
77	Axial Pressure Response From Conical Element Transducer	116

INTRODUCTION

Ultrasonic pulse-echo techniques have been implemented in a variety of acoustical systems. In nondestructive material testing it is used primarily for the dimensioning of parts and for the detection and determination of rejectable defects. In the medical field it is employed as a diagnostic tool for tissue characterization and as an alternative to conventional radiography. Ultrasonic pulse-echo methods have also been used in underwater acoustics in a variety of sonar systems.

With the widespread use of ultrasonics, these measurement techniques are becoming more refined. Consequently, greater resolution is being demanded from these systems. One of the areas which has received much attention has been the design of broadband transducers. The major effort here has been in the design of transducers having a time-limited response for maximum depth resolution. When such a transducer is pulsed, a particular phenomenon is noted in the acoustic field. Since the field is generated by pressure waves radiating from both the face and edge of the transducer's surface, multiple pulses could be introduced into the acoustic field, provided the transducer has a short enough time response. When the transducer is used in a pulse-echo mode, the question then becomes one of determining whether the multiple echos are caused by multiple targets in the acoustic field or by acoustic transients. It becomes apparent that a knowledge of the transient pressure field is necessary.

A number of authors have investigated the transient acoustic radiation from a uniformly vibrating piston for several geometries. Due

to its inherent symmetry properties, the circular piston has received much attention. Several excellent reviews have been given by Hanish (Ref.1), Freedman (Ref.2) and Harris (Ref.3). In addition, Freedman has discussed the transient radiation by transforming harmonic solutions to the time domain using time domain approximations; however, the method finds application only in narrow bandwidth studies. Several other authors have investigated direct time domain methods. Using integral methods Miles (Ref.4) has given the velocity potential response. Stepanishen (Ref.5) has developed an impulse response approach based on the exact time domain solution to the initial boundary value problem. Robinson, et al. (Ref.6) presented this impulse response using space-time plots obtained by convolution. Beaver (Ref.7) has computed the pressure waveforms resulting from a single cycle of a sine wave velocity. Weight and Hayman (Refs.8, 9) have compared the impulse response method with experiment using pulsed methods and stroboscopic schlieren sequences.

It is the intent of this thesis to investigate acoustic transient phenomena using the impulse response approach for a circular transducer. The harmonic pressure field will be investigated using Fourier transformations of the impulse response. A model will be developed to analytically represent the pulse-echo response of a transducer to various acoustic field points. A set of ultrasonic transducers with various bandwidths will be constructed and used to make nearfield measurements of acoustic transients. As a possible method for minimizing acoustic transients, the effect of focusing the acoustic field will be investigated experimentally.

CHAPTER I

THE NORMALIZED HARMONIC PRESSURE FIELD OF A CIRCULAR PISTON

To better understand acoustic transient phenomena, a knowledge of the harmonic pressure field is useful. The acoustic radiation from a circular piston will be represented using the impulse response function for selected acoustic field points. Utilizing both Fast Fourier Transformation methods and asymptotic methods, the harmonic pressure distributions will be presented for various points in the acoustic field.

The Impulse Response Approach

Consider now the case of a circular piston which is mounted in an infinite rigid circular planar baffle as shown in Figure 1. The velocity over the piston surface is considered to be uniform. The acoustic medium in the upper half space, $x_3 > 0$, is specified to be isotropic with a constant density, ρ , and velocity of propagation, c. Due to symmetry conditions the acoustic field need only be described in terms of a radial coordinate, r, and an axial coordinate, z.

The time dependent pressure at a point $\bar{x}$ is proportional to the time derivative of the velocity potential at that point $\bar{x}$. Stepanishen (Ref.5) has shown that the velocity potential may then be represented as a convolution of the time dependent piston velocity, v(t), with the impulse response of the piston for the spatial point of interest, $h(\bar{x},t)$, as shown in Equation (1). The impulse response is the velocity potential at a point x when the piston is impulsively excited.

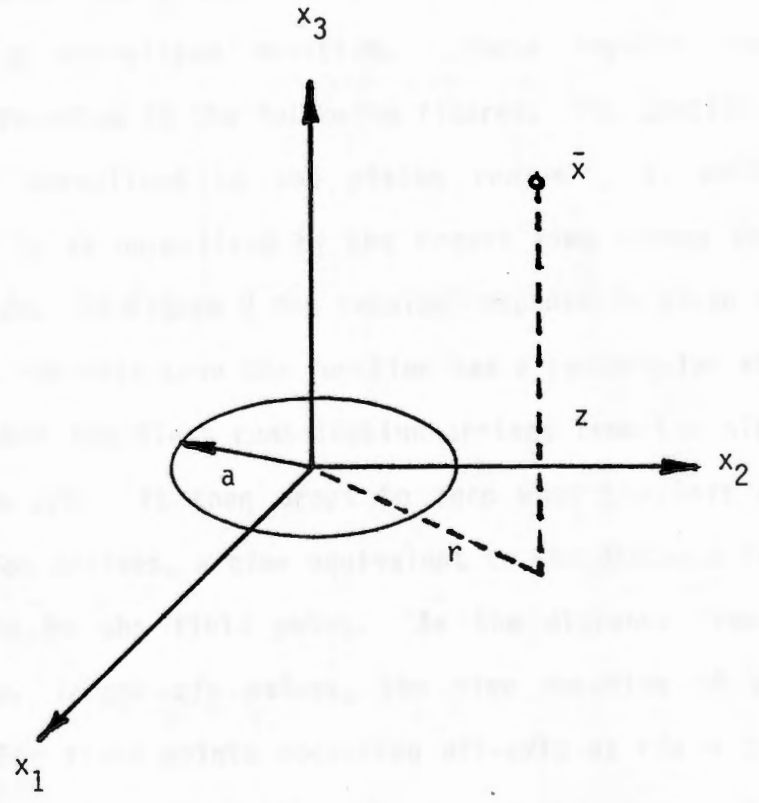

Figure 1. Circular piston mounted in an infinite rigid planar baffle.

$$p(\bar{x},t) = \rho\frac{\partial}{\partial t}\, v(t)*h(\bar{x},t) \qquad (1)$$

where * denotes convolution.

Stepanishen has provided expressions for the impulse response function in a normalized notation. These impulse responses are graphically presented in the following figures. The spatial coordinates r and z are normalized to the piston radius , a, while the time coordinate, τ , is normalized by the travel time across the radius of the piston, a/c. In Figure 2 the impulse response is given for the case when r/a = 0. In this case the function has a rectangular step response that begins when the first contribution arrives from the piston, a time equivalent to z/a. It then drops to zero when the last contribution from the piston arrives, a time equivalent to the distance from the edge of the piston to the field point. As the distance from the piston increases ,ie. larger z/a values, the time duration of the response decreases. For field points occurring off-axis at r/a = 1/2, as shown in Figure 3, the function still contains a step response, but its value does not immediately go to zero. The function begins tapering off after the contribution from the nearest edge arrives and ends when the last contribution arrives from the furthest edge of the piston. For field points chosen directly over the edge of the piston as shown in Figure 4, the impulse response no longer has a rectangular component. The peak amplitude has decreased; however,the response still has a duration equivalent to the difference between the nearest and furthest edge arrival times. Lastly, consider the case when the field point is selected far off axis at r/a = 2 as shown in Figure 5. The impulse

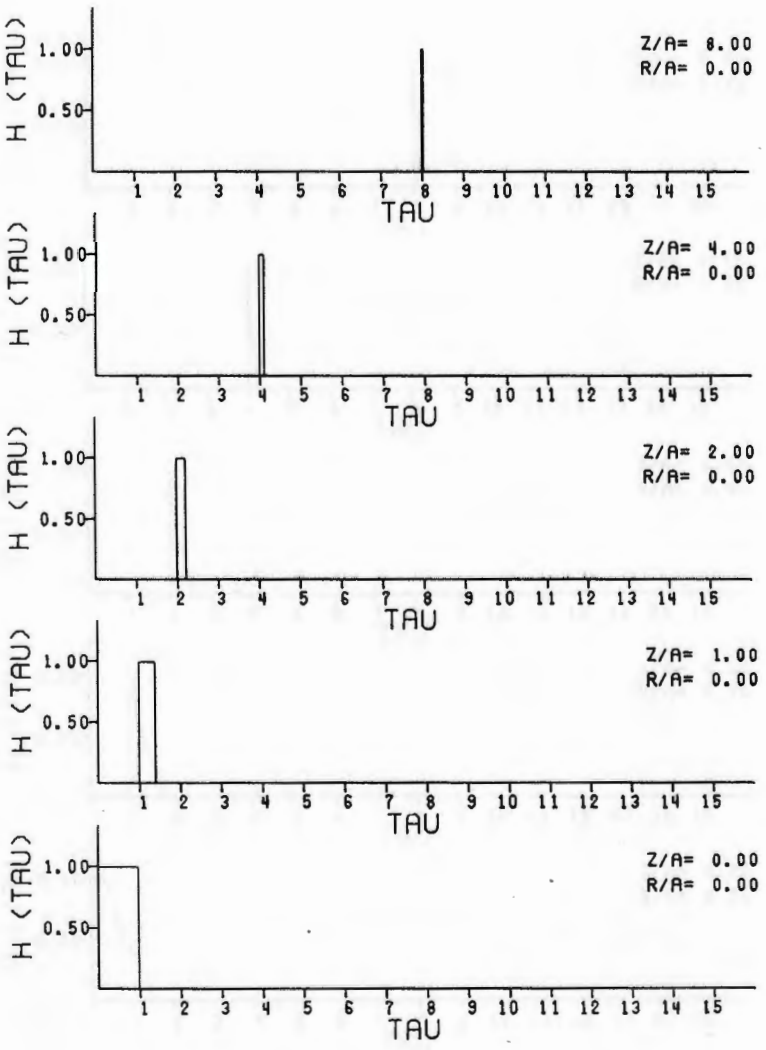

Figure 2. Impulse Responses for r/a = 0.

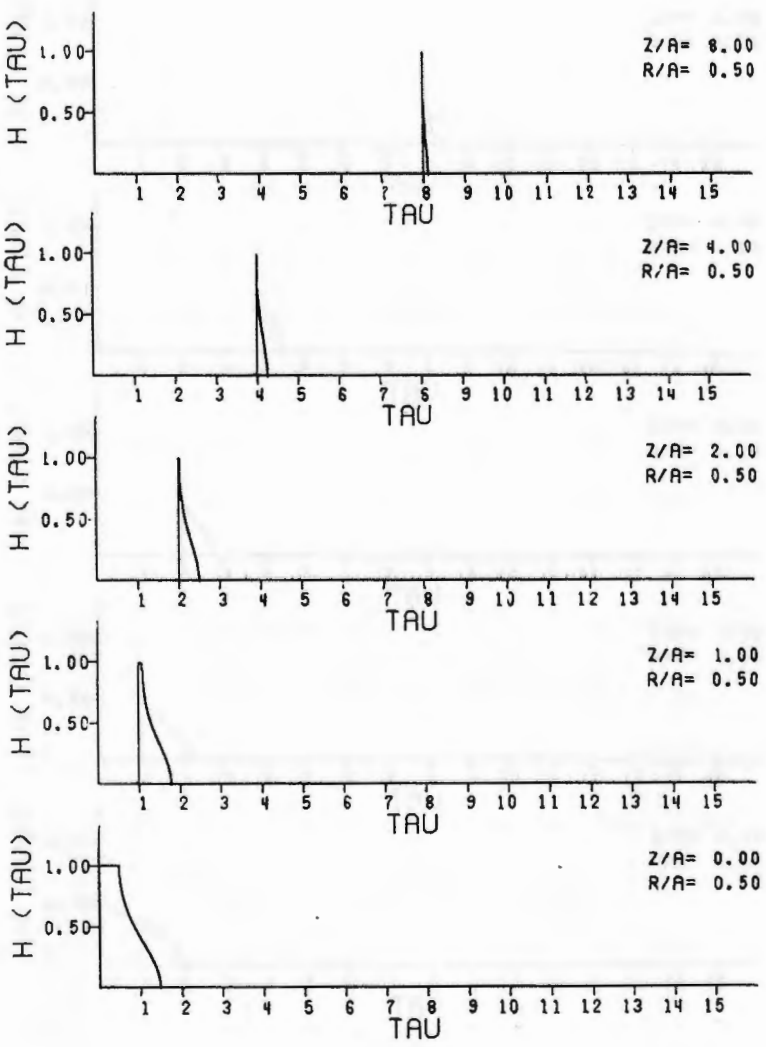

Figure 3. Impulse Responses for r/a = 0.5 .

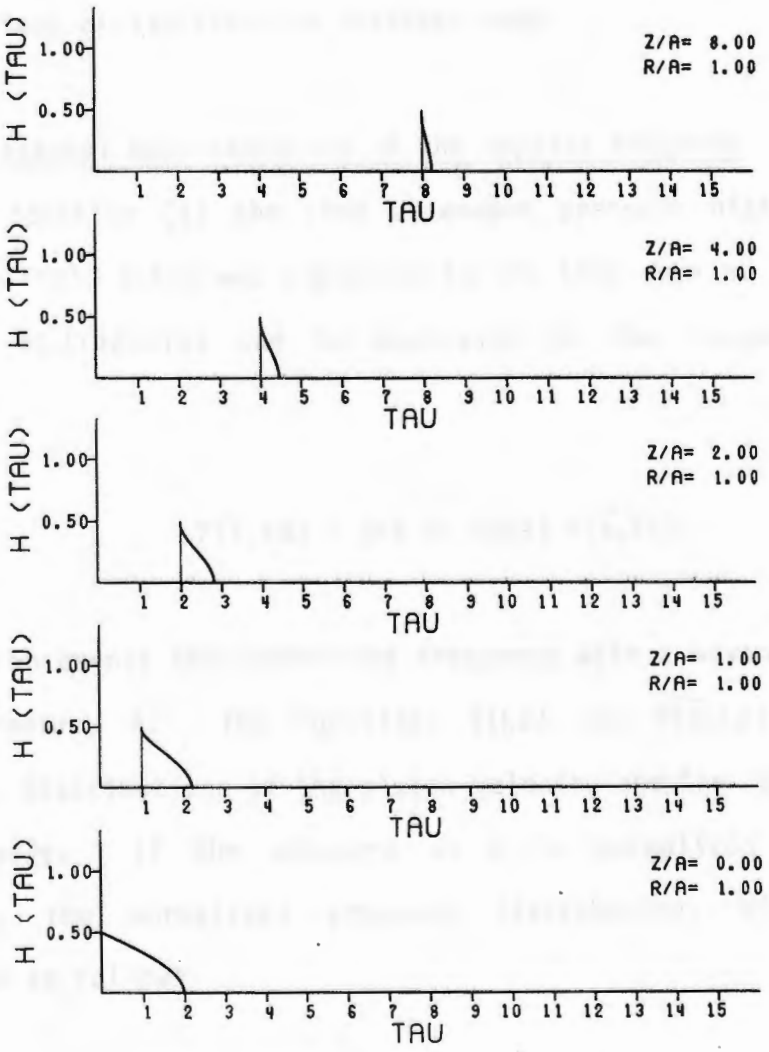

Figure 4. Impulse Responses for r/a = 1.

response now has an entirely different shape to it. When the first contributions from the piston arrive at the piston, the function increases in amplitude to a maximum. It then goes to zero when the last contributions arrive from the furthest edge.

Fourier Integral Representation of the Impulse Response

In Equation (1) the time dependent pressure distribution for a specified field point was expressed in the time domain. Similarly, the pressure distribution can be expressed in the frequency domain as follows:

$$P(\bar{x},ka) = jka\ \rho c\ V(ka)\ H(\bar{x},ka) \qquad (2)$$

Here ka represents the normalized frequency with a wavenumber, k, and a piston radius, a. The functions V(ka) and $H(\bar{x},ka)$ represent the frequency distributions of the piston velocity and the impulse response, respectively. If the pressure at $\bar{x}$ is normalized by the piston velocity, the normalized pressure distribution, $G(\bar{x},ka)$, can be expressed as follows:

$$G(\bar{x},ka) = \frac{P(\bar{x},ka)}{V(ka)} = jka\ \ c\ H(\bar{x},ka) \qquad (3)$$

This normalized pressure function represents the normalized harmonic pressure field at a spatial point $\bar{x}$, and can be obtained by evaluating the Fourier transform of the corresponding impulse response.

The Fourier transforms can be evaluated using standard FFT algorithms and by asymptotic techniques. In the FFT method, the impulse

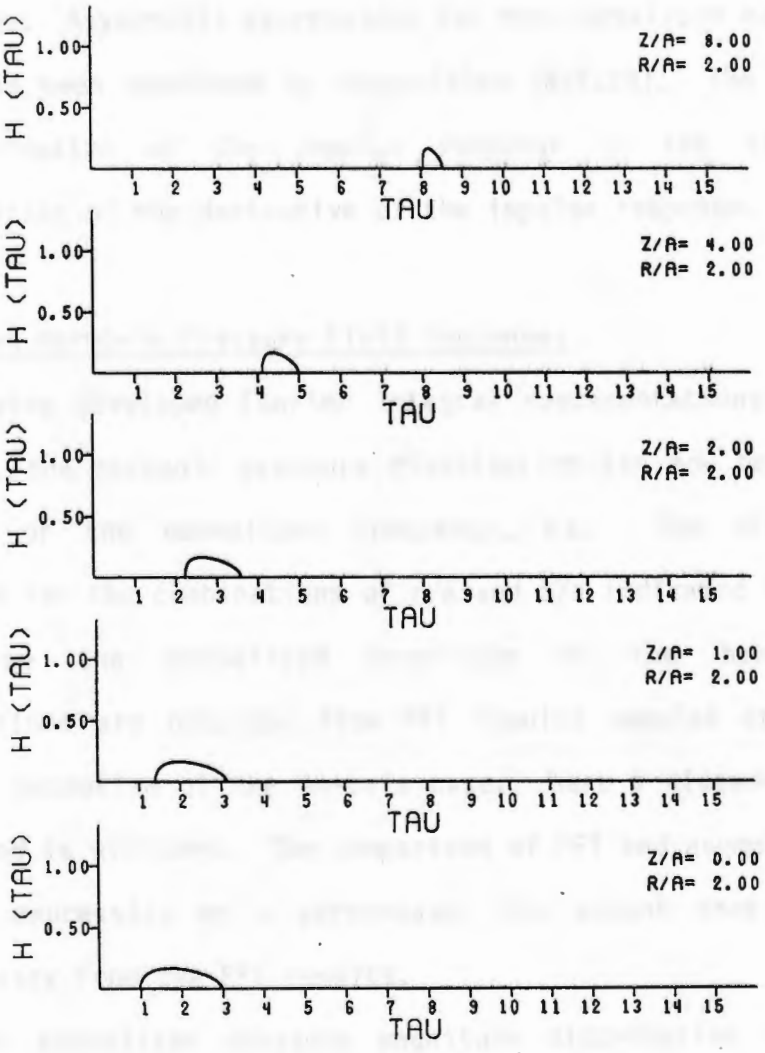

Figure 5. Impulse Responses for r/a = 2.

responses are sampled at a suitable rate over a specified interval. The normalized harmonic pressure is expressed as a Discrete Fourier Transform (DFT). The DFT is then evaluated using standard FFT algorithms. Asymptotic expressions for the normalized harmonic pressure field have been developed by Stepanishen (Ref.10). The method involves the examination of the impulse response in the vicinity of the singularities of the derivative of the impulse response.

Normalized Harmonic Pressure Field Responses

Having developed Fourier integral representations of the impulse response, the harmonic pressure distribution can now be presented as a function of the normalized frequency, ka. The distributions are presented for the combinations of r/a and z/a indicated in Figure 6. In each case the normalized magnitude of the harmonic pressure distributions are obtained from FFT results sampled at a rate of ka1 with the exception of the on-axis case. Here a closed-form expression exists and is utilized. The comparison of FFT and asymptotic methods is made by expressing as a percentage, the amount that the asymptotic results vary from the FFT results.

The normalized pressure magnitude distribution for the on-axis case at z/a = 1 is shown in Figure 7. The response has a sinusoidal characteristic that corresponds to the normalized time duration of the impulse response. As the distance from the piston is increased to four radii above the piston (z/a = 4) as shown in Figure 8, the period of oscillation has increased due to the decrease in the time duration of the impulse response.

In Figure 9 the harmonic pressure distribution is given for the

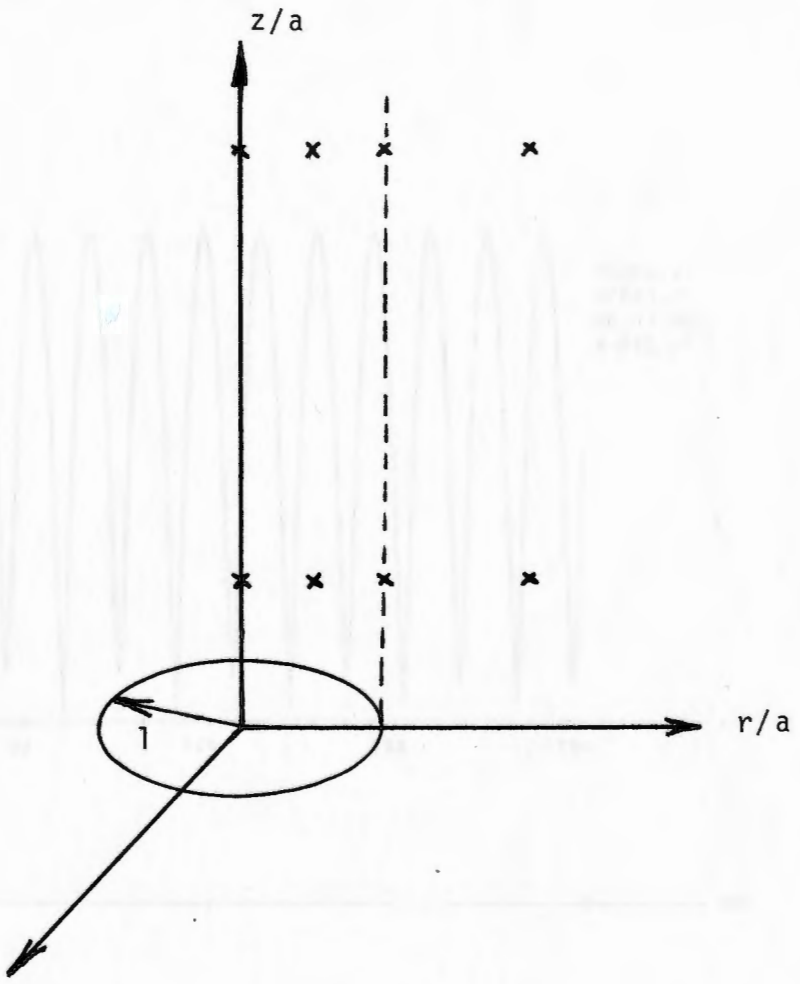

Figure 6. Spatial Points of Interest for Combinations of z/a = 1 and 4, and r/a = 0, ½, 1 and 2.

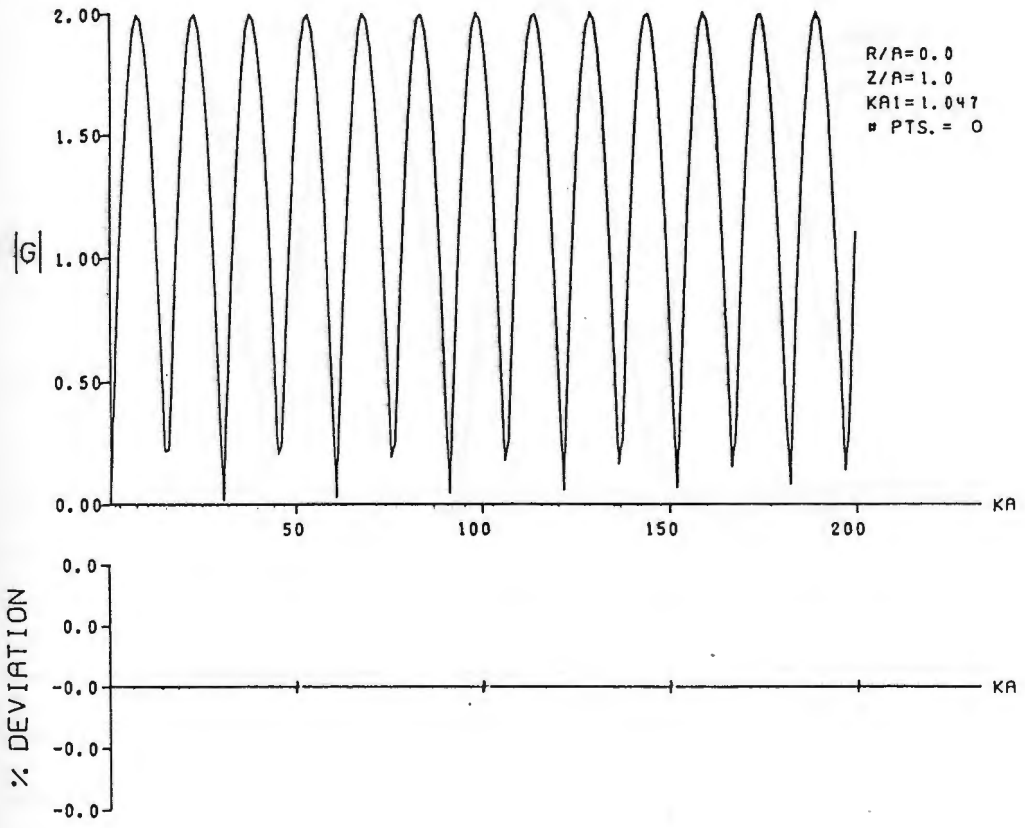

Figure 7. Normalized Harmonic Pressure Response, r/a = 0.0, z/a = 1.0.

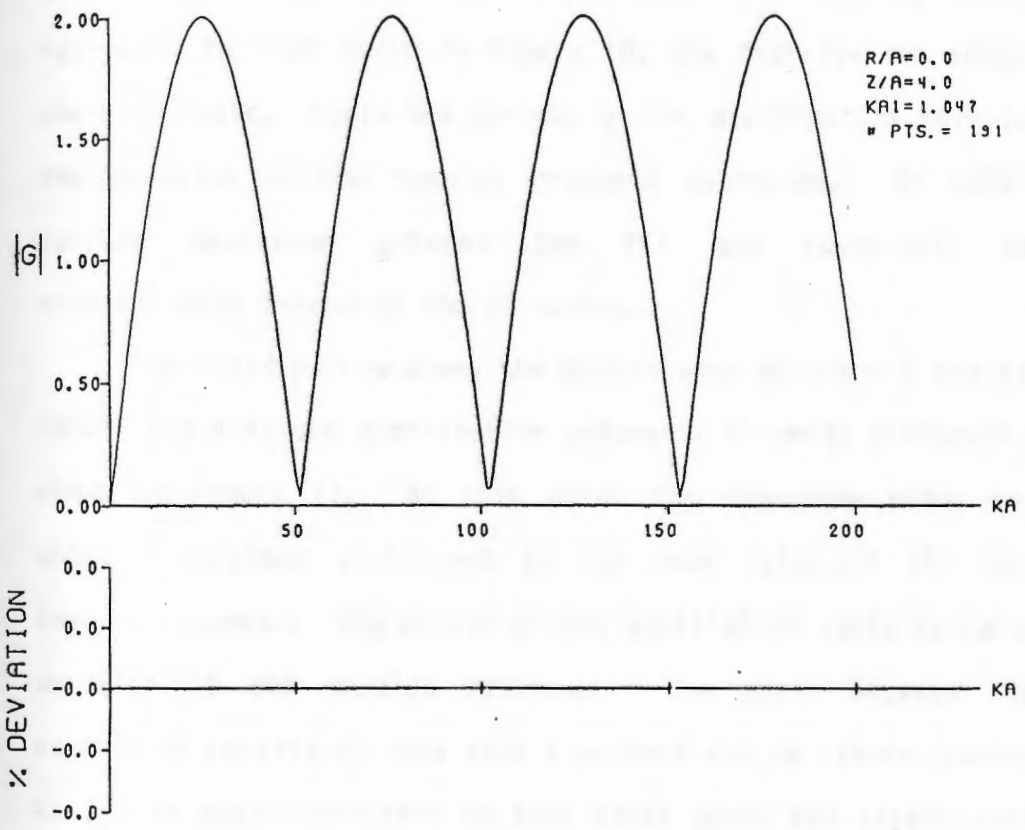

Figure 8. Normalized Harmonic Pressure Response, r/a = 0.0, z/a = 4.0.

off-axis case of r/a = 1/2 and z/a = 1. At this field point the magnitude tends to oscillate about unity for ka values greater than 10. For this case the major oscillation corresponds to the time duration of the rectangular portion of the corresponding impulse response, while the minor oscillation is related to the sloping portion of the same response. The percent deviation between the two methods has increased due to the inaccuracy of the FFT results for larger ka values. As z/a increased to four radii in Figure 10, the distribution shows a similar characteristic. Again the periods of the oscillations have increased as the duration of the impulse response decreases. In both cases the percent deviation between the FFT and asymptotic results is significantly larger at low ka values.

For field points along the piston edge at r/a = 1 and z/a = 1, the normalized pressure distribution assumes a slightly different feature as shown in Figure 11. At this point the magnitude tends to oscillate about a constant equivalent to the peak value of the corresponding impulse response. The period of the oscillation again is related to the duration of the impulse response. The error between the FFT and asymptotic results is less than a percent for ka values greater than 10. As z/a is again increased to four radii above the piston in Figure 12, the period of oscillation shows a similar change.

Lastly, the normalized harmonic pressure distribution is presented for the off piston case when r/a = 2 and z/a = 1 in Figure 13. In contrast to the preceding cases, the pressure magnitude does not exhibit an oscillatory nature about a constant value. It does, however, begin to oscillate about a value equal to the peak value of the corresponding impulse response function and then steadily decreases to zero. The same

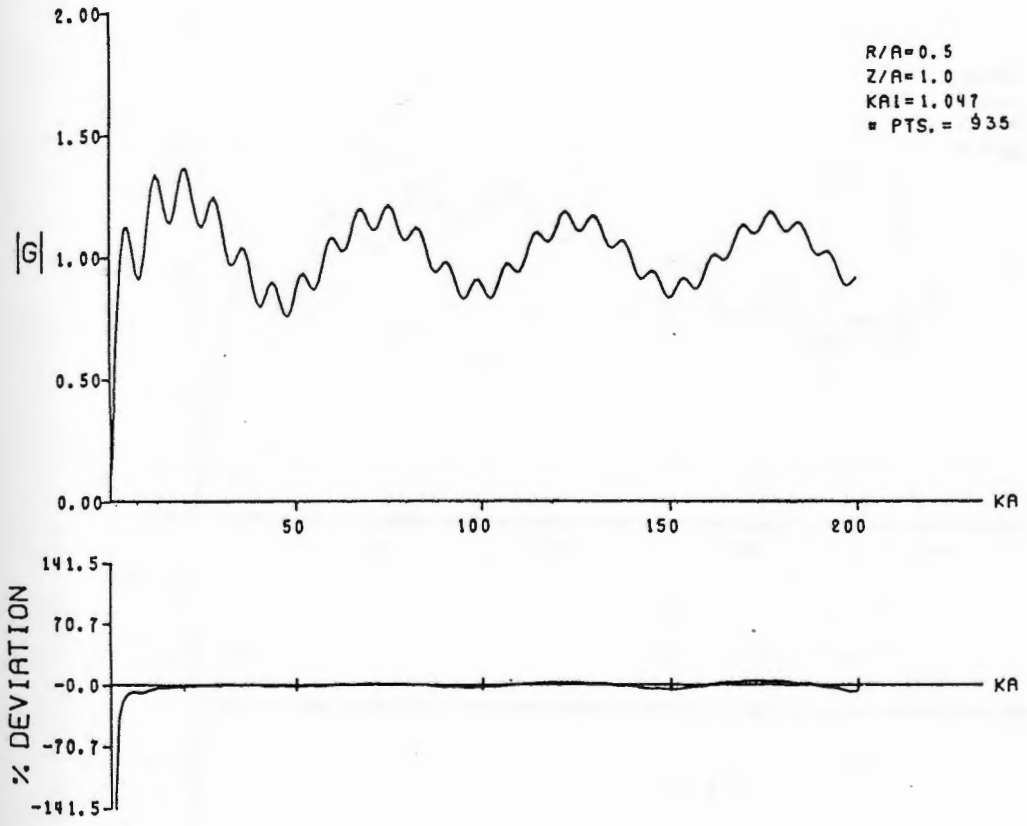

Figure 9. Normalized Harmonic Pressure Response, r/a = 0.5, z/a = 1.0.

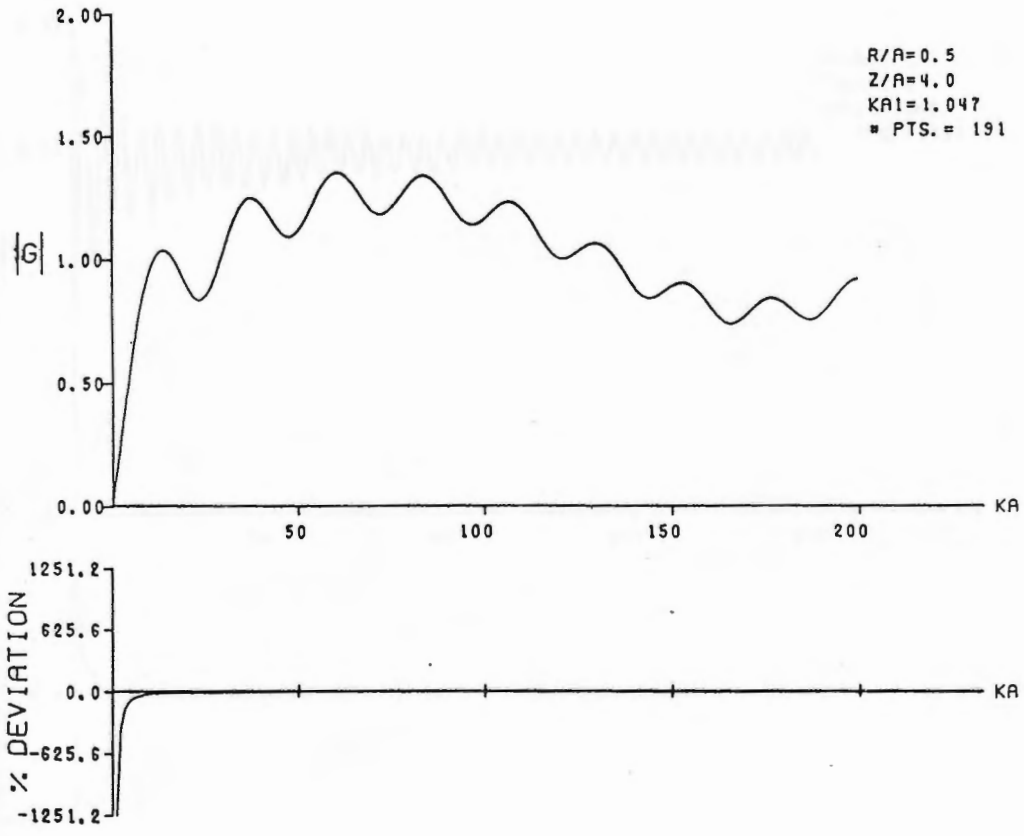

Figure 10. Normalized Harmonic Pressure Response, r/a = 0.5, z/a = 4.0.

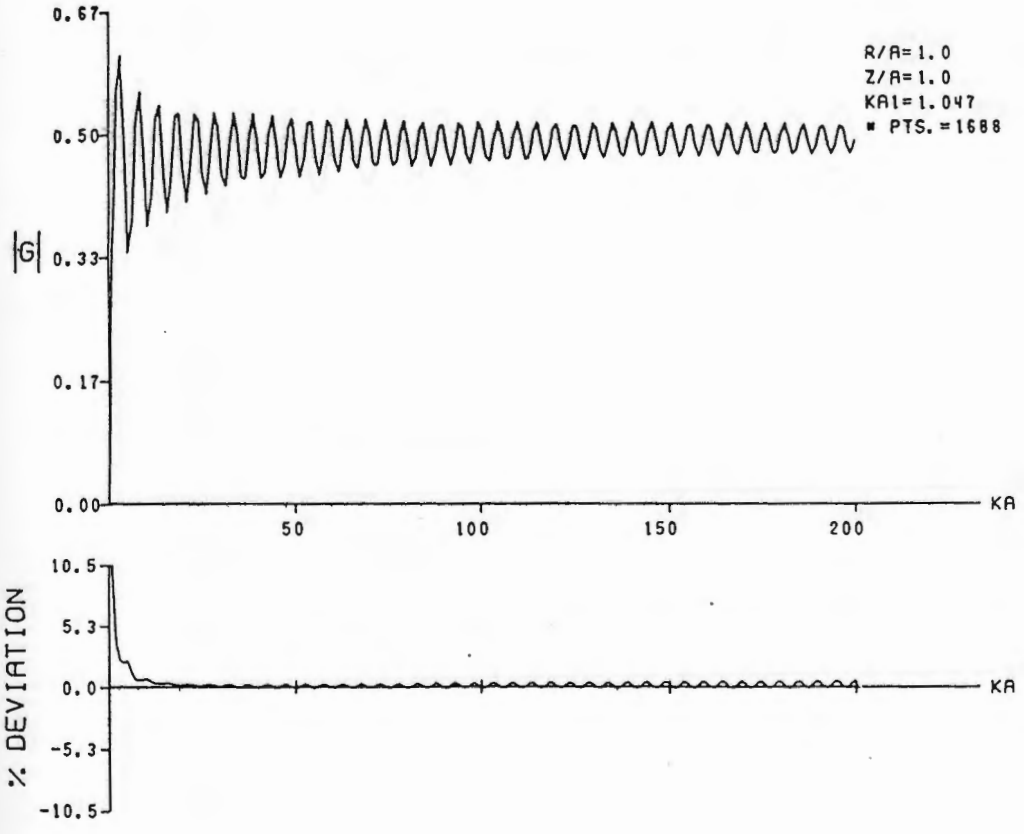

Figure 11. Normalized Harmonic Pressure Response, r/a = 1.0, z/a = 1.0.

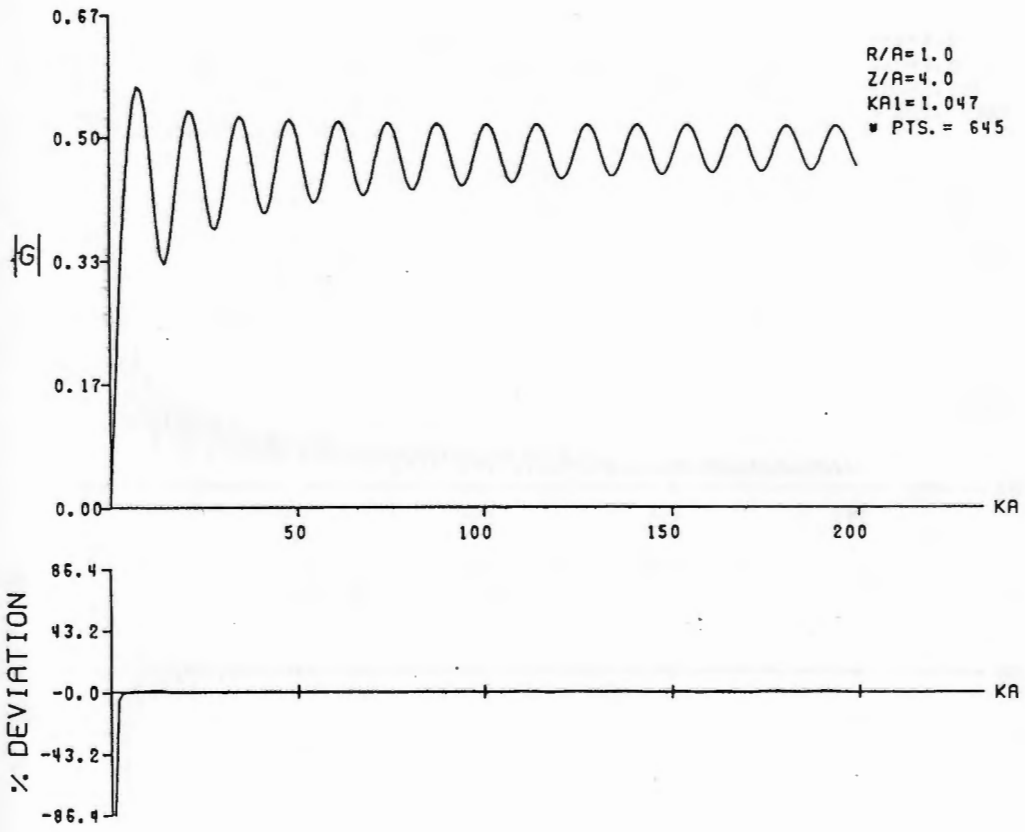

Figure 12. Normalized Harmonic Pressure Response, r/a = 1.0, z/a = 4.0.

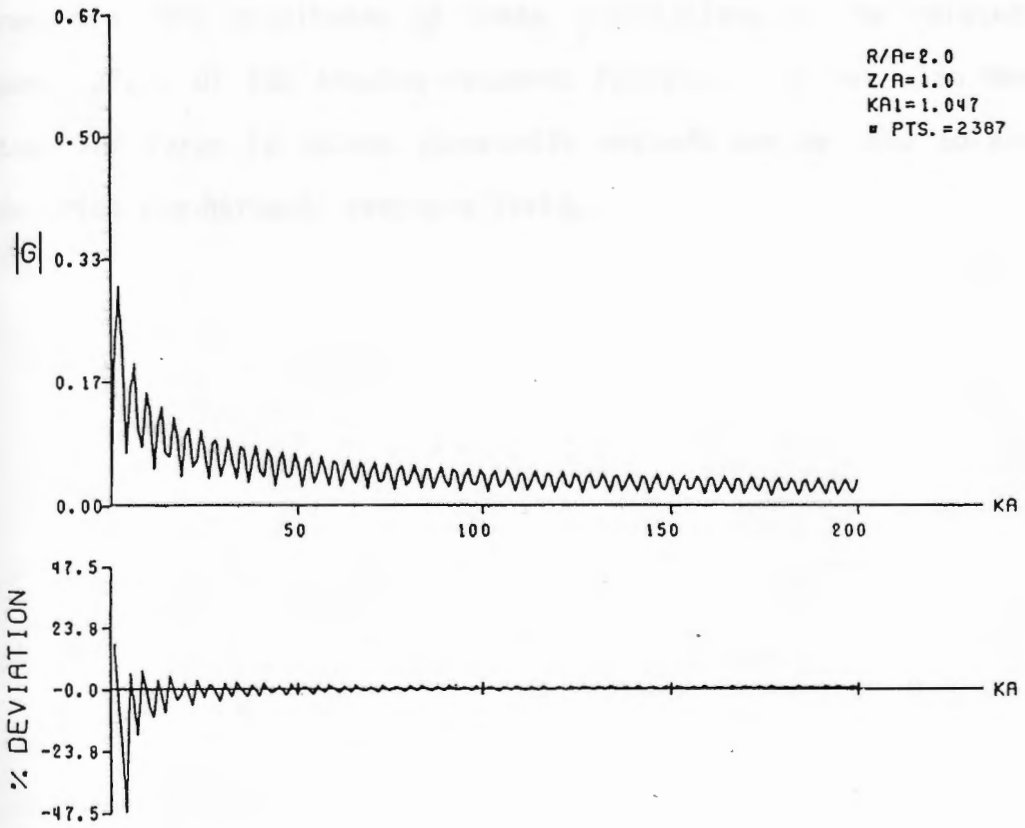

Figure 13. Normalized Harmonic Pressure Response, r/a = 2.0, z/a = 1.0.

phenomenon is noted in Figure 14 where r/a = 2 and z/a = 4. As in the previous cases, the period of oscillation corresponds to the duration of the impulse response. It is noted that the deviation between the FFT and asymptotic methods also are quite large for small ka values.

In summary, the normalized harmonic pressure distribution for a circular piston exhibits an oscillatory behavior with periods corresponding to the duration of various portions of the impulse response. The magnitudes of these oscillations can be related to the peak values of the impulse response function. It has also been shown that for large ka values asymptotic methods can be used to accurately describe the harmonic pressure field.

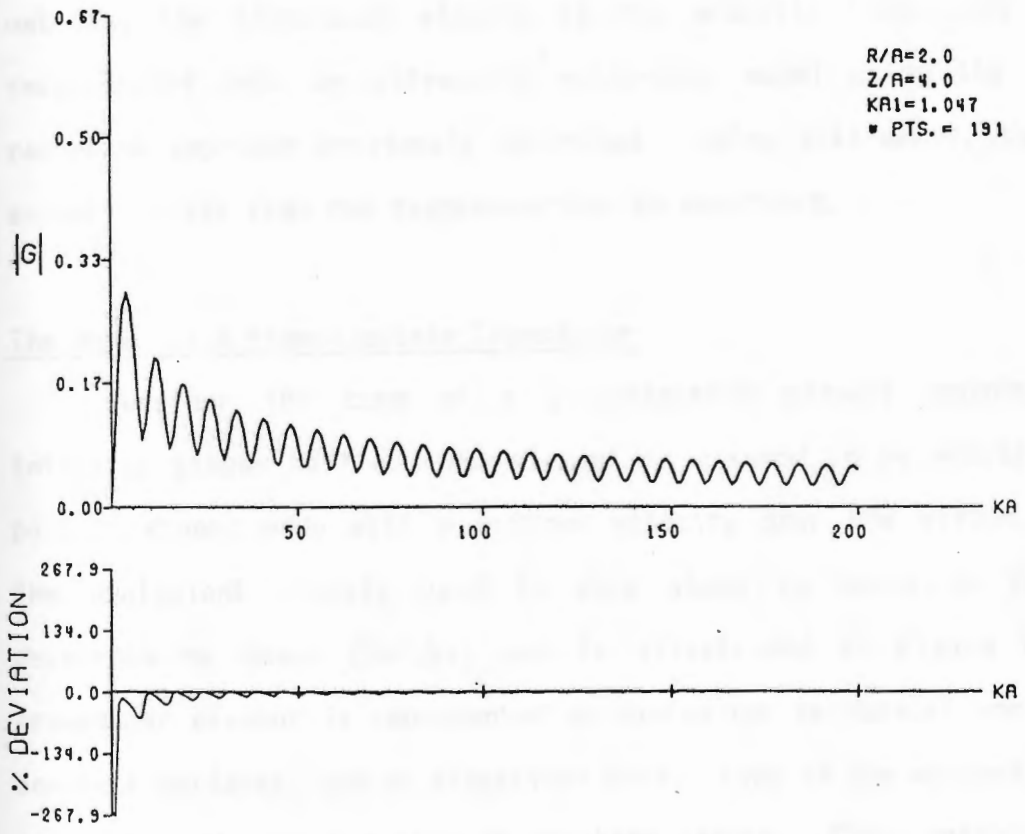

Figure 14. Normalized Harmonic Pressure Response, r/a = 2.0, z/a = 4.0.

CHAPTER II

PULSE-ECHO MODEL OF A CIRCULAR ULTRASONIC TRANSDUCER

Having investigated the harmonic pressure field for a circular piston, the pulsed response from a transducer operating in the pulse-echo mode is studied. The transducer is modeled by means of an equivalent circuit. This model is used to study various schemes for matching the transducer element to the acoustic load. It is then incorporated into an ultrasonic pulse-echo model using the acoustic radiation approach previously described. Using this model, the pulsed acoustic field from the transducer can be described.

The Model of a Piezoelectric Transducer

Consider the case of a piezoelectric element mounted in an infinite, planar baffle. The element is assumed to be vibrating in a pure thickness mode with a uniform velocity over the piston surface. The equivalent circuit used in this study is based on the model developed by Mason (Ref.11) and is illustrated in Figure 15. The transducer element is represented as having two mechanical ports (front and back surfaces) and an electrical port. Each of the mechanical ports is terminated into a series of matching layers. These matching layers can be described using a distributed parameter representation. The back mechanical port is terminated into a backing impedance, Zb. The front mechanical port is terminated into a radiation impedance, Zr, of the transmission medium and a force generator, F, that is used only in the receive mode. An optional electrical tuning network, Zt, is also included. The significance of the negative capacitance in the element

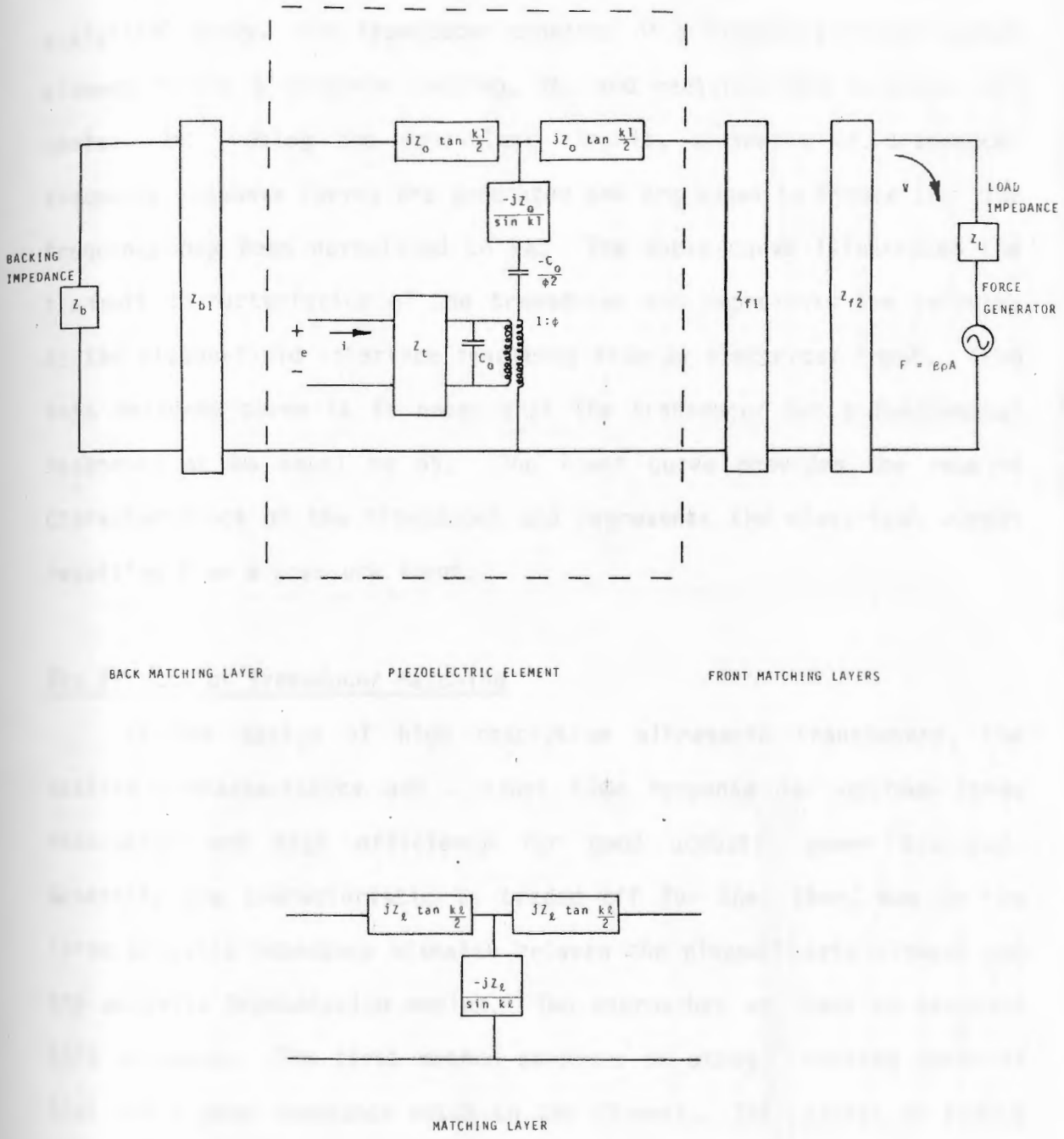

Figure 15. Transducer Equivalent Circuit

will be discussed later.

A 1.5 MHz, 2 cm. diameter transducer was selected for the analytical study. The transducer consists of a lithium sulfate crystal element having a corprene backing, Zb, and radiated into a castor oil medium, Zr. Using the equivalent circuit, a series of transducer frequency response curves are generated and are shown in Figure 16. The frequency has been normalized to ka. The upper curve illustrates the transmit characteristics of the transducer and represents the velocity at the piston-fluid interface resulting from an electrical input. From this response curve it is noted that the transducer has a fundamental resonance at ka equal to 65. The lower curve provides the receive characteristics of the transducer and represents the electrical output resulting from a pressure input.

The Effects of Transducer Matching

In the design of high resolution ultrasonic transducers, the desired characteristics are a short time response for optimum range resolution and high efficiency for good acoustic power transfer. Generally one characteristic is traded off for the other, due to the large acoustic impedance mismatch between the piezoelectric element and the acoustic transmission medium. Two approaches are used to minimize this mismatch. The first method consists of using a backing material that has a good impedance match to the element. This serves to reduce the reverberation time within the element and thus decreases the transducer's time response. There is a serious drawback with this approach. Since a large portion of the acoustic energy is transferred into the backing , a smaller amount is transmitted into the acoustic

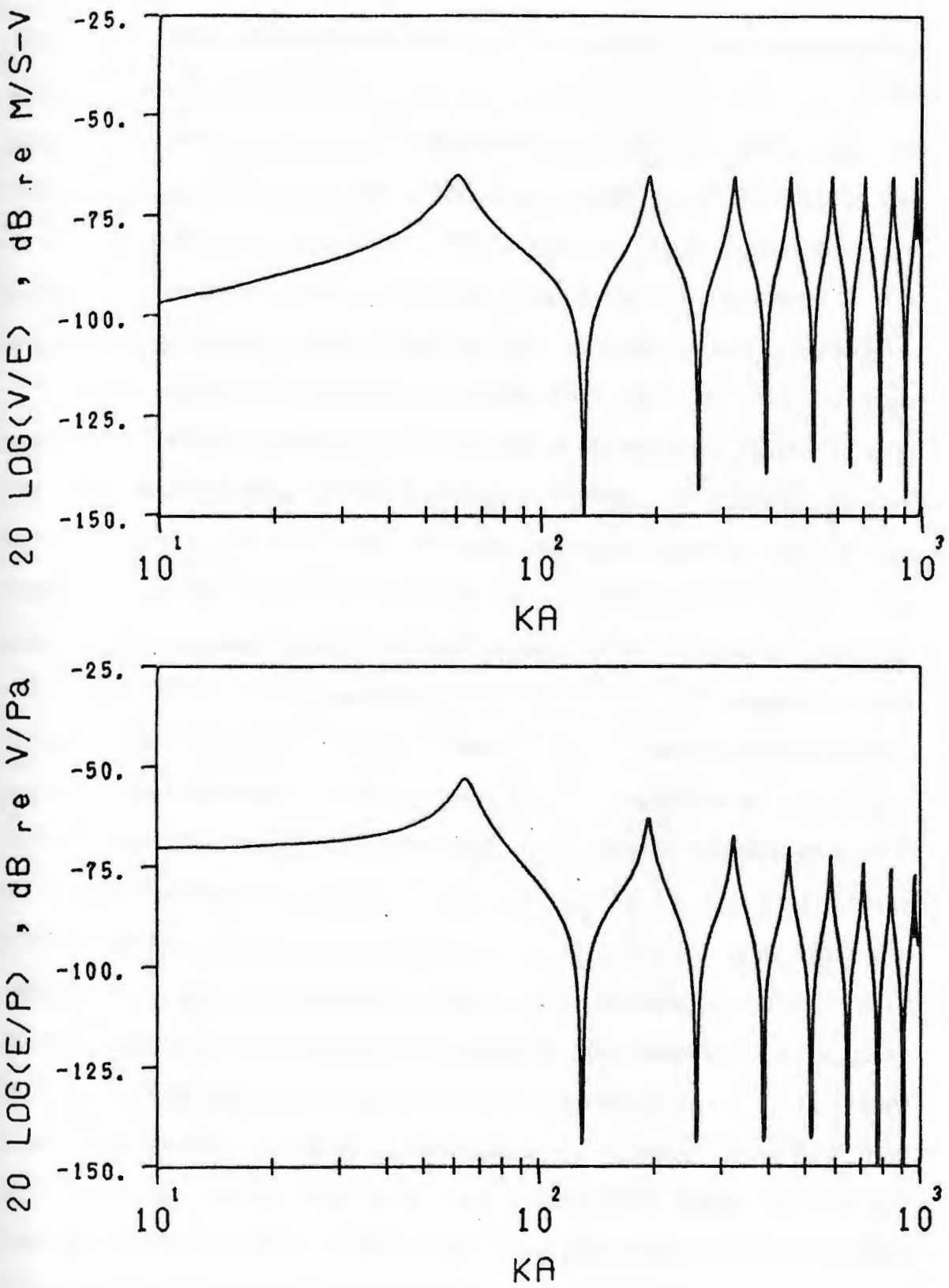

Figure 16. Transducer Transmit and Receive Responses.

load. The second approach involves the use of quarter-wavelength thick acoustic transformers between the element and the load. This method was apparently first suggested by McSkimin (Ref.12) who noted that an increase in bandwidth could be obtained with good power transfer if two or more transformers were used. Sittig (Ref.13) later showed that the number of transformers should be kept low since reverberation in the multiple layers would tend to mask the zone in front of the transducer.

Other studies have been conducted that utilize both of these approaches. Kossoff (Ref.14) has reported using matching layers on both the front and back ends of the transducer element. In contrast to this method, Souquet, et al., (Ref.15) have employed matching only on the front end, while totally mismatching the element to the backing. The goal here is to make the transducer appear to be air-backed for high efficiency, while at the same time providing structural support for the element. Desilets, et.al. (Ref.16) have utilized the equivalent circuit proposed by Krimholtz, et.al. (Ref.17) for optimizing transducer characteristics. This model treats the piezoelectric element as a pair of quarter-wavelength layers combined by a frequency-dependent electroacoustic coupling transformer. Using this approach, Desilets implemented a binomial matching scheme for transducer matching. Goll (Ref.18) has utilized standard transmission line formulas for matching both backed and unbacked transducers to the acoustic load. This scheme treats the element as being semi-infinite in extent. There are many other matching schemes that have been investigated which are far too numerous to mention here. The intent is to present a few of the better known approaches and to make a determination of the merits of each.

The impedance formulas used in the above schemes are summarized in

Table I for both single and double matching layers. Here Z1 represents the impedance of the matching layer nearest to the element of impedance Zx. In the case of a second matching layer, Z2 corresponds to the layer impedance next to the acoustic load, Zr.

TABLE I. Impedance Formulas for Matching Layers

Matching Scheme	Single Layer Z1	Double Layer Z1	Double Layer Z2
Semi-Infinite Method (17)	$\sqrt{Zx\ Zr}$	$\sqrt[4]{Zx^3\ Zr}$	$\sqrt[4]{Zx\ Zr^3}$
Unbacked Method (14)	$\sqrt[3]{2\ Zx\ Zr^2}$	-	-
Binomial Method (15)	$\sqrt[3]{Zx\ Zr^2}$	$\sqrt[7]{Zx^4\ Zr^3}$	$\sqrt[7]{Zx\ Zr^6}$

To compare the three methods, a transducer having a 1" diameter and a 2.25 MHz fundamental resonance is modeled using the equivalent circuit when a single quarter wavelength matching layer attached to the front end. Two different backing conditions are considered. The first backing has an acoustic impedance near the element's acoustic impedance, while the second type is modeled as air-backed.

The time and frequency pulse-echo responses are provided by the model. From these responses, four transducer performance parameters are used to compare the matching methods: center frequency, bandwidth, loop gain and damping factor. The center frequency describes the frequency of mechanical vibration of the transducer. The bandwidth is the frequency range and is defined by the points 6 dB down from the maximum

amplitude of the frequency spectrum. The loop gain provides a measure of the transducer's sensitivity and is defined as 20 log of the voltage ratio of the echo signal to the pulse applied to the transducer. The damping factor is a measure of pulse length and is defined as the number of half cycles whose amplitudes are greater than or equal to one-half the amplitude of the first half cycle.

The time and frequency responses for the transducers are shown in Figure 17 and summarized in Table II by the performance parameters just discussed. For the air backed case each of the three matching schemes cause a downshift in the transducer's center frequency, while the loop gain remains essentially the same. However, for the semi-infinite and unbacked methods the frequency spectrum shows two resonances and yields a long time response. For the cases when the transducer backing is reasonably matched to the element, the transducer bandwidth shows a significant increase, while the pulse length shows a correponding decrease. All of the transducer responses for this case are very similar, indicating that the predominate factor on the transducer response is its backing condition. The major sacrifice though is the drop in loop gain.

The Pulse-Echo Model

In the previous discussion an analytical model of an ultrasonic transducer was presented and utilized to study various impedance matching schemes. The model can be combined with the acoustic radiation approach described in Chapter I and implemented into a complete ultrasonic pulse-echo system. A diagram of this model is presented in

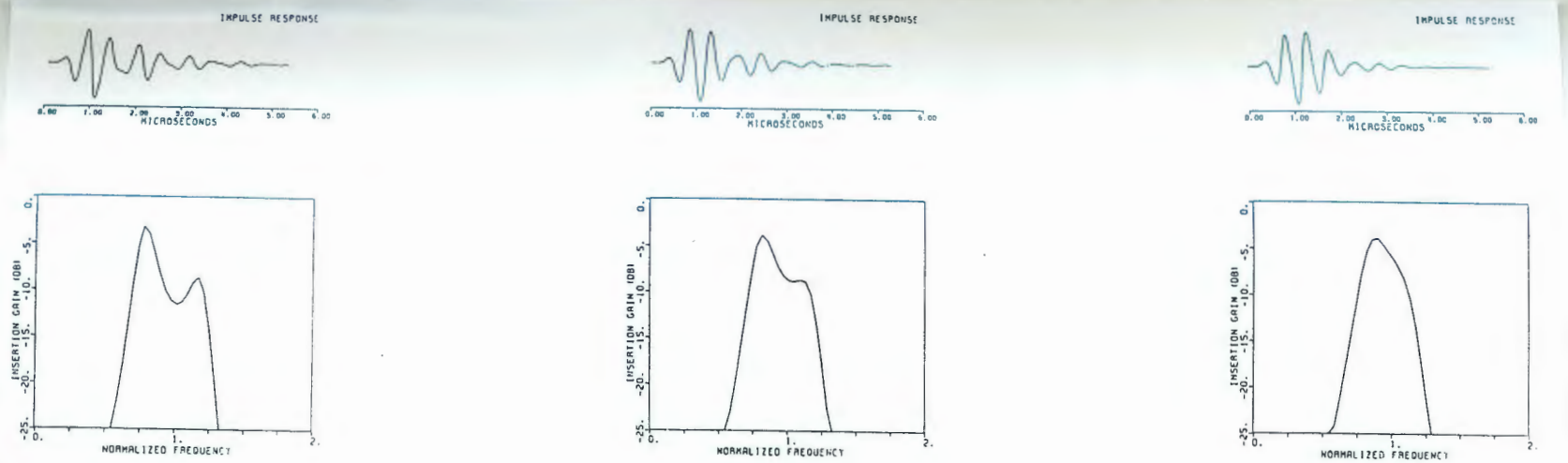

(a) Semi-infinite method, air-backed

(b) Unbacked method, air-backed

(c) Binomial method, air-backed

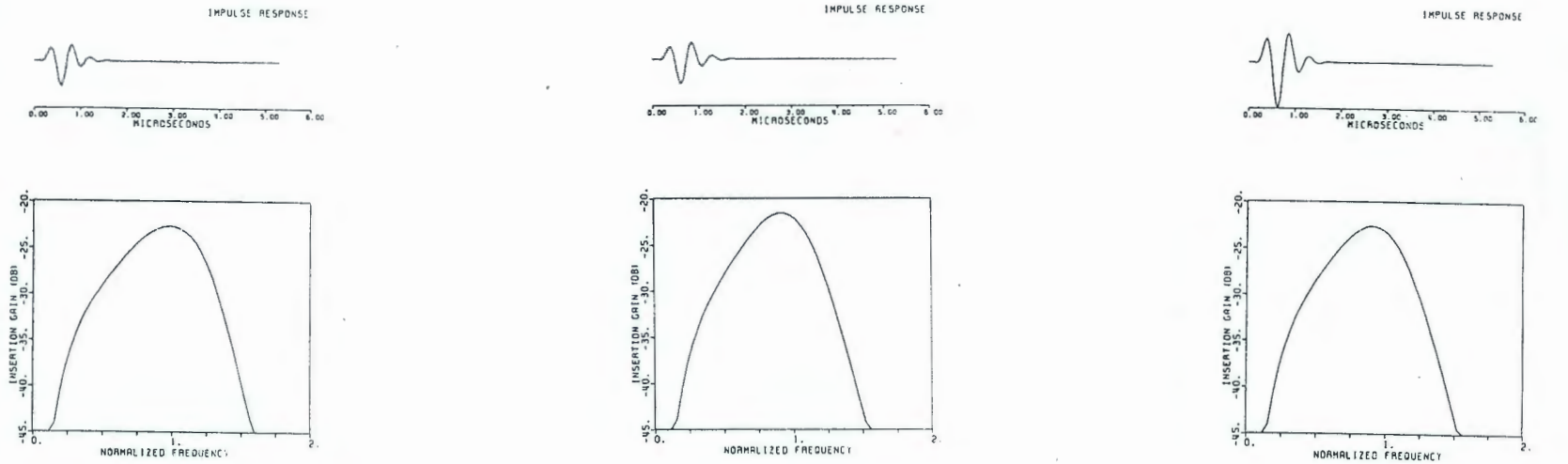

(d) Semi-infinite method, backed

(e) Unbacked method, backed

(f) Binomial method, backed

Figure 17. Comparison of Matching Schemes.

TABLE II. Effect of Various Matching Schemes on Transducer Response

Matching Scheme	Backing Impedance (Mrayls)	Center Frequency (MHz)	6 dB Bandwidth (%)	Damping Factor	Loop Gain (dB)
Semi-Infinite	0	1.76	55.0	8	-38.9
Unbacked	0	1.85	47.6	7	-38.4
Binomial	0	2.02	34.8	6	-38.6
Semi-Infinite	18	2.07	80.9	3	-50.6
Unbacked	18	1.93	72.7	4	-50.5
Binomial	18	1.89	79.1	3	-51.2

Note: Zx = 20.5 Mrayls, Zr = 1.5 Mrayls

Figure 18. The quantity e (τ) corresponds to the electrical input applied to the transducer that causes the transducer to vibrate with a velocity v(τ). This velocity in turn generates a time-dependent pressure p (τ) at a point $\bar{x}$ in the acoustic medium. The pressure wave then reflects off a target and propagates back to the transducer piston. The reflected wave p (τ) then generates a blocked force f(τ) on the transducer face that in turn causes an output voltage e (τ). The transmit and receive transducer responses, G1 and G2, correspond to the responses given in Figure 17. The acoustic radiation field is described using the impulse response technique developed by Stepanishen (Refs.4,18). The impulse response is evaluated using time domain

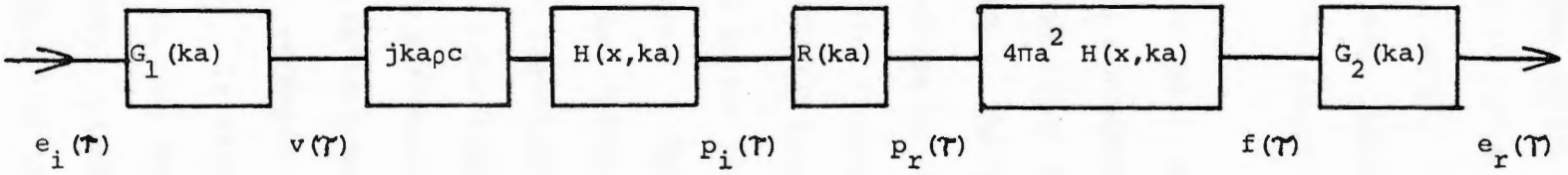

$$G_1(ka) = \frac{V(ka)}{E_i(ka)}$$

$$H(x,ka) = \int_{-\infty}^{\infty} h(x,\tau) e^{-jka\tau} \, d\tau$$

$$R(ka) = 1$$

$$G_2(ka) = \frac{E_r(ka)}{F(ka)}$$

Figure 18. Ultrasonic Pulse-Echo Model.

expressions and inverse Fourier transformed yielding a frequency domain representation of the impulse response $H(\bar{x},ka)$. For the purposes of this study, only point reflectors are considered and so the reflection coefficient R(ka) is unity. The transducer initially described can now be investigated using standard FFT methods to obtain time domain responses for specific acoustic field points and for specific electrical inputs.

The transducer will be excited with two different transmit voltages to simulate a broadband and a narrowband electrical input. The broadband input corresponds to a half cycle of a 10 MHz sine wave as shown in Figure 19. The associated velocity at the face of the transducer is normalized to the maximum value in the waveform, ie., the extreme value. Again τ corresponds to the normalized time across the transducer radius. The individual pulses that make up the transmit velocity correspond to the reflections of longitudinal waves within the piezoelectric element. The unique exponential phenomena occurring between the individual pulses is due to the presence of the negative capacitance in the transducer equivalent circuit as previously noted. If this negative capacitance is eliminated from the circuit, the velocity exhibits a different characteristic as shown in Figure 20. In this case only the reflections at the faces of the element are observed. For the case of a narrowband electrical input, three cycles of a 1 MHz sine wave is used. In Figure 21 the velocity distribution for this input exhibits a beating behavior due to the difference between the transducer fundamental resonance frequency and the input frequency. It should be noted that the transducer velocity is much larger for the narrowband input than for the broadband input.

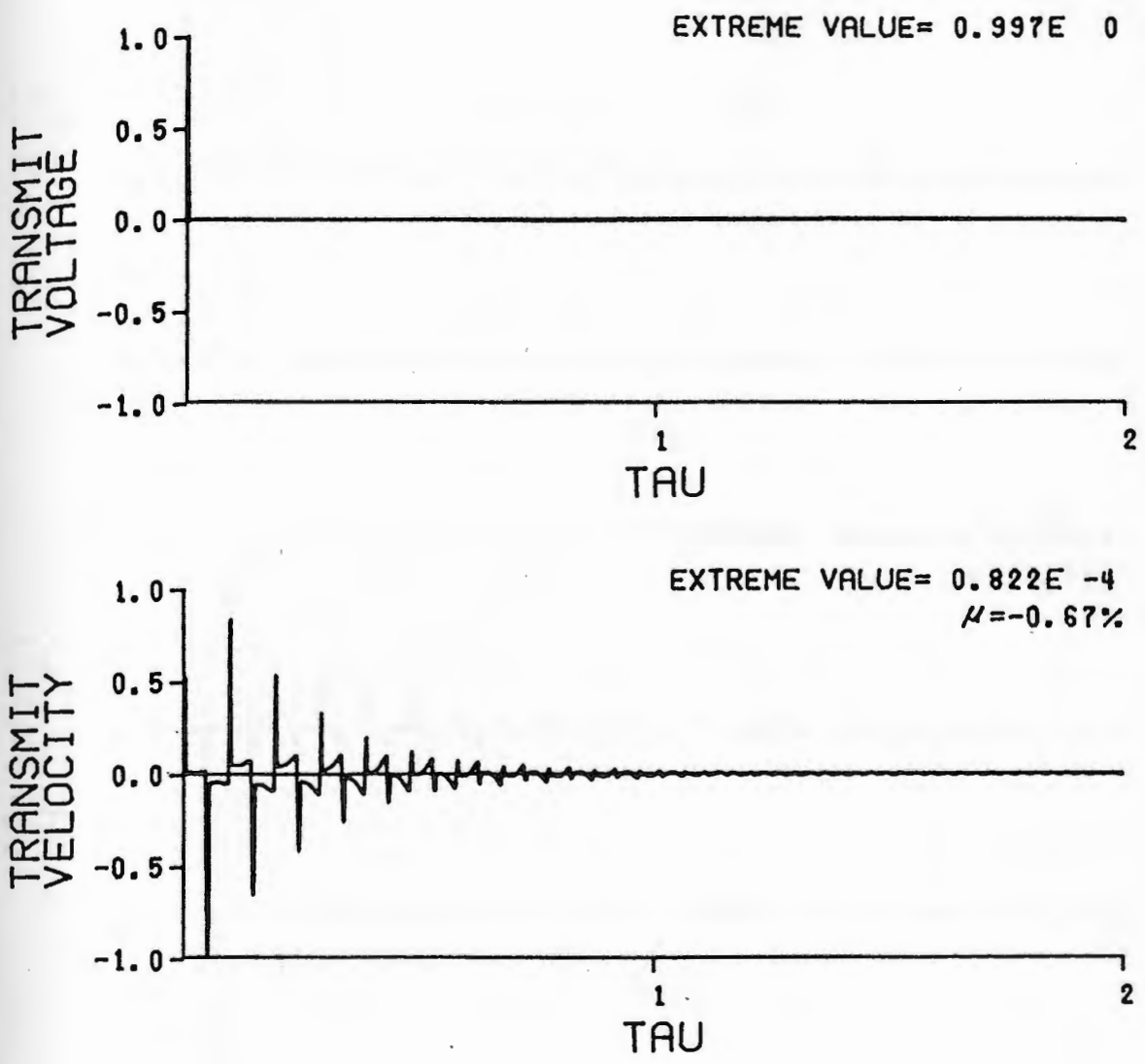

Figure 19. Velocity Response For Broadband Excitation.

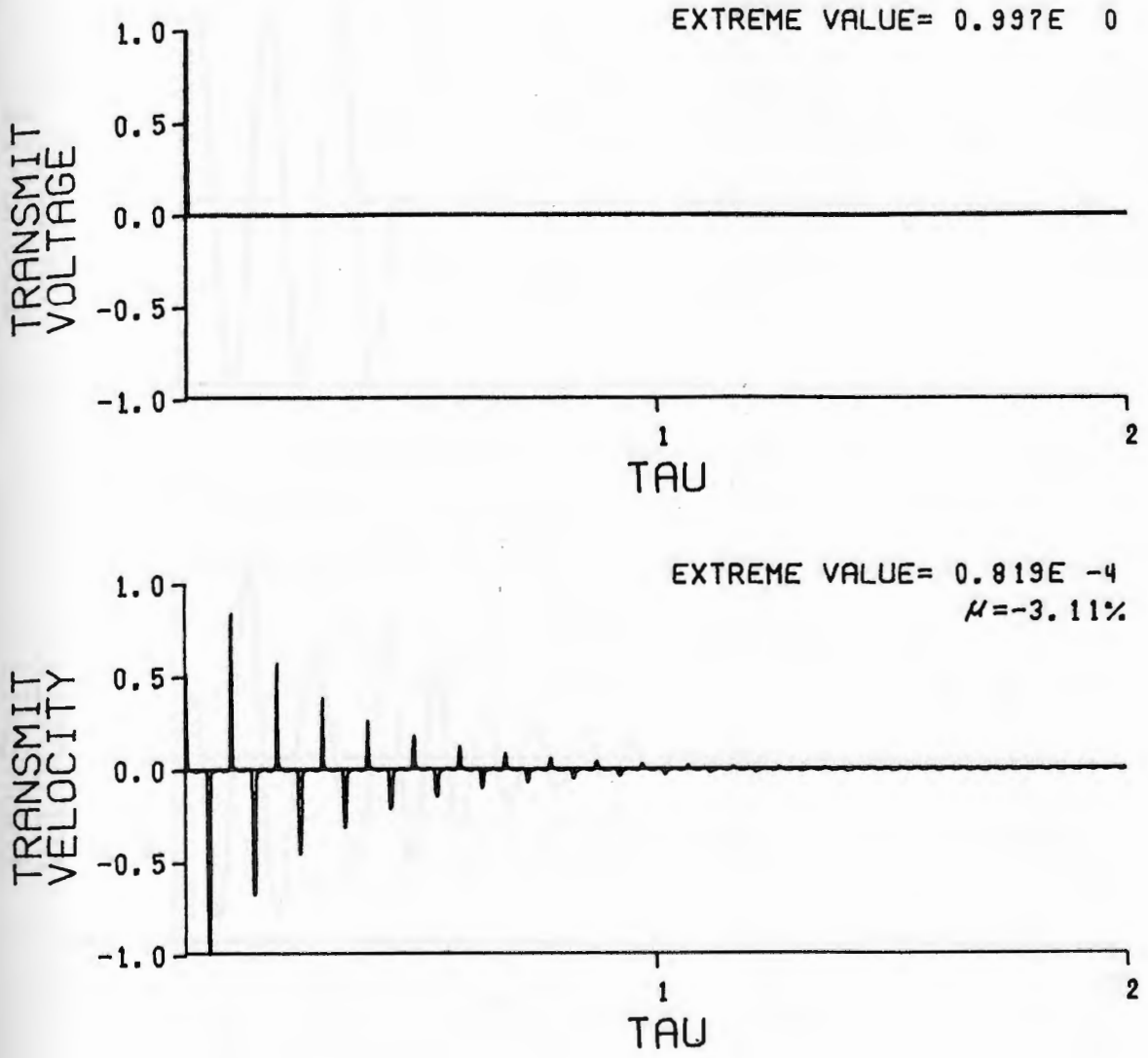

Figure 20. Velocity Response For Broadband Excitation Without Negative Capacitance.

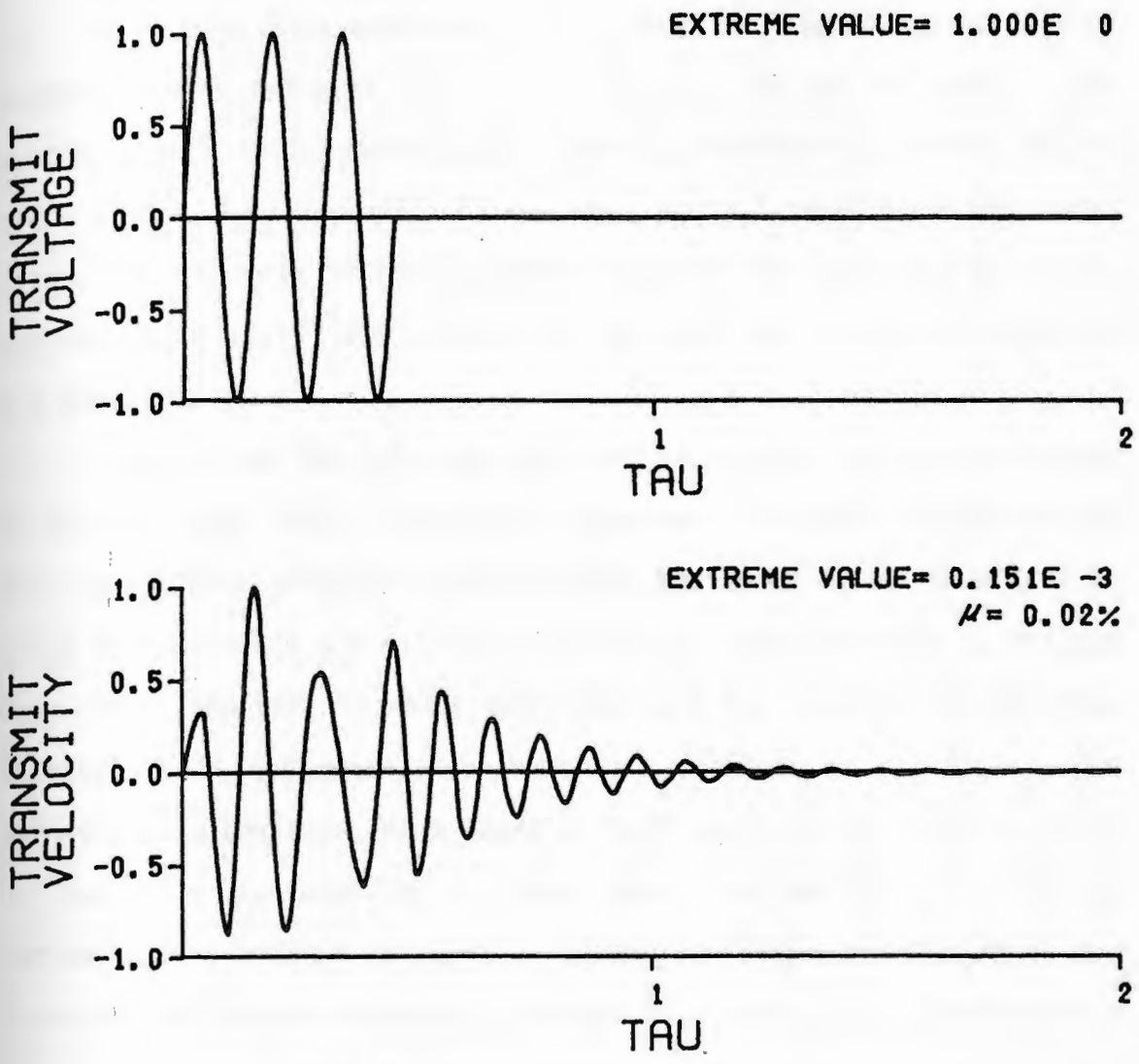

Figure 21. Velocity Response For Narrowband Excitation.

Using this pulse-echo model, the normalized time histories for the acoustic field pressures and receive voltages can be evaluated. The spatial points to be investigated again correspond to combinations of r/a = 0, 0.5, 1, 2 and z/a = 1, 4. The numerical results are presented first, for the case of no transducer dynamics (an idealized thickness expander transducer), and second, for the case when transducer dynamics are included.

Consider now the case when the electrical input is the half cycle 10 MHz sine wave with no transducer dynamics. In Figure 22 the receive voltage and field pressure time responses are shown for an on-axis field point at a distance z/a = 1 from the piston. Each response is delayed by a normalized time τ which corresponds to the acoustic travel time. Although it is not readily apparent, the pressure at the field point consists of a positive and a negative half cycle 10 MHz sine wave that is separated in time by a time equal to the duration of the corresponding impulse response. Since no transducer dynamics are involved, the receive voltage is equivalent, apart from a scale factor, to the blocked force on the element. The reflected signal also undergoes a lengthening in time as it is received at the piston. This characteristic is related to the piston's impulse response function. The transmit velocity is initially convolved with the impulse response and generates a time dependent pressure at the field point. When the pressure wave is reflected off of a point target at that position, it is again convolved with the same impulse response as it is received at the piston.

In the next three figures the radial distance from the piston center is increased to r/a = .5, 1 and 2 in Figures 23, 24 and 25,

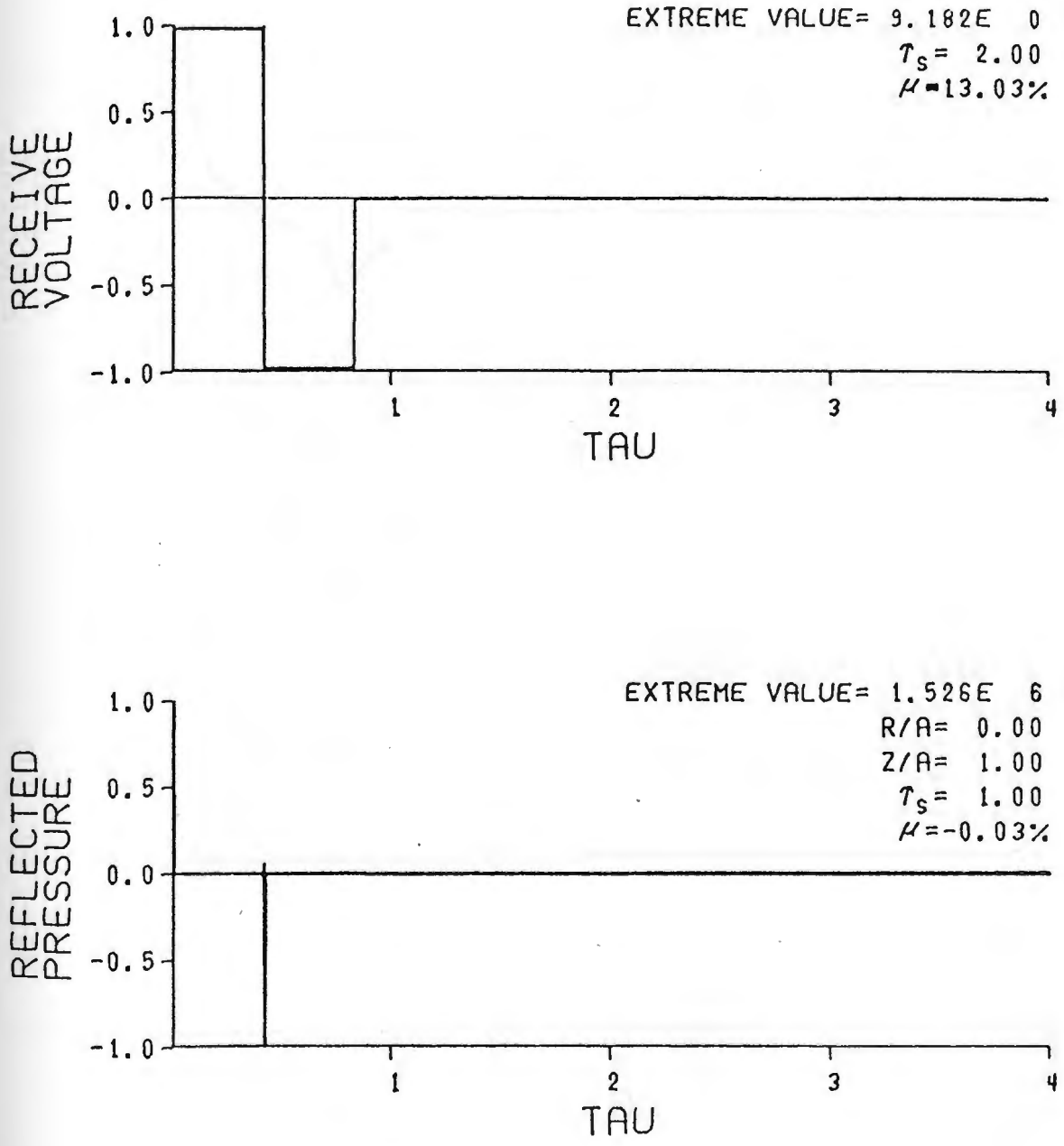

Figure 22. Pulse-Echo Response,No Dynamics, Broadband Input,r/a=Q.,z/a=1.

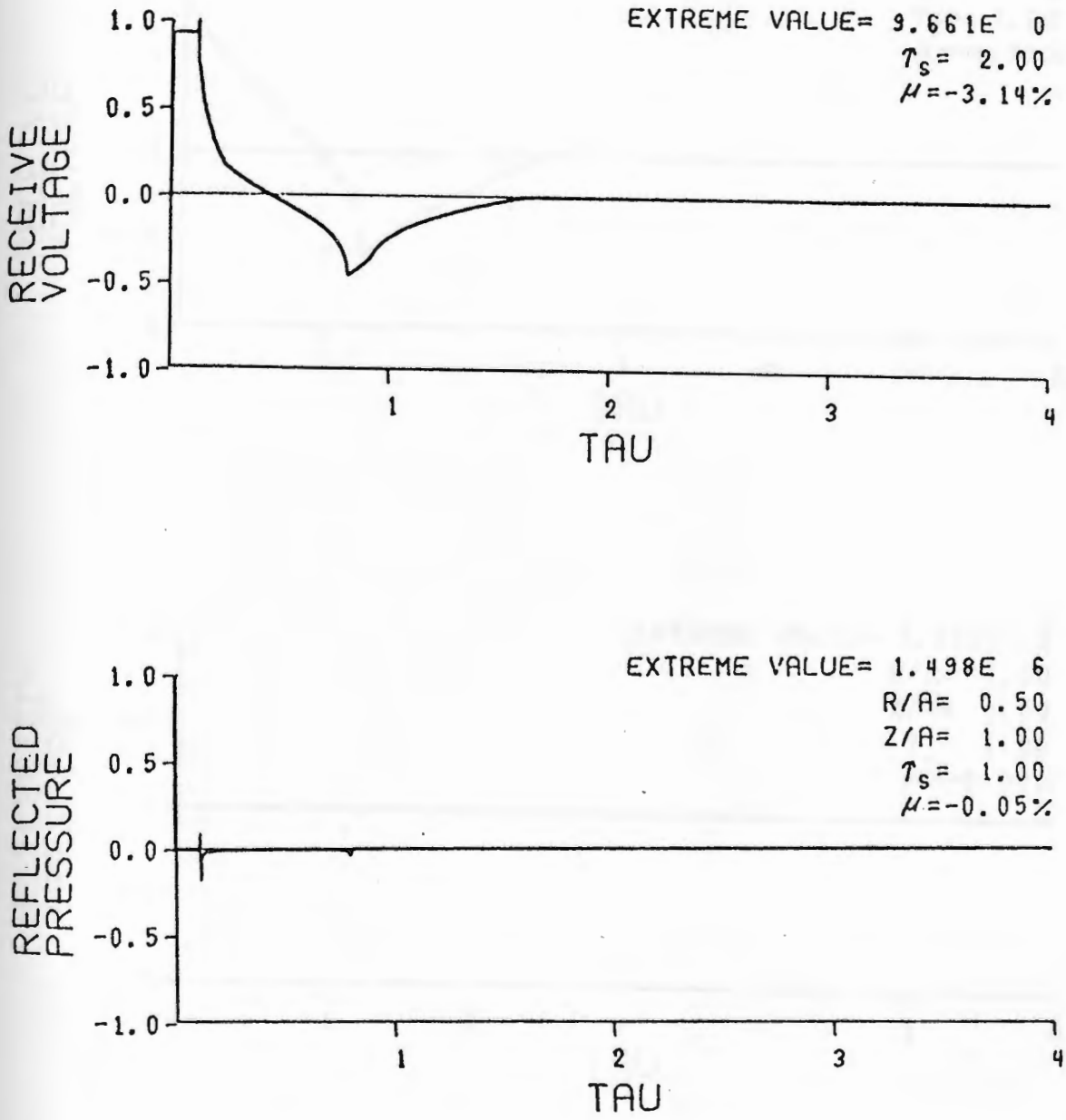

Figure 23. Pulse-Echo Response,No Dynamics, Broadband Input,r/a=.5,z/a=1.

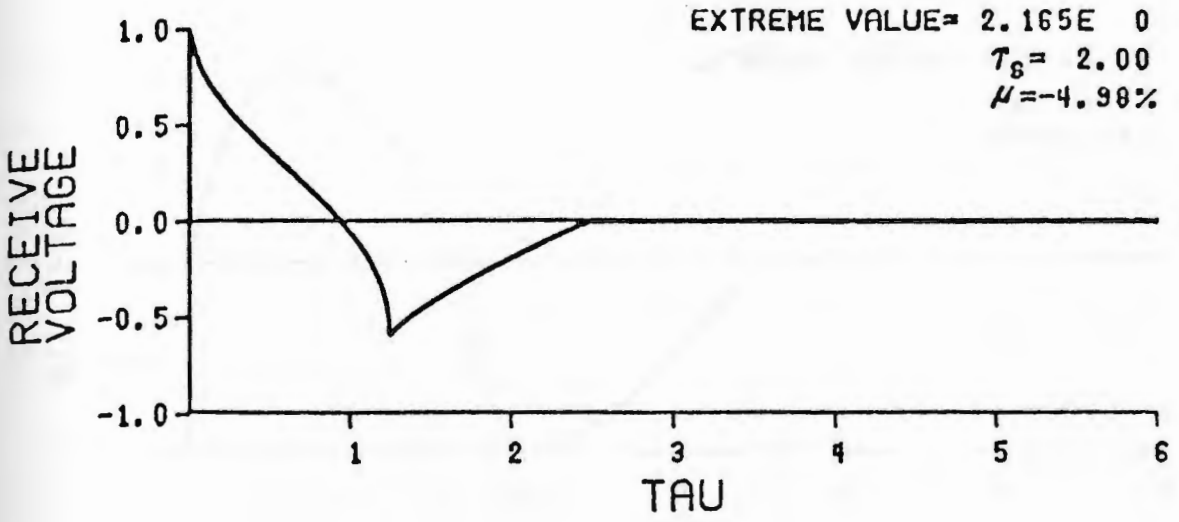

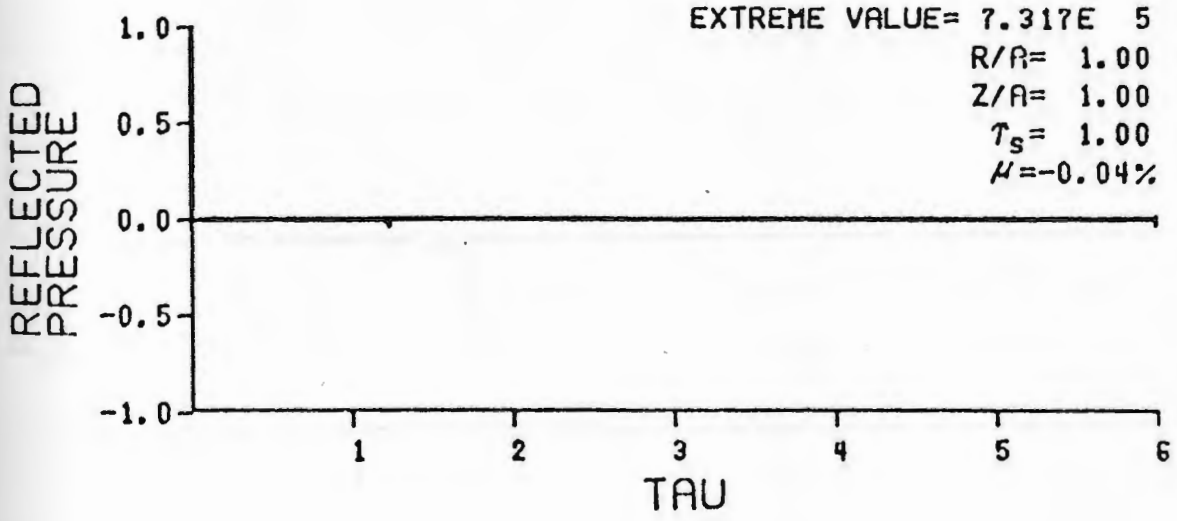

Figure 24. Pulse-Echo REsponse, No Dynamics, Broadband Input,r/a=1.,z/a=1.

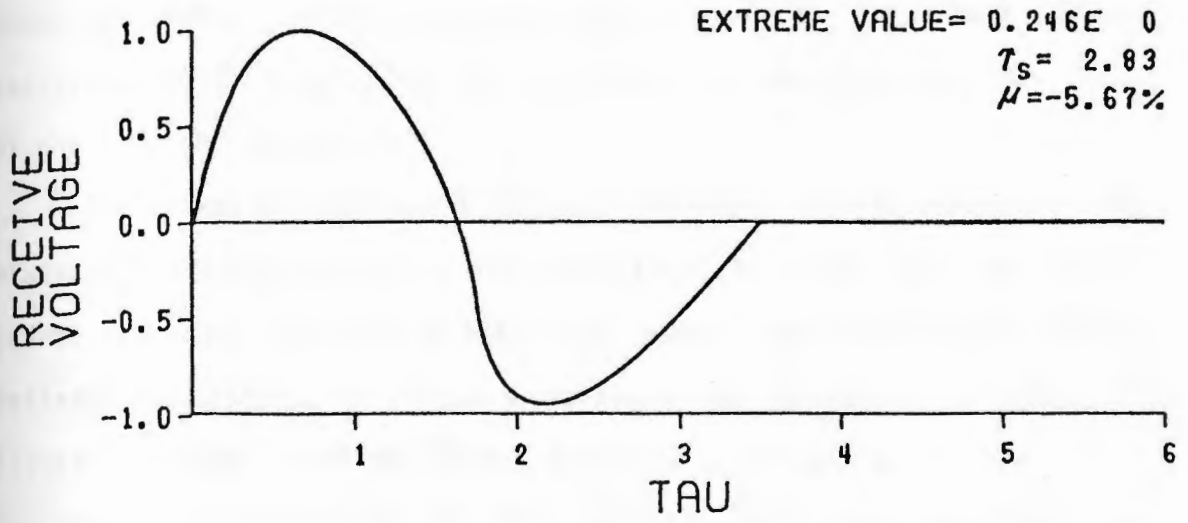

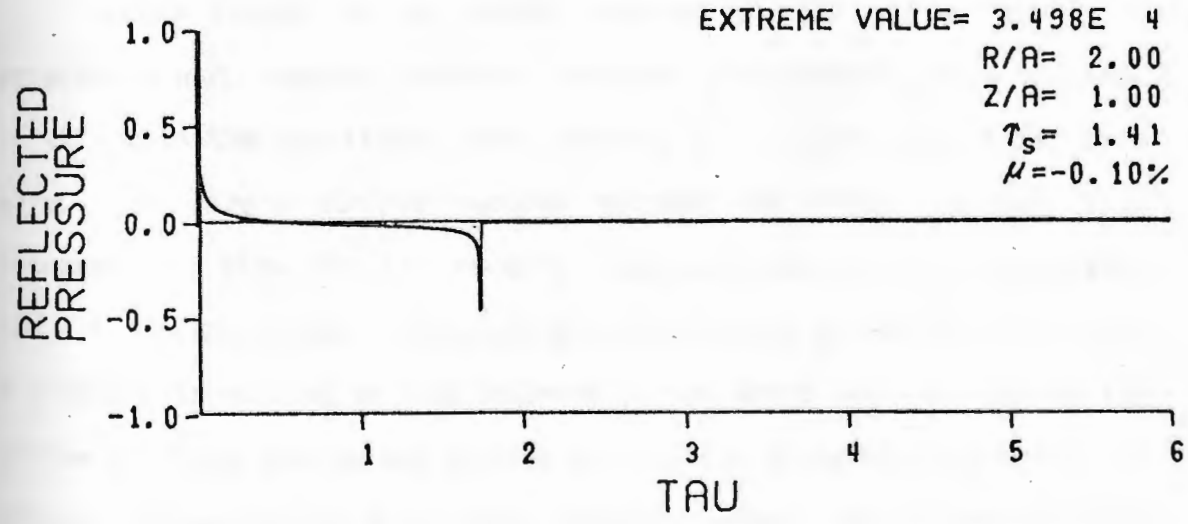

Figure 25. Pulse-Echo Response, No Dynamics, Broadband Input, r/a=2., z/a=1.

respectively. The most obvious characteristic is the increase in pulse duration. As the radial distance is increased, the duration of the impulse response increases. A marked decrease in signal amplitude is noted for radial distances greater than r/a = .5. The shape of the receive signals in each case has a tendency to correlate with the shape of the impulse response.

The effect of increasing the axial distance to z/a = 4 on the time histories is apparent in the next four figures. Again the same radial points are used. For the on-axis field point, the time duration of the reflected pressures and receive voltages has decreased as shown in Figure 26. Again when the radial distances are increased to r/a = .5 , 1, and 2 as in Figures 27, 28, and 29, the pulse durations are lengthened. It is noted that the amplitudes of the pressures and voltages are similar to those in the previous case when z/a = 1.

Having looked at the pulse response of the piston due to a broadband input, consider now the case when a narrowband input is used. In this case the electrical input consist of 3 cycles of a 1 MHz sine wave. In Figure 30 the receive voltage and field pressure time responses are shown for the on-axis field point occurring at a distance z/a = 1 from the piston. Although the short pulse excitation results in a pressure consisting of two separate pulses which are replicas of the piston velocity, the pulses overlap and yield a distorted waveform. The receive voltage consists of three distinct pulses, one of which is out of phase with the other two. The pulse lengthening noted in these responses is due to the duration of the impulse response and to the increased input duration.

In the next three figures the radial distance from the piston

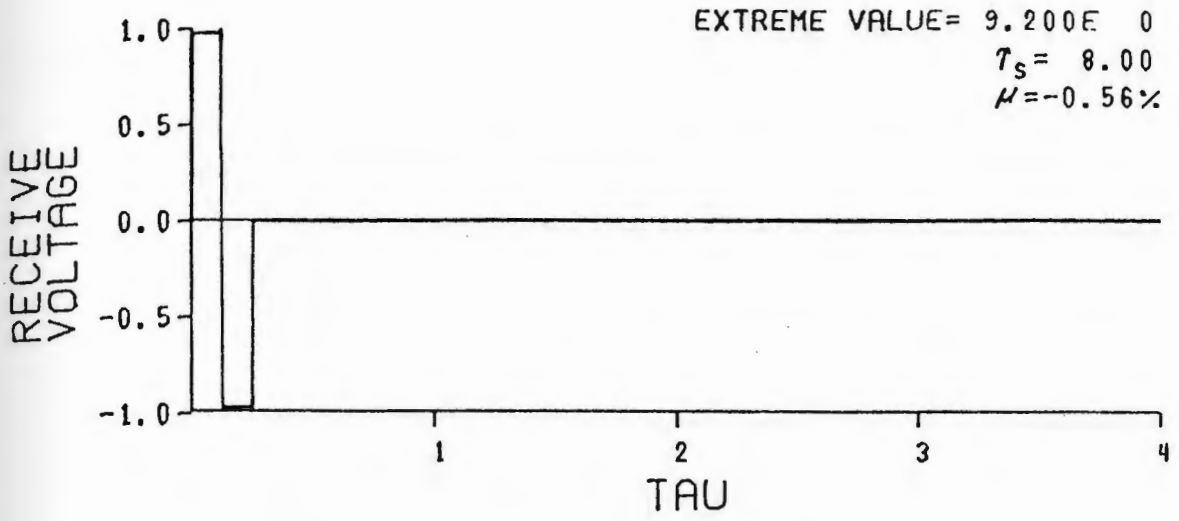

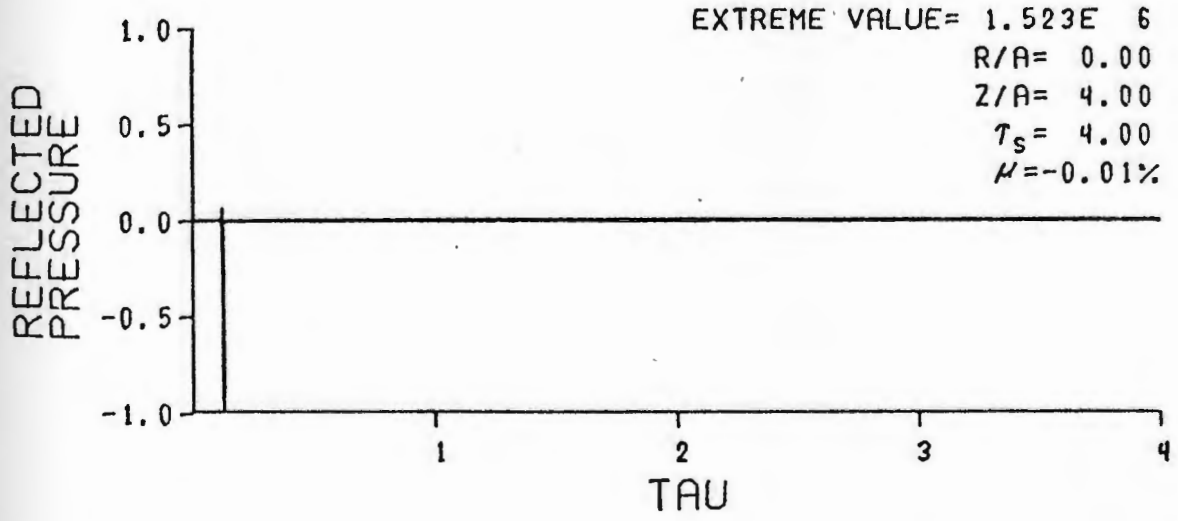

Figure 26. Pulse-Echo Response, No Dynamics, Broadband Input, r/a=0.,z/a=4.

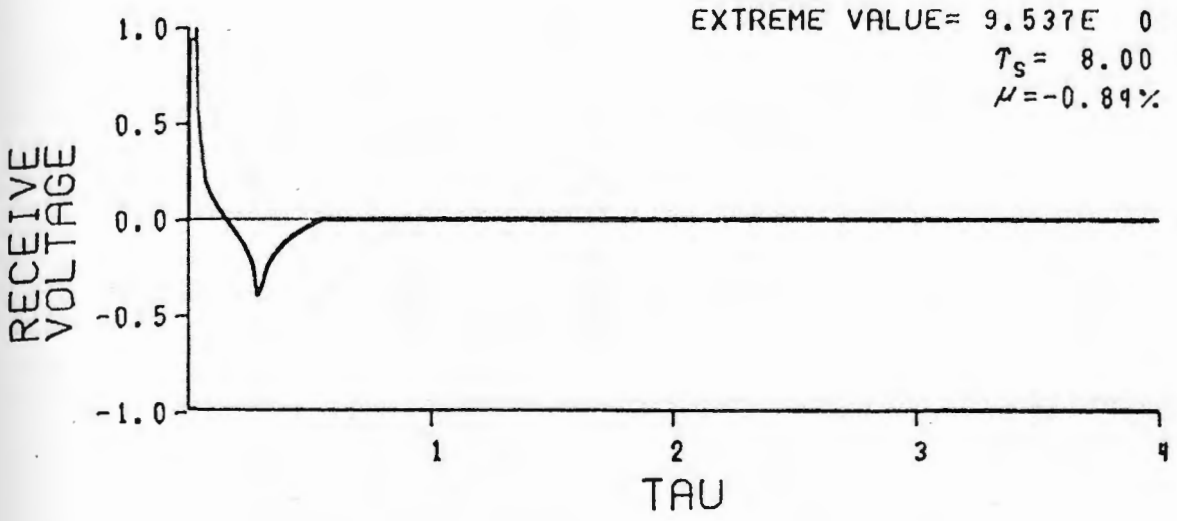

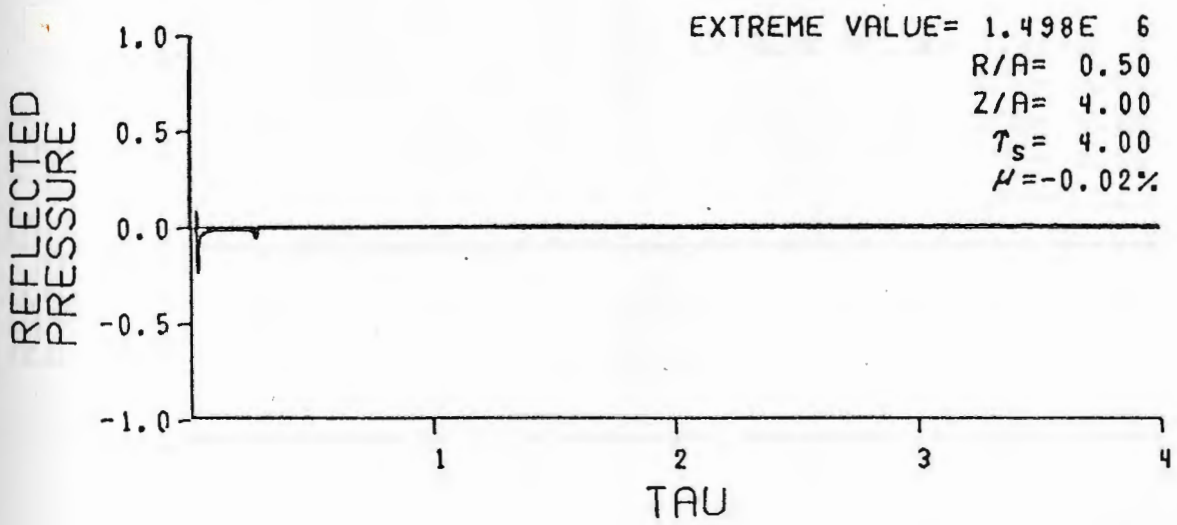

Figure 27. Pulse-Echo Response, No Dynamics, Broadband Input, r/a=.5, z/a=4.

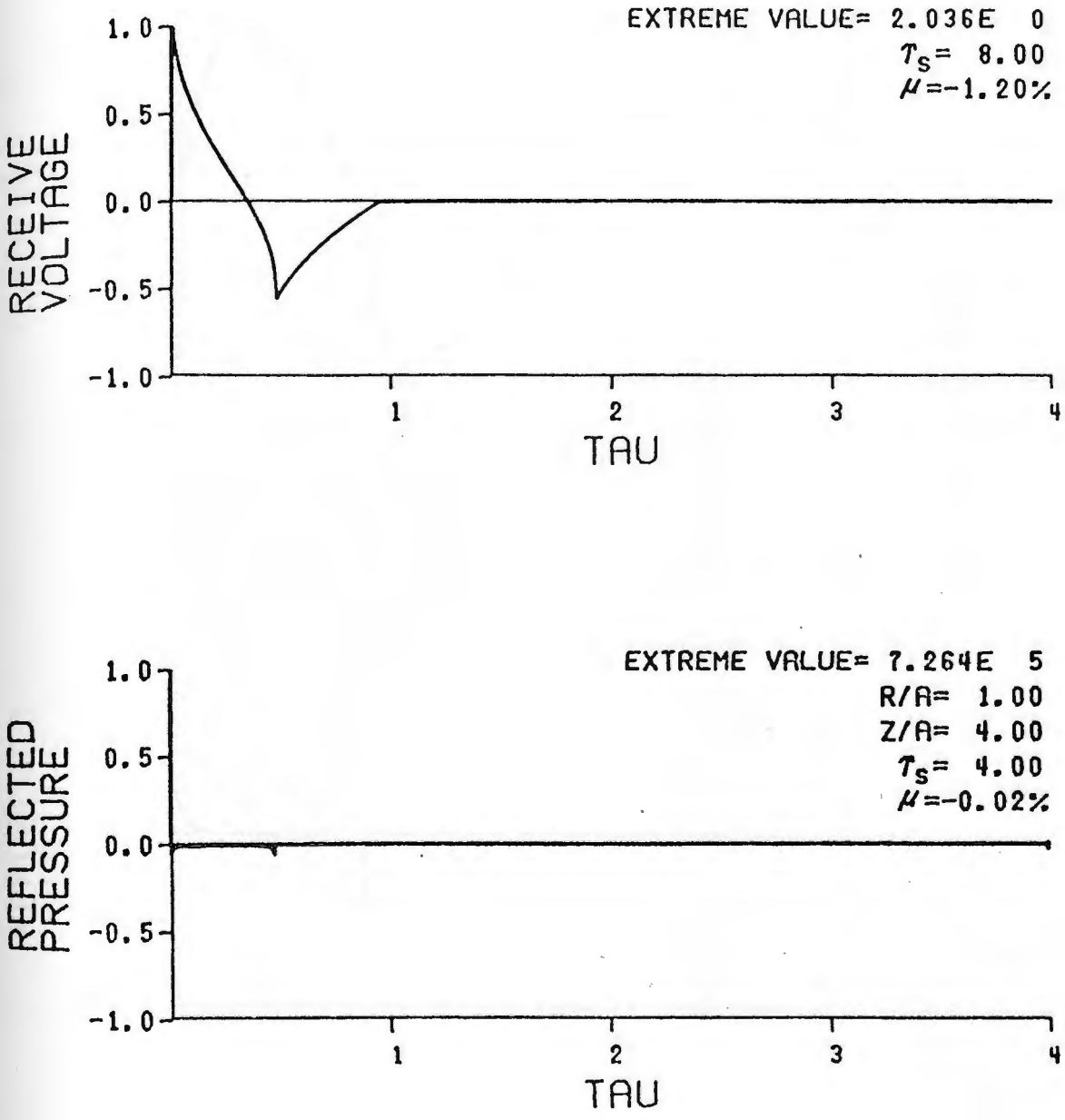

Figure 28. Pulse-Echo Response, No Dynamics, Broadband Input, r/a=1.,z/a=4.

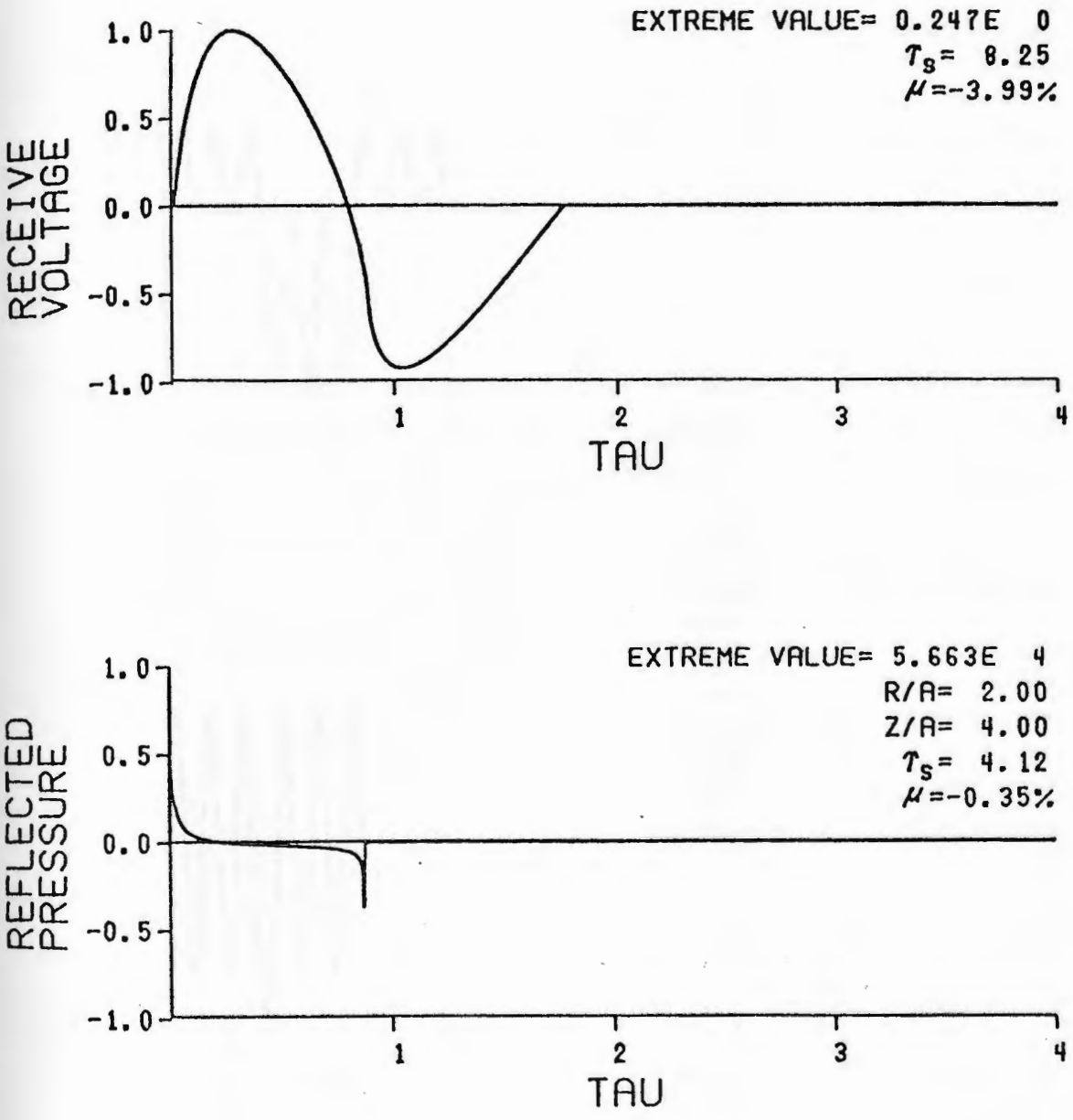

Figure 29. Pulse-Echo Response, No Dynamics, Broadband Input, r/a=2.,z/a=4.

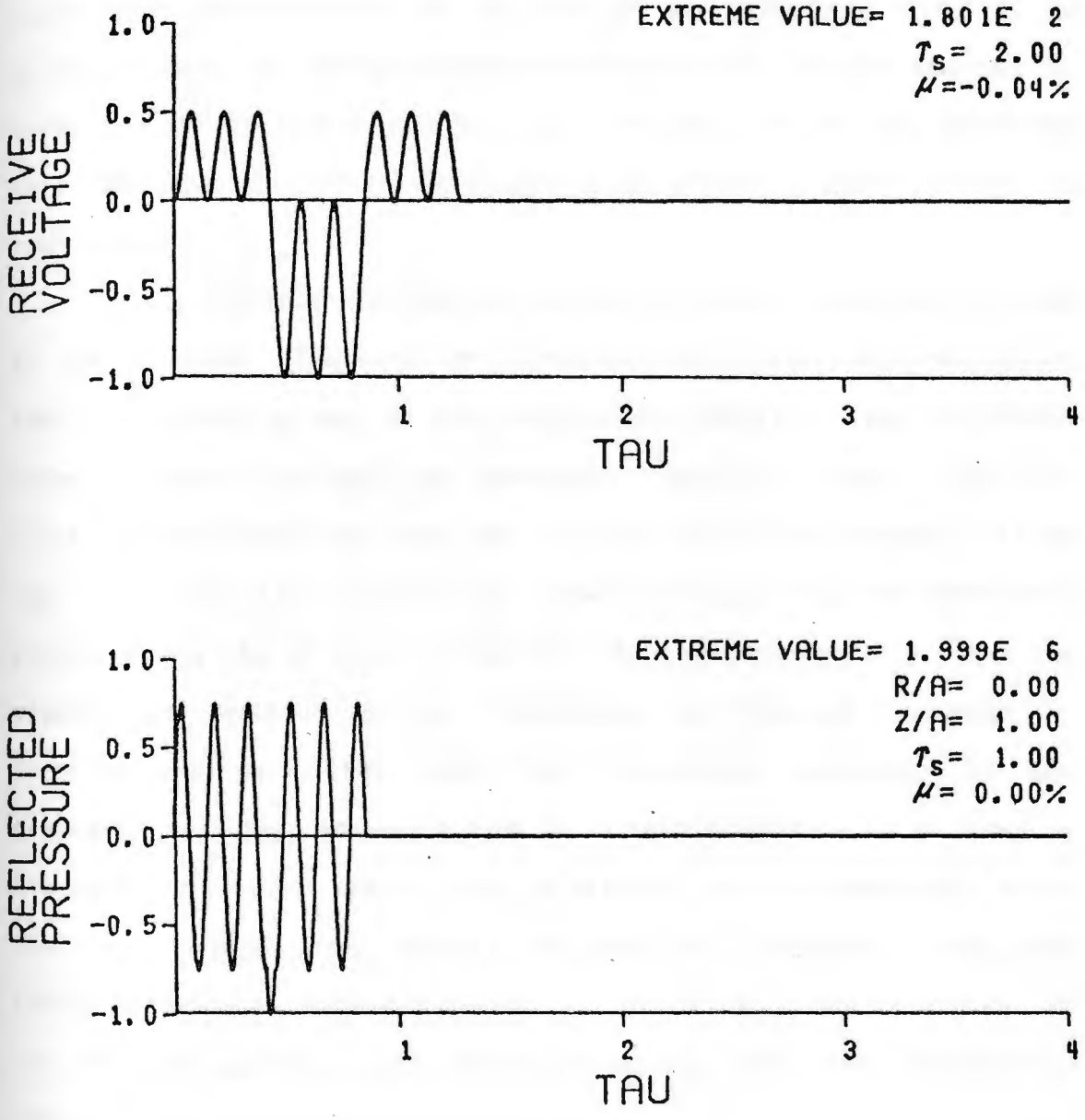

Figure 30. Pulse-Echo Response, No Dynamics, Narrowband Input, r/a=0.,z/a=1.

center is increased to r/a = .5, 1 and 2 in Figures 31, 32 and 33, respectively. In contrast to the on-axis case, the impulse response no longer has a rectangular shape for off-axis points. Thus the transmitted pressures are not replicas of the velocity. Again as in previous cases, the reflected pressures and receive voltages increase in duration, as the radial distance is increased. Unlike the broadband case, the amplitudes of the responses do not exhibit a uniform change as r/a increases.

In the previous discussions transducer dynamics were not included in the analysis. The next set of figures will illustrate the effect that the transducer has on the pressure and receive voltage responses using the same broadband and narrowband electrical inputs. Consider first the broadband case when the axial distance from transducer is at z/a = 1. For the on-axis case shown in Figure 34, the reflected pressure consists of two replicas of the transmit velocity. As the signals are received by the transducer, the response increases in duration and oscillates about the fundamental resonance of the transducer. As the radial distance is increased to r/a = .5 as shown in Figure 35, a second distinct pulse is starting to form immediately after the first; however, the overall amplitude has decreased. When the radial distance is increased to r/a = 1 and 2 as shown in Figures 36 and 37, the multiple pulse structure becomes much more distinctive, though larger amplitude decreases are noted.

If the same transducer is provided with a narrowband input, a similar response is noted. Consider now the on-axis case when the axial distance corresponds to z/a = 4 as shown in Figure 38. The reflected pressure no longer consists of replicas of the transmit velocity. The

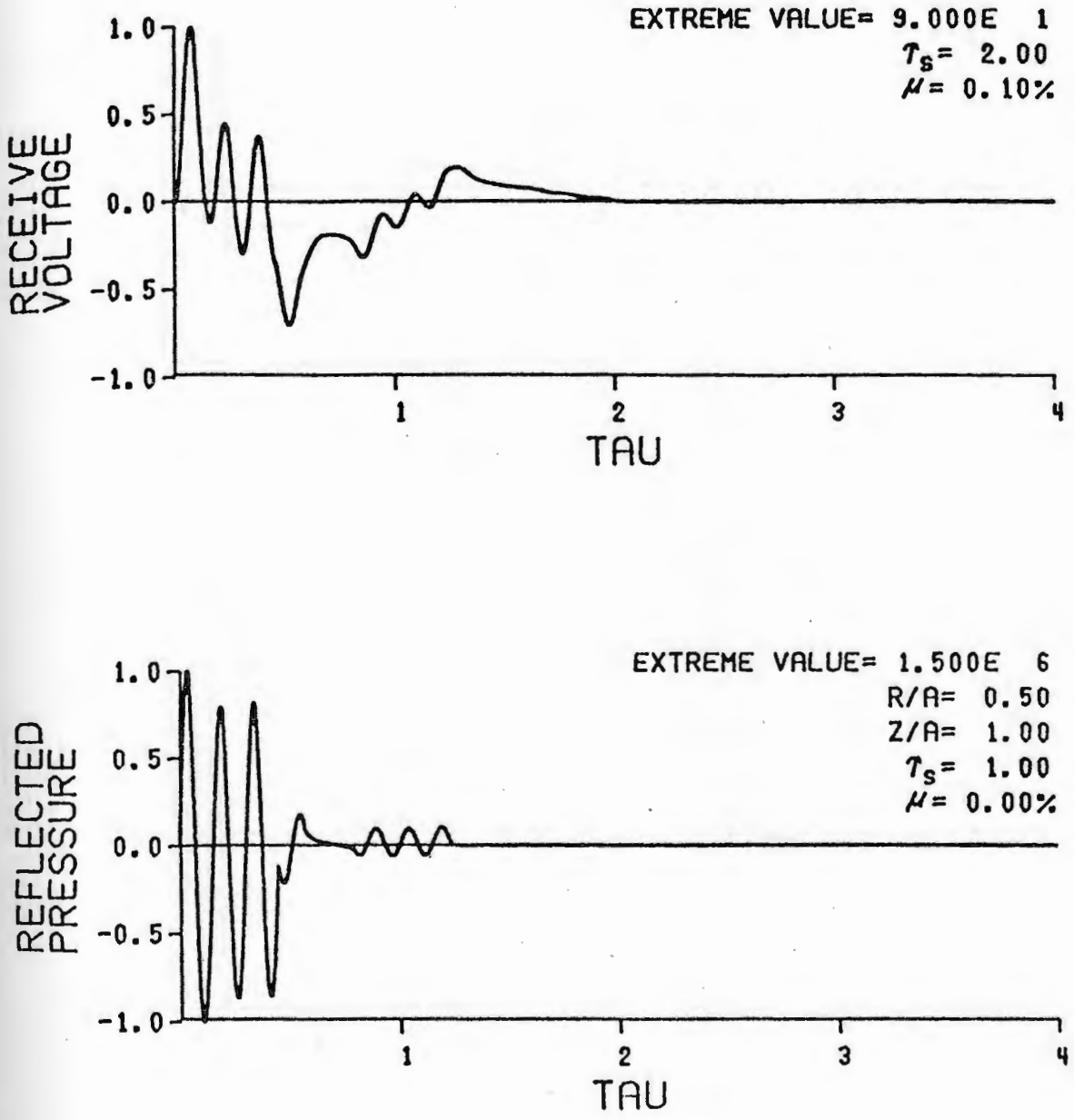

Figure 31. Pulse-Echo Response, No Dynamics, Narrowband Input, r/a=.5,z/a=1.

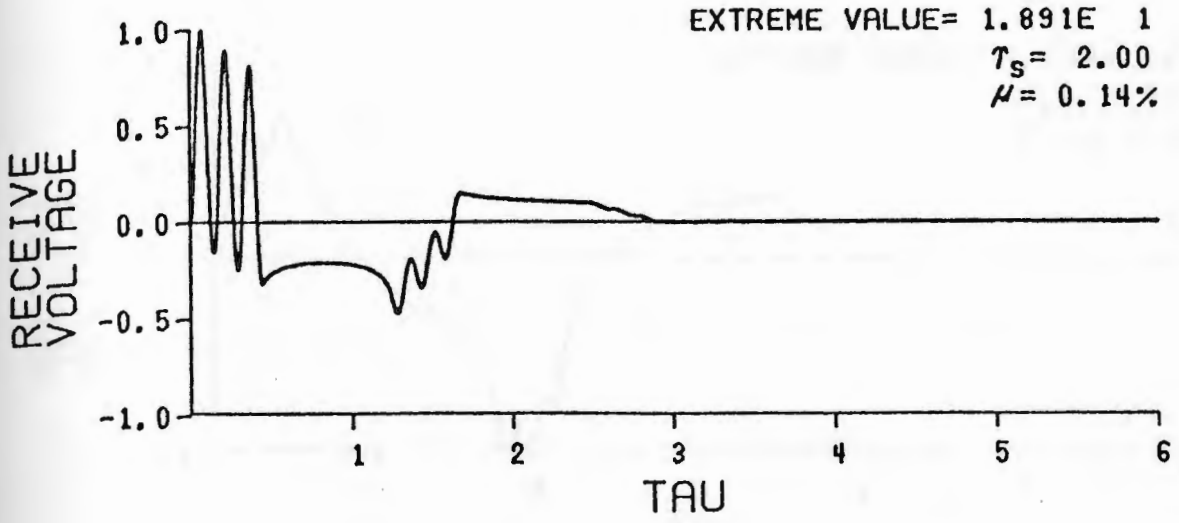

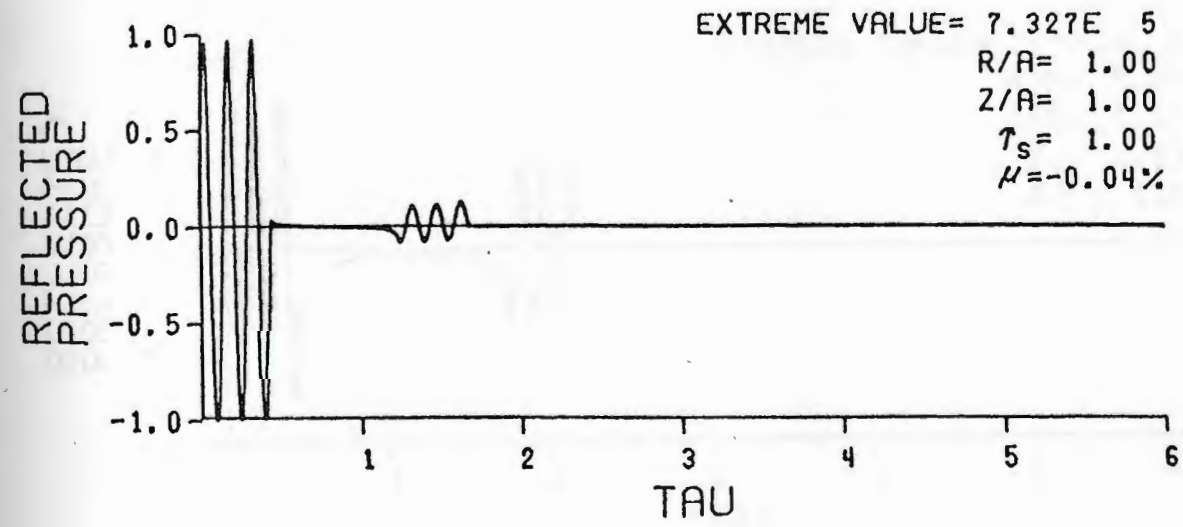

Figure 32. Pulse-Echo Response, No Dynamics, Narrowband Input, r/a=1.,z/a=1.

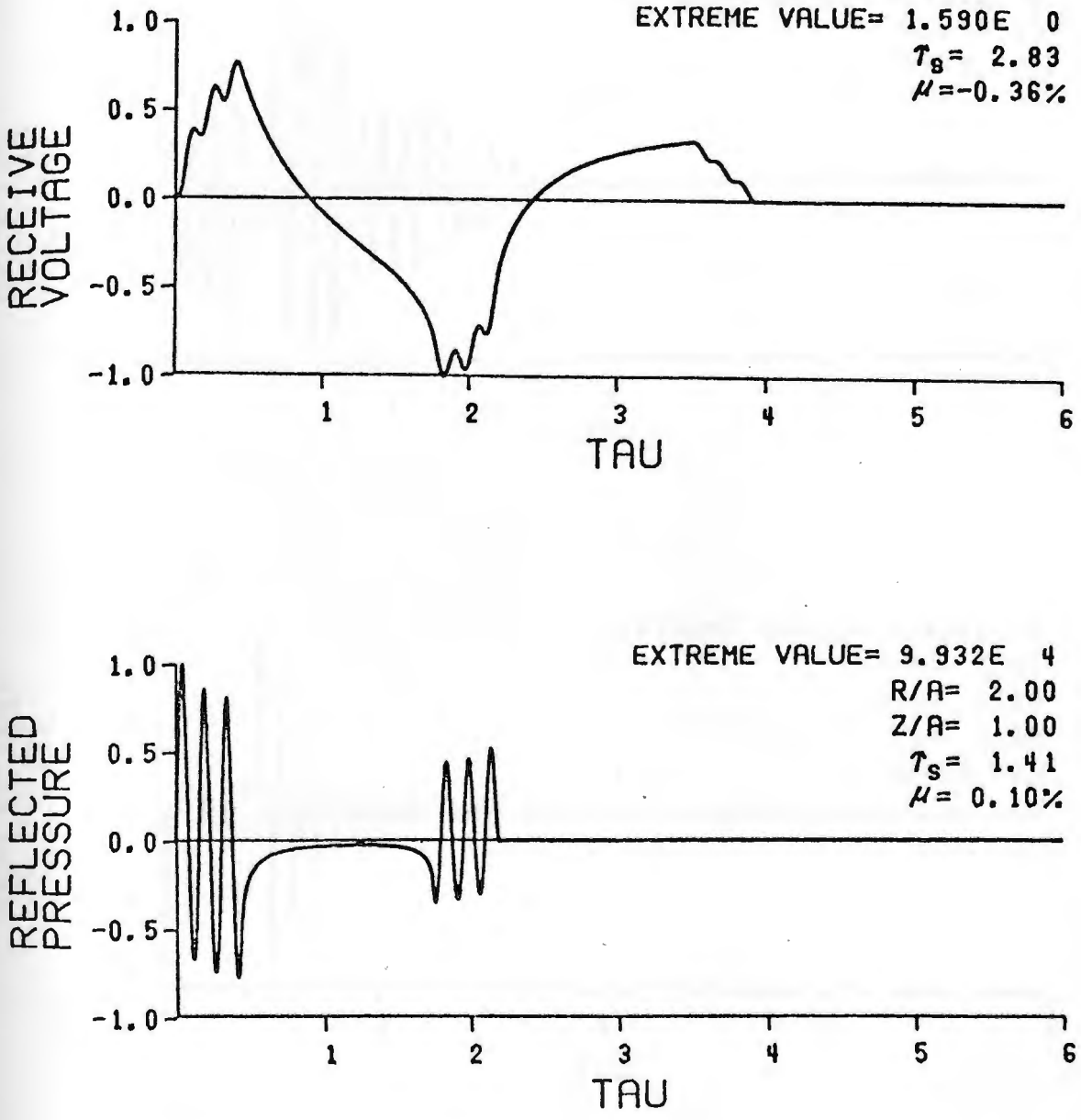

Figure 33. Pulse-Echo Response, No Dynamics, Narrowband Input, r/a=2.,z/a=1.

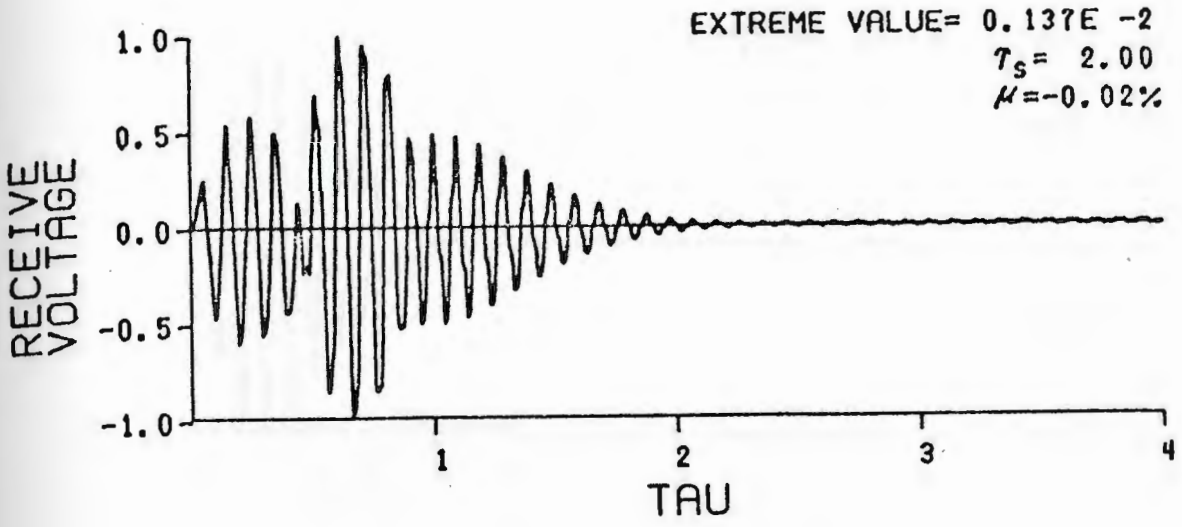

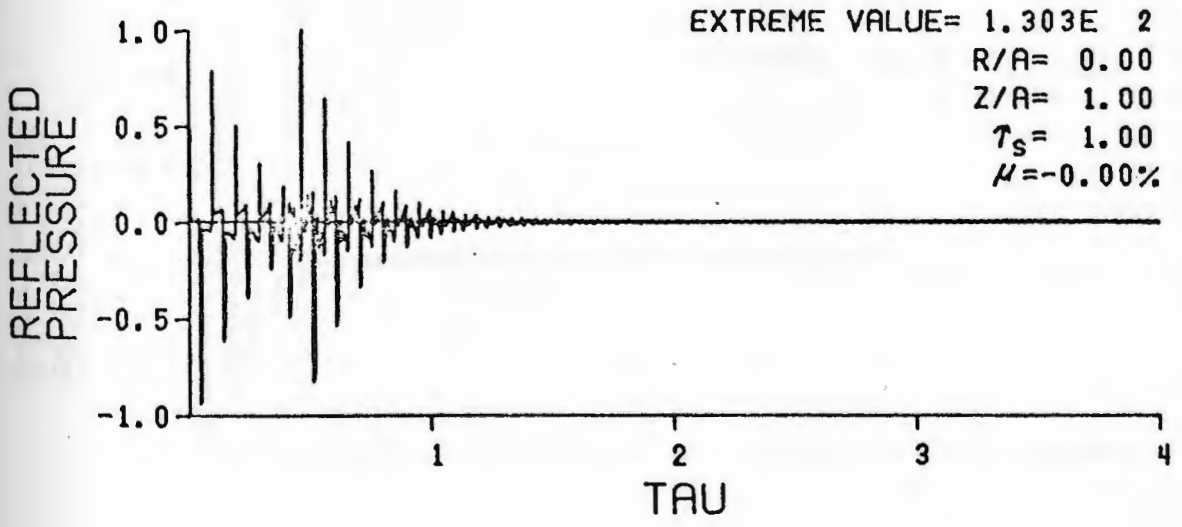

Figure 34. Pulse-Echo Response, Dynamics, Broadband Input, r/a=0.,z/a=1.

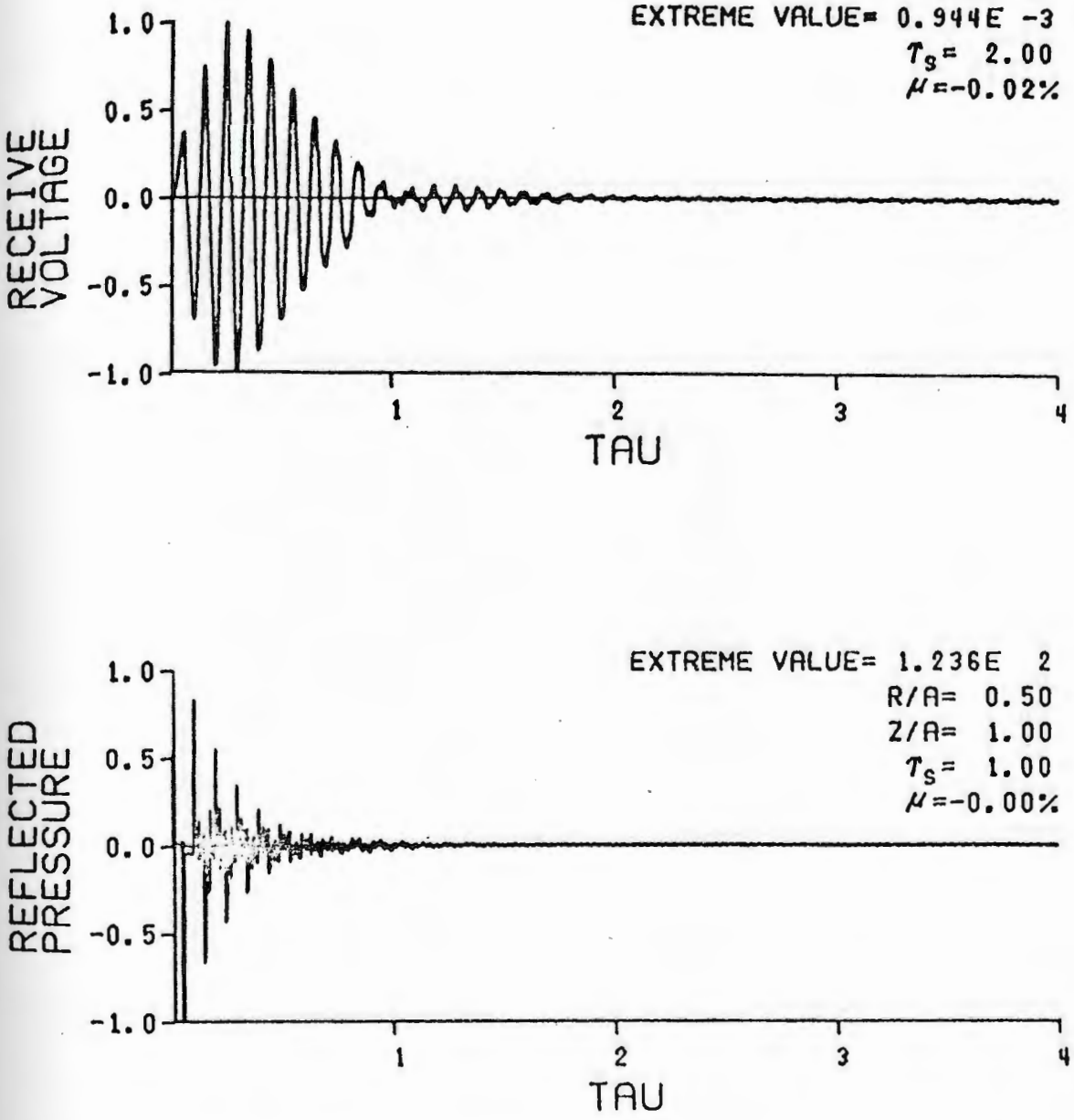

Figure 35. Pulse-Echo Response, Dynamics, Broadband Input, r/a=.5,z/a=1.

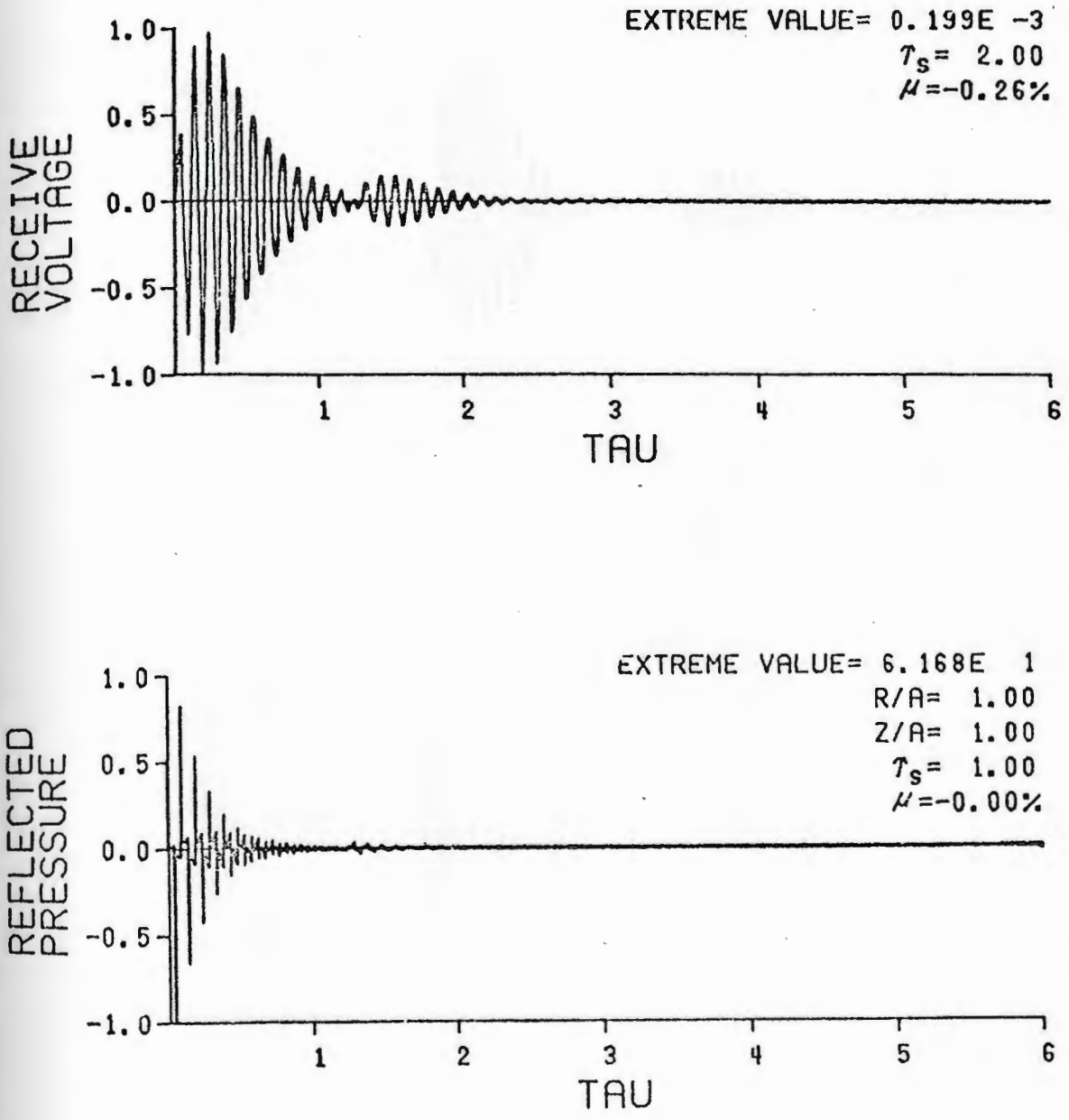

Figure 36. Pulse-Echo Response, Dynamics, Broadband Input, r/a=1.,z/a=1.

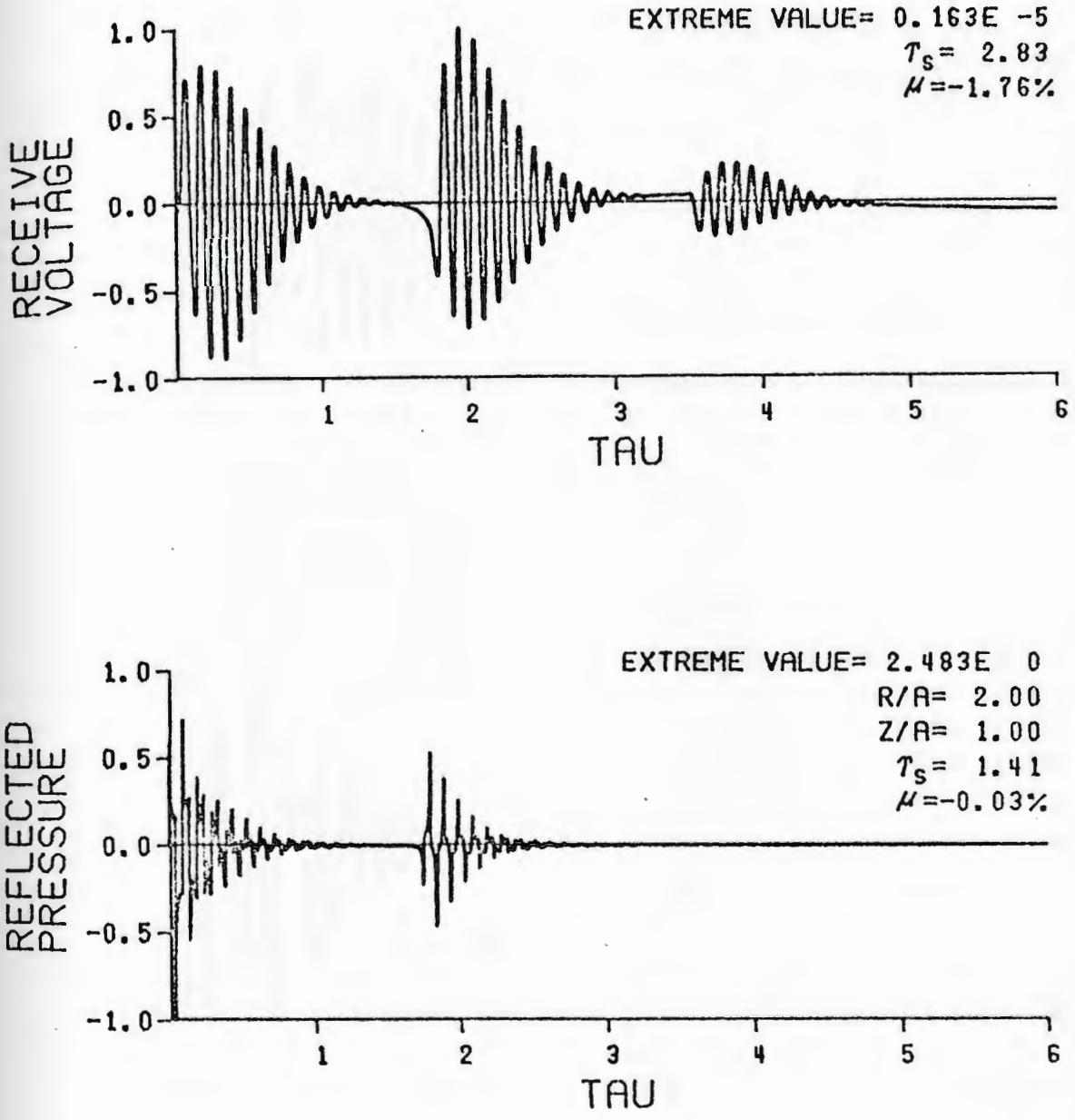

Figure 37. Pulse-Echo Response, Dynamics, Broadband Input, r/a=2.,z/a=1.

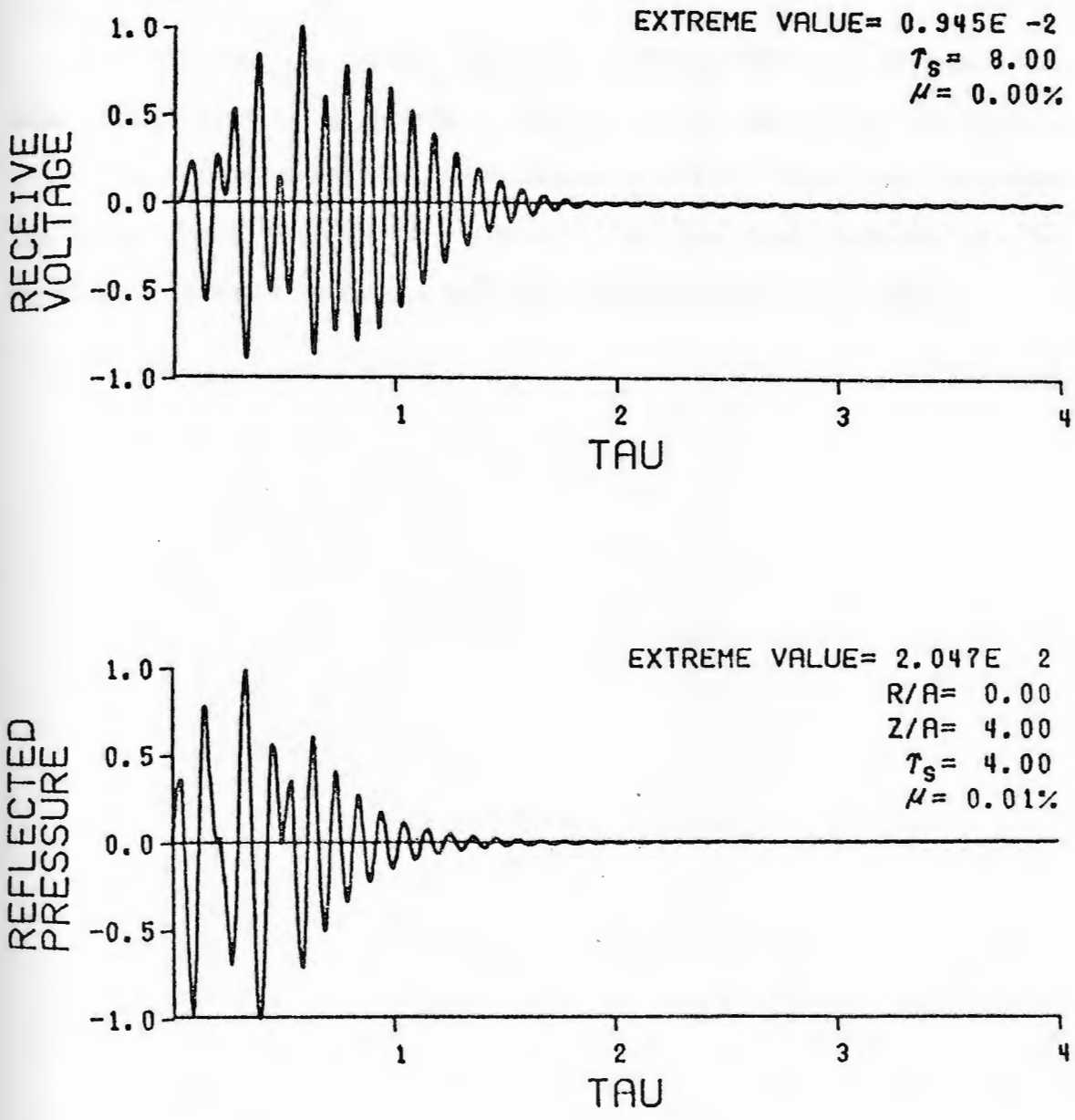

Figure 38. Pulse-Echo Response, Dynamics, Narrowband Input, r/a= 0.,z/a=4.

receive voltage exhibits a similar modulated response. As the radial distance is increased to r/a = 1 and 2 as shown in Figures 39 and 40, the responses exhibit a multiple pulse structure having an extremely long duration.

In summary, the pulsed acoustic response from a transducer has been investigated for a variety of spatial points and electrical inputs. It has been shown that the pulsed acoustic field effectively lengthens the duration of the acoustic pulses. If the time response of the transducer is short enough, a multiple pulse structure can occur.

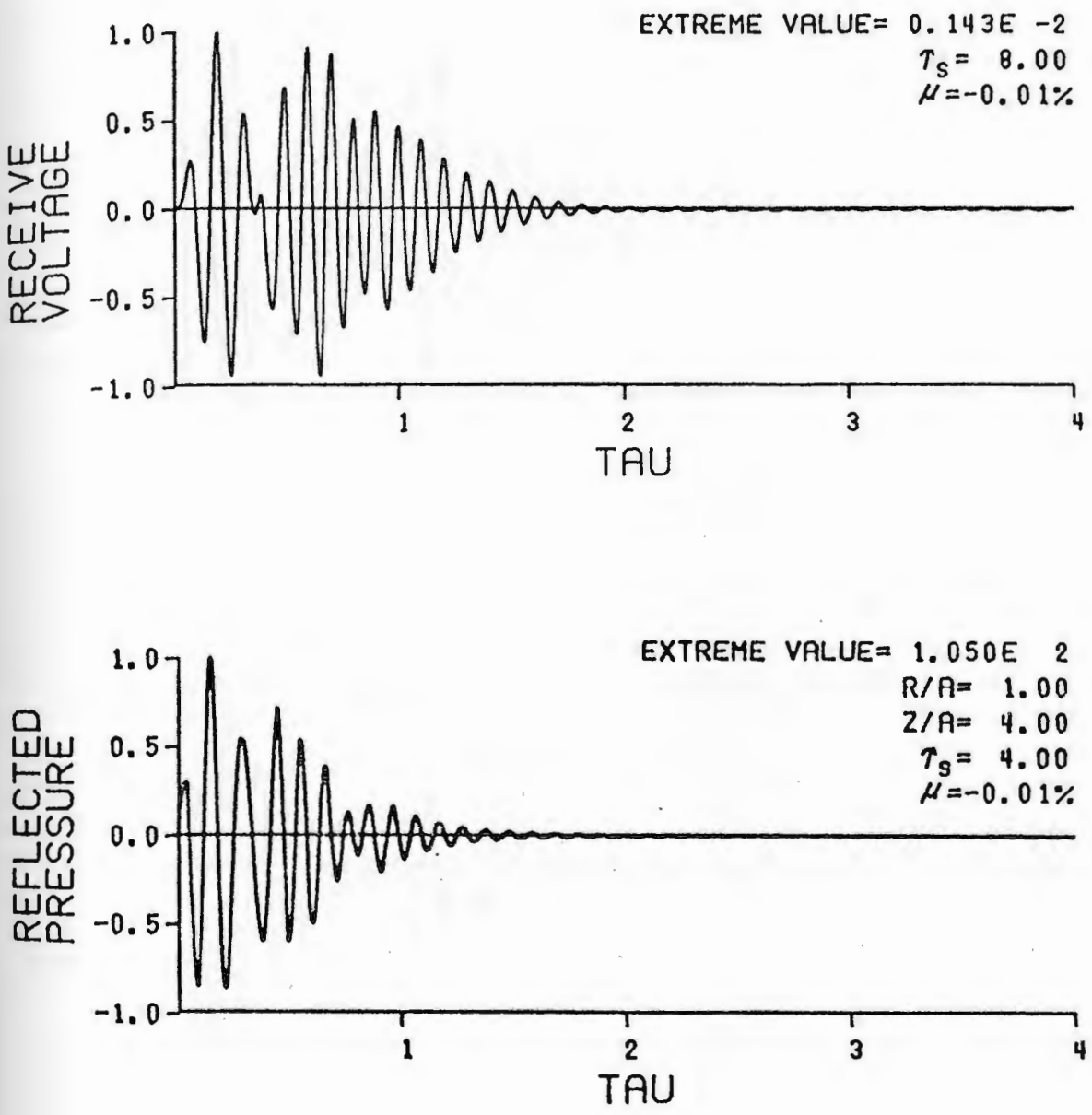

Figure 39. Pulse-Echo Response, Dynamics, Narrowband Input,r/a=1.,z/a=4.

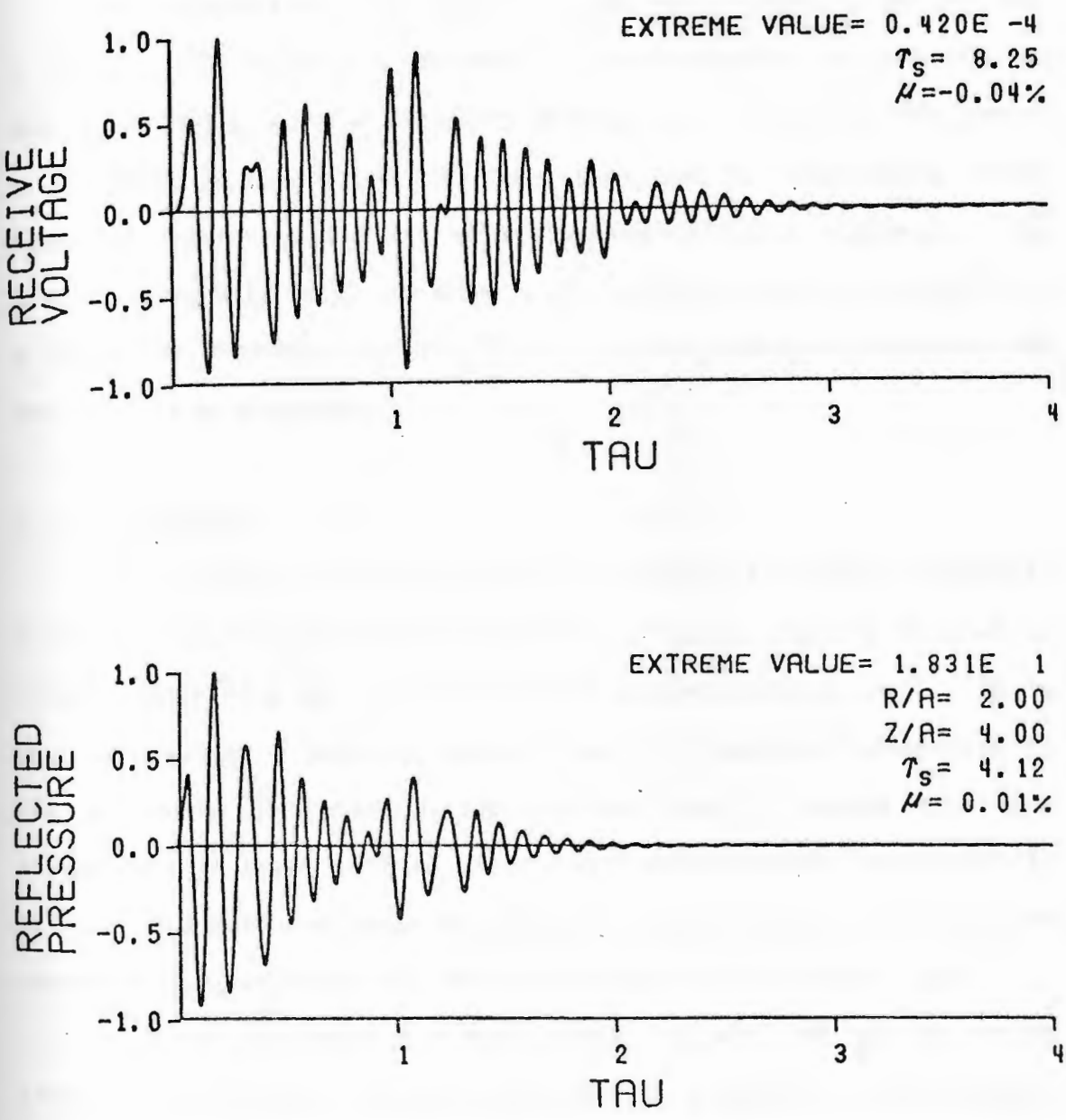

Figure 40. Pulse-Echo Response, Dynamics, Narrowband Input, r/a=2.,z/a=4.

Chapter III

ULTRASONIC TRANSDUCER CONSTRUCTION

The construction of ultrasonic transducers is more of an art than a science. To build a transducer to specifications obtained from an analytical model, careful attention must be paid to detail. The number of variables in manufacture is large, such that two transducers having identical components can end up having two different responses. The process is largely trial and error until one has enough experience with a particular method. In this light, various transducer construction methods will be discussed.

Review of Methods

The principal components of a typical broadband ultrasonic transducer are illustrated in Figure 41. Here a backing is used to absorb energy from the back face of the piezoelectric element. It is desirable to use a backing material that is completely absorptive so that no energy is reflected back to the element, thereby causing a voltage signal later in time after the transducer has been initially pulsed. The matching layer on the other hand is used to increase the amount of energy transferred from the element to the acoustic load.

A number of methods have been proposed to match the backing to the element. The simplest technique consists of selecting a material that has an acoustic impedance near that of the element's impedance. The major problem with this method is that the backing must be quite long to prevent any reverberation within the backing from affecting the element. It is desirable that the backing approximate a semi-infinite condition.

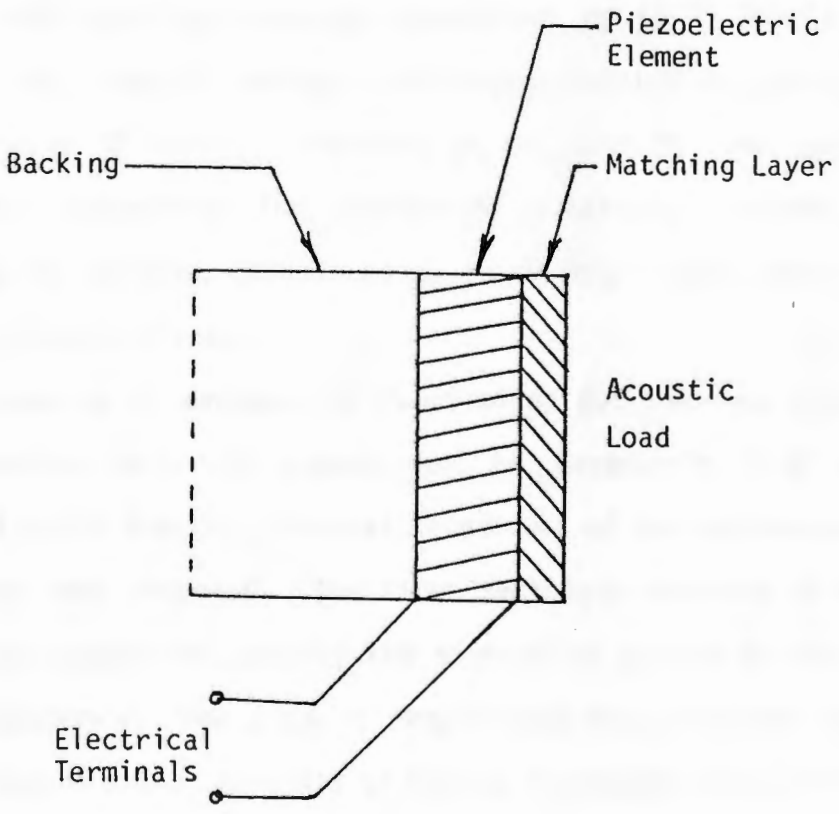

Figure 41. Physical Configuration of Transducers.

Another technique for manufacturing backings uses a composite of tungsten and polyvinyl powders that are combined in known ratios and hot pressed into a dense slug. Lees, et al. (Ref.20) has formulated composites with specified acoustic impedances up to 42 Mrayls., while Larson, et al. (Ref.21) using a different fabrication has obtained impedances up to 32 Mrayls. Rokhlin, et al. (Ref.22) has used metal-metal powder composites for fashioning backings. Using forming pressures up to 10 kbar, impedances up to 40 Mrayls have been obtained with tungsten-tin mixtures.

The majority of methods for fabricating backings use a tungsten-epoxy composite which is chosen due to tungsten's high acoustic impedance (Z = 104 Mrayls). Several techniques of making tungsten-epoxy backings have been proposed. The first technique consists of making a tungsten-epoxy paste and pouring the mixture in a mold containing the element. Impedances from 3 to 10 Mrayls have been obtained with this method. A second method consists of making a tungsten-epoxy mixture and forcing the excess epoxy out in tightly toleranced mold. Backing impedances from 10 to 14 Mrayls have been obtained using a 25 ksi pressure. A third method consists of centrifuging the tungsten-epoxy mixture to the desired packing ratio. Using a three inch arm spinning at 3400 rpm, impedances of 12 Mrayls have been achieved. Using the same technique Kossoff (Ref.14), reporting that the backing impedance depends upon the particle size, spinning speed and arm radius, has obtained impedances ranging from 6 to 16 Mrayls. A fourth method reported by Kino and Desilets (Ref.23) utilizes vacuum impregnation of epoxy into a compressed tungsten powder slug. Backing impedances from 12 to 40 Mrayls have been reported. Again this author has obtained an impedance

of 13 Mrayls using this technique; however, elaborate molds were not employed.

The matching layer may be fabricated in a number of ways. Usually a ceramic, glass or hard-curing epoxy is selected with the desired acoustic impedance obtained from the previously discussed matching formulas. If such a material is not available, a filler such as a metallic powder may be added. Careful attention must be made when a filled composite is employed as a matching layer, as losses in the composite could significantly affect the final transducer response. Once the material for the matching layer is obtained, the piece may be lapped to the desired quarter wavelength thickness.

General Construction Procedure

Four transducers have been constructed having different bandwidths and time responses. A lead metaniobate ceramic (Keramos, K-81) was selected for the study as a result of its high inherent damping and low acoustic impedance (Zx = 20 Mrayls). The elements were chosen to be one inch in diameter with a resonant frequency of 2.25 MHz. Several of the transducers were fabricated with an air backing (Zb = 0 Mrayls) or a high impedance backing (Zb = 18 Mrayls), while some had quarter wave matching layers (Zr = 3.0 Mrayls), as indicated in Table III.

The high impedance backing was fabricated from a tungsten-epoxy composite using a new technique called the forced impregnation technique. The major advantage of this method is that backings with high acoustic impedances can be reliably fabricated. In this method epoxy was impregnated into a slug of compressed tungsten powder in a mold. The mold assembly consisted of a steel cylinder whose inside

TABLE III

Matching Conditions of Test Transducers

Transducer	Backing Type	Matching Layer
# 1	Air	None
# 2	Air	Yes
# 3	High Impedance	None
# 4	High Impedance	Yes

diameter was equal to the element's diameter. The cylinder was placed magnetized, polished steel plate. A tungsten powder (GTE Sylvania Corp., M-55) was poured into the mold and compressed with a 50 ksi ram pressure. An epoxy that cured to a tough resilient gel (Emerson & Cuming, Eccogel 1265) was chosen due to its high acoustical losses. The epoxy was poured into the mold containing the compressed tungsten powder. An O-ring was inserted into the mold and the epoxy was impregnated into the tungsten using a ram force of 100 to 300 pounds. When the tungsten slug was saturated with epoxy, as evidenced by seepage from the base plate, the load was released, the O-ring removed and the excess epoxy gently wiped from the top of the mixture. A ram pressure of 25 ksi was then slowly applied to the mixture and held at that pressure for three minutes at 200°F. Afterwards the base plate was removed carefully, so as not to disturb the tungsten-epoxy composite. The backing was then carefully forced into a fiberglass retaining ring having the transducer element already epoxied in place. The element-ring and backing assembly was clamped and placed into an oven at 200°F for four hours to allow the backing to cure in place. Once completed,

the backing had an impedance of 18 Mrayls.

The air-backed transducers required a different fabrication technique. As they would be used in water, the element's back had to be encapsulated such that the element would essentially see an air load. This was accomplished by placing several pieces of cork sheet cut to the diameter of the element and snuggly placed in contact with the element. Since the impedance of cork (Z = 0.1 Mrayls) was much lower than that of the element (Z = 20 Mrayls), the element would see an air load. A high viscosity RTV compound was used to encapsulate the cork into place. During the repair on one of the transducers, it was found that no RTV had seeped onto the element through the cork and that the element did in fact see an air load.

To match the element to the water load, a matching layer impedance of 3.6 Mrayls was obtained using the binomial transformer formula discussed in Chapter II. For the matching layers a low viscosity epoxy (Mereco, Metacast 401) was selected having an impedance of 3.0 Mrayls. The uncured epoxy was evacuated to remove air bubbles entrapped during mixing, poured directly onto the element and allowed to cure at 150°F for one hour. The transducer matching layer was then lapped to a thickness of 0.011 inches, the quarter wavelength thickness at the element's resonant frequency. The thickness of the layer was verified using standard ultrasonic pulse-echo methods using a 15 MHz, 1/4 inch diameter delay line probe.

The electrical leads were soldered to each side of the element using a silver plated ribbon wire. The wire (0.015" wide by 0.001" thick) was first tinned with solder. The wire was then soldered to the element using a flux that allowed momentary contact of the soldering

iron to the element. The electrical leads were connected to a coaxial cable (Belden, RG-174) and imbedded with a potting epoxy to ensure electrical isolation.

Special Fabrication Considerations

Different backing impedances can be obtained by varying the size of the tungsten particles and the compressive pressures applied to the backing composite during fabrication. Backing impedances ranging from 3 to 23 Mrayls can be realistically obtained by varying these two factors using the Eccogel 1265 epoxy. Higher impedances can be obtained if a rigid curing epoxy is used in place; however, the losses in the backing are only on the order of 8 dB/cm. Using the Eccogel 1265 or an equivalent epoxy, losses of 50 dB/cm can be easily obtained for the backing described (Zb = 18 Mrayls).

A word of mention should be made concerning the determination of the backing's acoustic impedance. Generally the density and sound velocity are measured and then multiplied together. However, when very lossy backings are employed, the sound velocity measurement is not an easy one to make. The acoustic impedance of interest is the backing impedance that the element would see in actual operation, ie., the backing's "reflective" impedance. This measurement can be obtained using standard ultrasonic pulse-echo techniques. Here a high frequency delay line probe is used to look at the signal from the backing-element interface from the front face (no matching layer) and compared with the signal from an air-element interface. The difference in signal amplitude and phase determines the reflection coefficient of the element-backing interface. Since the impedance of the element is known,

the backing's "reflective" impedance can readily be obtained. It is this impedance that the author has used to determine the backing impedances using the methods discussed.

In reference to the preparation of the piezoelectric element for bonding, it has been suggested (Ref.16) that it be cleaned in an organic solvent, heated for several hours to remove any absorbed solvents and assembled in a dust free, laminar flow hood. While this procedure is good practice, the extreme clean conditions are not completely necessary. It has been found that an adequate cleaning procedure consists of the removal of the oxide coating on the electrode surface with a hard eraser followed by a quick rinse in acetone. This method assures a thin, strong bond line.

Heat and pressure have an effect of the piezoelectric element. A different lead metaniobate element (Keramos, K-83) was held at 200°F for four hours, the normal cure for Eccogel 1265 at that temperature. Once the element had cooled to room temperature, the element had lost 5 dB in loop gain. The ceramic had a relatively low Curie temperature of 450°F. The element was then loaded with a 25 ksi ram pressure and an additional loss of 2 dB was noted. The element also responded with excessive ringing in its time response, possibly due to microcracks in the ceramic.

The attachment of the electrical leads to the element also requires special consideration. The connection can be accomplished either by a hot solder joint or with conductive epoxy. When hot soldering, a small tipped soldering iron should be used in conjuction with a temperature control to minimize the amount of localized heating on the element. When using conductive epoxy, it has been noted that in

some cases the joint may burn out causing the connection to be broken. This phenomenon generally occurs with epoxies having a low silver content or if the epoxy is used beyond the expiration date.

Chapter IV

EXPERIMENTAL RESULTS OF TRANSDUCERS

In the previous discussions a model of an ultrasonic transducer was described that incorporated both transducer dynamics and the acoustic field characteristics. The transducer response was analyzed for various reflectors in the acoustic field. A set of transducers was then built with different matching conditions. In the present discussion the analytical and experimental responses of these transducers are compared. After these responses have been studied, pulsed acoustic measurements will be made on each transducer for reflectors placed at different points in the acoustic field.

Transducer Responses

In Chapter II an equivalent circuit for a thickness expander transducer was described for analyzing the transmit and receive characteristics of the transducer separately. The same circuit is used to obtain the pulse-echo response of the transducer in the form of a two-way voltage transfer function. The frequency response is obtained from the magnitude of the transfer function, while inverse Fourier techniques are used to obtain the time response of the transducer. Experimentally the pulse-echo response of the transducer can be obtained by impulsively exciting the transducer and reflecting the acoustic energy off a water/air interface at normal incidence. The pulse-echo time response of the tranducer is obtained from the received voltage pulse. This pulse can then be spectrum analyzed to obtain the frequency characteristics of the transducer.

The experimental set up for characterizing the ultrasonic transducers is shown in Figure 42. The ultrasonic equipment consists of a pulser and a receiver (Metrotek MP203, MR101) to obtain the time response that is viewed on an oscilloscope (Tektronix 7704A). The time signal is then windowed by a stepless gate (Metrotek MG701) and input into a spectrum analyzer (Tektronix 7L12) that provides the frequency response. The transducer under evaluation is mounted in a water tank to an adjustable carriage system such that the transducer will radiate off the water/air interface as shown in Figure 43. Since the total energy in any cross-sectional plane of the transducer nearfield is constant, the water path distance must be less than the nearfield length to obtain a valid characterization. The nearfield length, N_o ,is the distance from the transducer of maximum pressure where the strong pressure fluctuations in the nearfield yield to a more uniform pressure response in the farfield and is defined as

$$N_o = \frac{D^2}{4\lambda} \tag{4}$$

where D is the diameter of the transducer element and λ is the wavelength in the acoustic medium. The water path distance is chosen to be 90% of the nearfield length. The transducer is normalized to the water/air interface to obtain maximum signal return. The transducer is excited with a spike pulse having a peak voltage of -100 volts and a 10 nanosecond rise time. Both the pulser and receiver have input impedances of 50 ohms.

Using this arrangement the pulse-echo responses of the transducers have been obtained and compared to the analytical responses from the

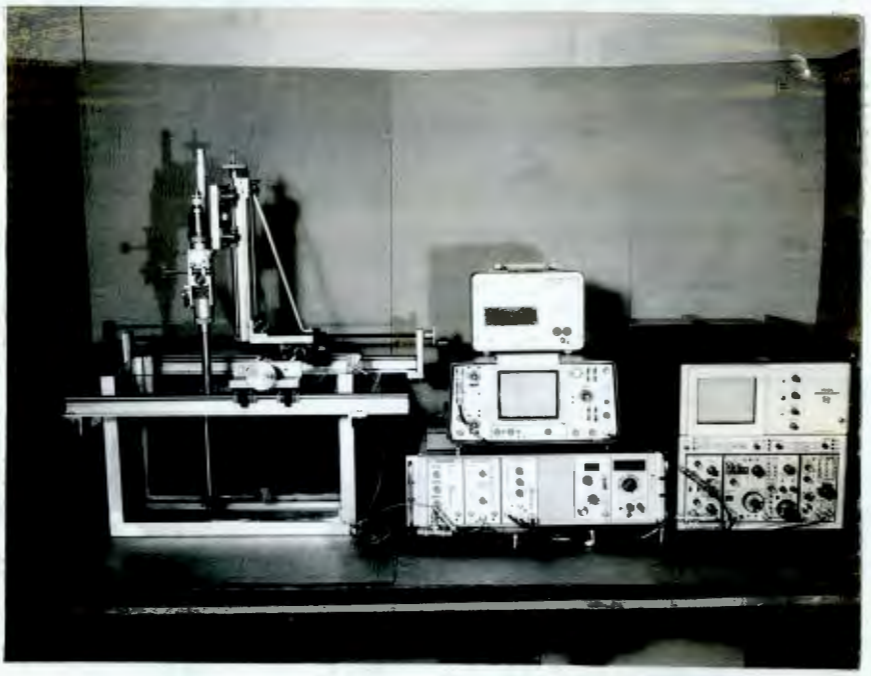

Figure 42. Experiment test equipment.

Figure 43. Experimental test setup.

model. For each experimental characterization the ultrasonic settings were identically maintained. The results are presented in the following figures and summarized in Table IV using the four performance parameters discussed in Chapter II for comparison.

TABLE IV

Comparison of Analytical and Experimental Transducer Responses

Transducer Number	Response Type	Center Frequency (MHz)	Bandwidth (%)	Loop Gain (dB)	Damping Factor (½cycles)
1	Anal	2.20	8.0	-44.4	21
	Exp	2.28	12.7	-46.4	17
2	Anal	2.11	25.0	-39.3	8
	Exp	2.17	34.1	-37.4	8
3	Anal	1.63	124.3	-58.3	2
	Exp	2.00	70.0	-58.8	4
4	Anal	1.85	85.7	-52.1	3
	Exp	2.18	56.0	-51.4	4

In Figure 44 the analytical pulse-echo response for transducer #1 is presented in three plots. First, the time response is presented as the impulse response of the transducer operating in a pulse echo mode. Second, the frequency spectrum is plotted as the magnitude of the voltage transfer function with the frequency normalized to the transducer element's resonant frequency. The last plot presented is the complex electrical input impedance and is also normalized to the

DISTRIBUTED PHARMETER MODEL

PIEZOELECTRIC ELEMENT PARAMETERS (MKS)

FREQUENCY = 2.25 MHZ

DIAMETER = 25.40 MM

DENSITY = 6200.

VELOCITY = 3302.

DIELECTRIC CONSTANT = 300.

ELECTROMECHANICAL COUPLING COEFF. = 0.43

BACKING IMPEDANCE = 0.0 -

RADIATION IMPEDANCE = 1.5

CABLE CAPACITANCE (PF) = 560.

CENTER FREQUENCY = 2.20 MHZ

PEAK INSERTION GAIN = -0.4 DB

TOTAL POWER GAIN = 77.4 DB

BANDWIDTH (-6 DB) = 8.0 %

SPECTRUM SYMMETRY DIFF.(-12 DB) = 100.0 %

SPECTRUM SYMMETRY DIFF.(-20 DB) = 100.0 %

DAMPING = 21.HALF-CYCLES

LOOP GAIN = -44.4 DB

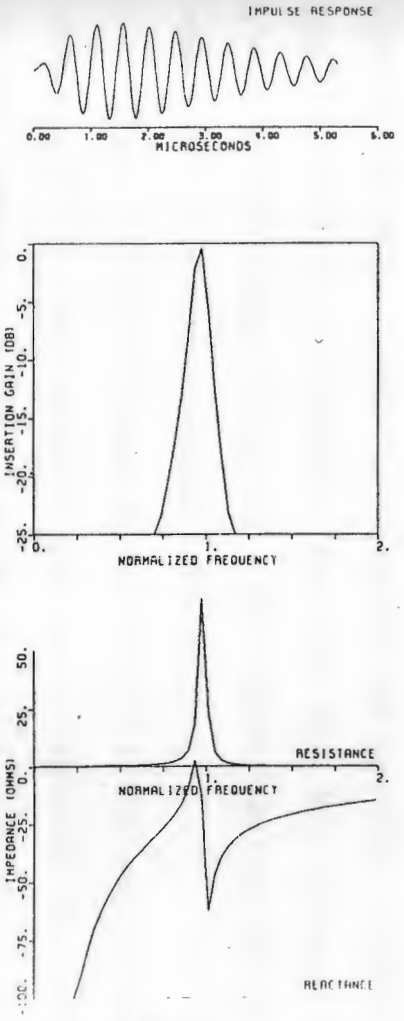

Figure 44. Transducer #1 analytical response.

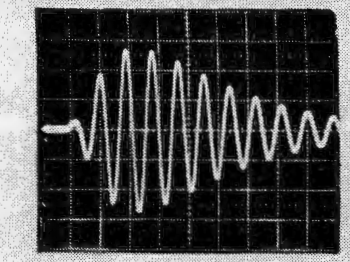

(a) RF waveform (0.2v/ Vdiv, 0.5μsec/ Hdiv).

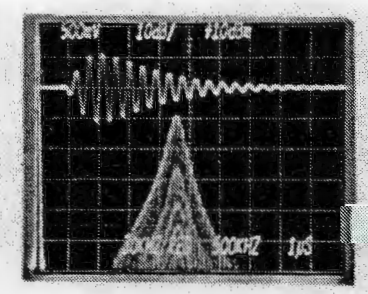

(b) Spectrum analysis.

Figure 45. Transducer #1 experimental response.

fundamental frequency. This transducer represents a piezoelectric element that is air-backed without a matching layer. It is noted that the element response exhibits a long pulse length of 10.5 cycles with a very narrow bandwidth of 8%. The experimental response of the same transducer in Figure 45 shows good agreement with the analytical results. For purposes of completeness, the electrical input impedance of the transducer would have been measured; however, since the appropriate equipment was not available, the measurement was not made.

The analytical and experimental responses for transducer #2 are given in Figures 46 and 47, respectively. The matching conditions on this transducer correspond to an unbacked element with a quarter wavelength epoxy matching layer. In this case the matching layer shortens the pulse length to 4 cycles and provides a corresponding threefold increase in bandwidth. The layer also has increased the loop gain of the transducer element by 5 dB. Again there is good agreement between the analytical and experimental results.

If the transducer element is now matched solely on the back of the element without a front matching layer as in transducer #3, a completely different response is noted. Figures 48 and 49 give the analytical and experimental responses for this case. The pulse length of the transducer has dramatically decreased compared to the unbacked cases, while the bandwidth has showed a corresponding increase as expected. Moreover, the loop gain decreased 14 dB. It is noted that the modeled results deviate from the measured results, particularly for the center frequency and bandwidth measurements. This disagreement is thought to be due to the excitation of other modes of vibration in the piezoelectric element. The model used here is valid only for one

DISTRIBUTED PARAMETER MODEL

PIEZOELECTRIC ELEMENT PARAMETERS (MKS)

FREQUENCY = 2.25 MHZ

DIAMETER = 25.40 MM

DENSITY = 8200.

VELOCITY = 3302.

DIELECTRIC CONSTANT = 300.

ELECTROMECHANICAL COUPLING COEFF. = 0.43

FRONT MATCHING LAYER PARAMETERS

1. DENSITY = 1184.

VELOCITY = 2540.

THICKNESS = 0.28 MM

BACKING IMPEDANCE = 0.0

RADIATION IMPEDANCE = 1.5

CABLE CAPACITANCE (PF) = 560.

CENTER FREQUENCY = 2.11 MHZ

PEAK INSERTION GAIN = -2.9 DB

TOTAL POWER GAIN = 80.0 DB

BANDWIDTH (-6 DB) = 25.0 %

SPECTRUM SYMMETRY DIFF. (-12 DB) = 0.0 %

SPECTRUM SYMMETRY DIFF. (-20 DB) = 33.3 %

DAMPING = 8. HALF-CYCLES

LOOP GAIN = -39.3 DB

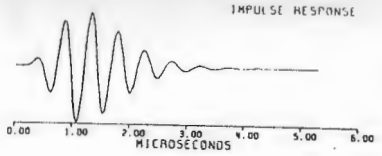

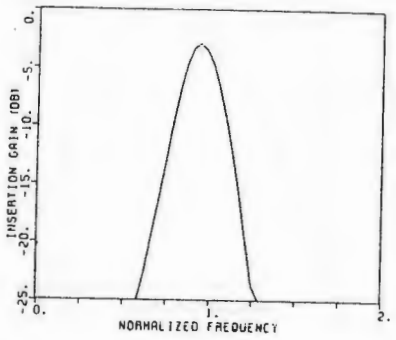

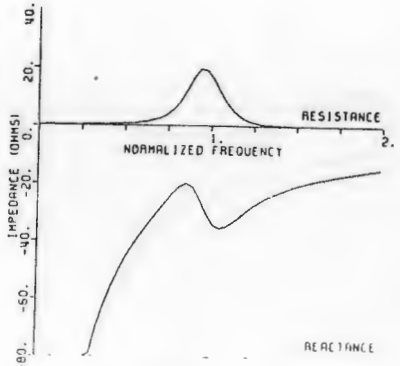

Figure 46. Transducer #2 analytical response.

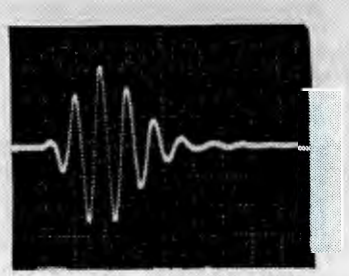

(a) RF waveform (0.5v/ Vdiv, 0.5usec/ Hdiv).

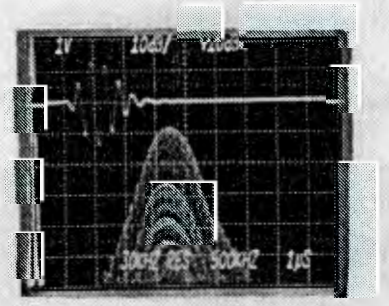

(b) Spectrum analysis.

Figure 47. Transducer #2 experimental response.

DISTRIBUTED PARAMETER MODEL

PIEZOELECTRIC ELEMENT PARAMETERS (MKS)

FREQUENCY = 2.25 MHZ

DIAMETER = 25.40 MM

DENSITY = 6200.

VELOCITY = 3302.

DIELECTRIC CONSTANT = 300.

ELECTROMECHANICAL COUPLING COEFF. = 0.43

BACKING IMPEDANCE = 18.0

RADIATION IMPEDANCE = 1.5

CABLE CAPACITANCE (PF) = 560.

CENTER FREQUENCY = 1.63 MHZ

PEAK INSERTION GAIN = -31.3 DB

TOTAL POWER GAIN = 33.6 DB

BANDWIDTH (-6 DB) = 124.3%

SPECTRUM SYMMETRY DIFF. (-12 DB) = 26.1 %

SPECTRUM SYMMETRY DIFF. (-20 DB) = 52.2 %

DAMPING = 2. HALF-CYCLES

LOOP GAIN = -58.5 DB

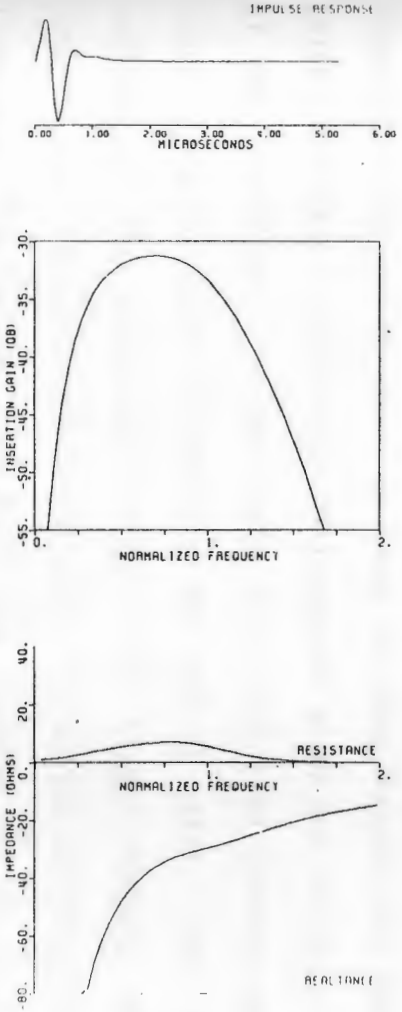

Figure 48. Transducer #3 analytical response.

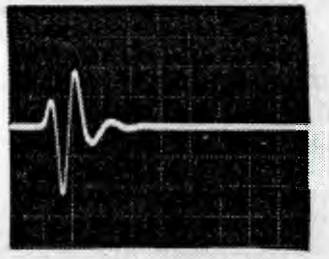

(a) RF waveform (0.05v/ Vdiv, 0.5usec/ Hdiv).

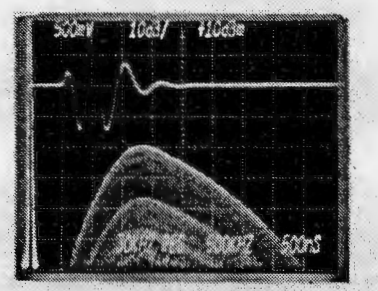

(b) Spectrum analysis.

Figure 49. Transducer #3 experimental response.

dimensional vibrations in the transducer and consequently cannot take other modes into account.

Finally, consider the responses for transducer #4 shown in Figures 50 and 51. The transducer has a high impedance backing as in the previous case, but this time a front matching layer has been added. The transducer still maintains a short pulse length, while the loop gain has increased 6 dB. Again the bandwidth and center frequency measurements do not agree completely with the analytical results.

During the course of the experiment, several spurious artifacts were noted in the time responses of the transducers. These pulses, as shown in Figure 52, occurred shortly after the transducer had been pulsed and were not due to reflectors in the acoustic field. For transducers #1 and #3 where no front matching layers were employed, a pulse consistently occurred 16 microseconds after the initial excitation of the transducer. It was noted that this time corresponds to the travel time for sound to travel a one inch in water. When the front surface of the transducer element was finger damped, the pulse disappeared. In an attempt to determine the origin of the pulse, a thin fiberglass ring having a one-half inch diameter was centered on each element face. The pulse shifted in time to eight microseconds after initial excitation, corresponding to a one-half inch travel in water. A three-quarter inch diameter ring was centered on the face of each transducer. The pulse artifact now shifted to twelve microseconds after initial excitation, corresponding to a three-quarter inch travel in water. It is now thought that these artifacts arise from radial modes being excited that originate at the transducer center, propagate radially outward to a reflecting surface such as an edge and return to

DISTRIBUTED PARAMETER MODEL

PIEZOELECTRIC ELEMENT PARAMETERS (MKS)

FREQUENCY = 2.25 MHZ

DIAMETER = 25.40 MM

DENSITY = 6200.

VELOCITY = 3302.

DIELECTRIC CONSTANT = 300.

ELECTROMECHANICAL COUPLING COEFF. = 0.43

FRONT MATCHING LAYER PARAMETERS

1. DENSITY = 1184.

VELOCITY = 2540.

THICKNESS = 0.28 MM

BACKING IMPEDANCE = 18.0

RADIATION IMPEDANCE = 1.5

CABLE CAPACITANCE (PF) = 560.

CENTER FREQUENCY = 1.85 MHZ

PEAK INSERTION GAIN = -23.9 DB

TOTAL POWER GAIN = 46.2 DB

BANDWIDTH (-6 DB) = 85.7 %

SPECTRUM SYMMETRY DIFF. (-12 DB) = 0.0 %

SPECTRUM SYMMETRY DIFF. (-20 DB) = 11.1 %

DAMPING = 3. HALF-CYCLES

LOOP GAIN = -52.1 DB

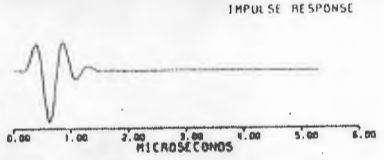

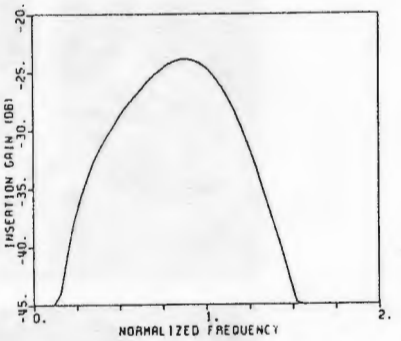

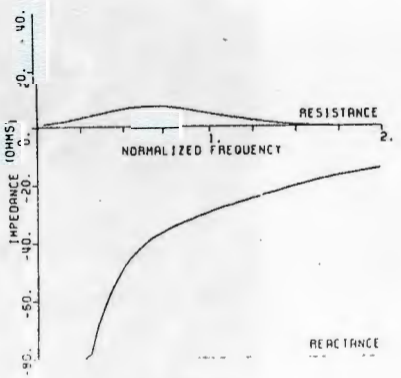

Figure 50. Transducer #4 analytical response.

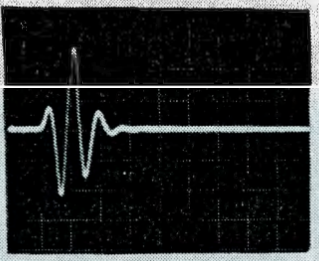

(a) RF waveform (0.1v/ Vdiv, 0.5μsec/ Hdiv).

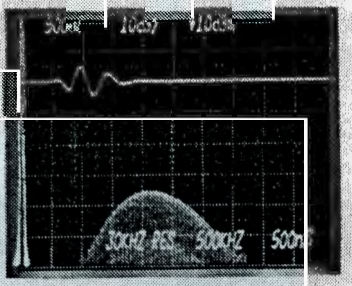

(b) Spectrum analysis.

Figure 51. Transducer #4 experimental response.

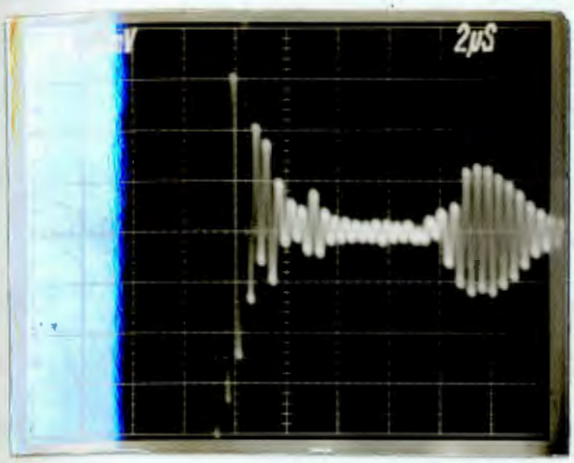

(a) Transducer #1
(no backing, no layer).

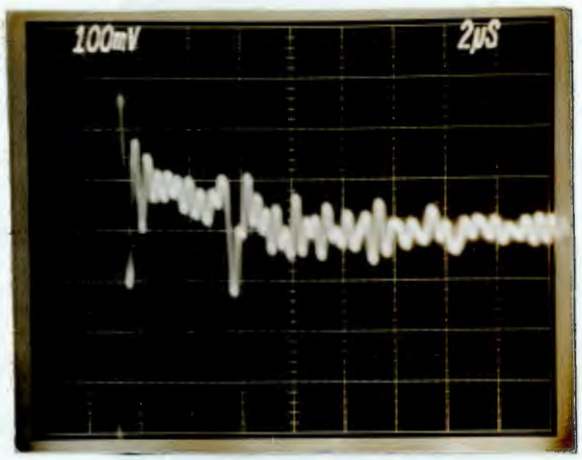

(b) Transducer #2
(no backing with layer).

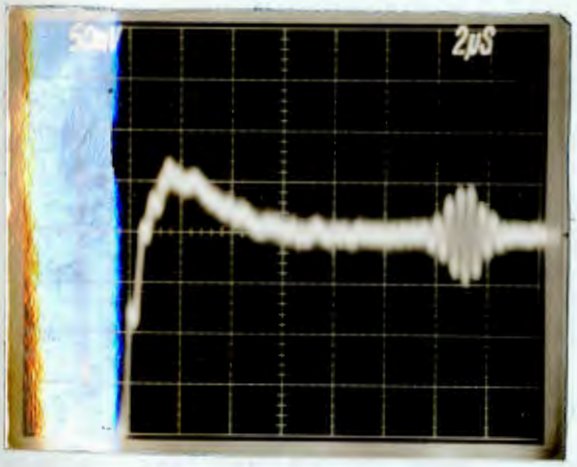

(c) Transducer #3
(backing, no layer).

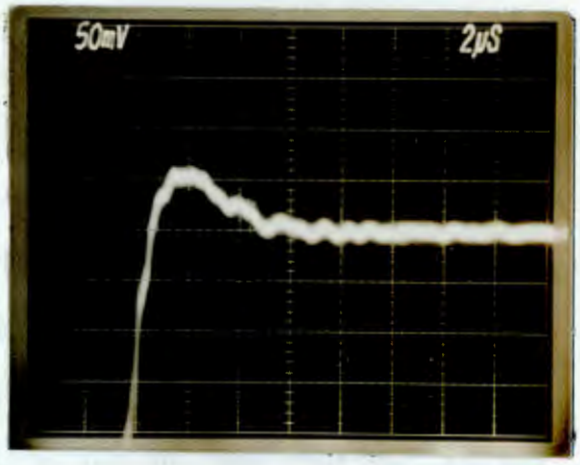

(d) Transducer #4
(backing with layer).

Figure 52. Time domain artifacts of transducers.

the center. The presence of a matching layer apparently serves to dampen out these pulses. It was also noted in each case that if the fiberglass ring was moved off center, the pulse would gradually disappear.

When matching layers were employed as in transducers #2 and #4, a different phenomenon was noted. When the transducer was unbacked as for #2, a spurious pulse occurred 7.5 microseconds out in time. In light of the previous discussion on radial modes, it was noted that this time corresponded to a one inch travel time in the ceramic element. If radial modes were being excited in the element, the presence of a backing should dampen out these vibrations. This appears to be the case for transducer #4 where the element is backed with a front matching layer. The response displays no acoustic artifacts.

Pulsed Acoustic Field Measurements

Having considered the effect of transducer construction methods on the pulse-echo response, the pulsed acoustic fields from these transducers are now investigated. The transducers are pulsed with a negative spike pulse have a peak voltage of -180 volts and a 10 nanosecond rise time. The internal impedances of the pulser and receiver are set to 50 ohms. The output of the receiver to the oscilloscope is also terminated into 50 ohms. A three-sixteenths inch diameter steel ball is chosen as the acoustic reflector. As the ball has a diameter corresponding to five wavelengths, it can be regarded as an idealized reflector. The transducer under evaluation is mounted on the carriage assembly and normalized to the tank bottom. The steel ball reflector is then placed off the tank bottom approximately one inch

(about 34 microseconds round trip). To provide a one-to-one comparison amongst the various measurements, the settings of the ultrasonic equipment are held constant for all transducers. For this study it is desired that spatial points be sampled in the acoustic nearfield. As the nearfield length for these transducers is nine inches, axial distances of two, four and eight inches from the transducer face are chosen. These distances correspond to z/a = 4, 8 and 16. Radial points corresponding to r/a = 0, 0.5 and 1.0 are chosen.

Consider now the pulse-echo responses from transducer #1 which corresponds to an unbacked element radiating directly into water. For the on-axis case shown in Figure 53 it is seen that the echo consists of a long, modulated pulse. Due to the inherently long pulse length of the transducer (3.7 microseconds from the characterization) and narrow bandwidth (13%), the pressure contributions from the transducer face and edges tend to merge together yielding a long acoustic pulse length. However, as the distance from the transducer is increased a shortening of pulse length is noted, as the differences in the time of arrivals between the face and edge pressures is decreased. The peak amplitude of of the signal also reaches a maximum at z/a = 16 where the field point is in the vicinity of the nearfield length. Note the additional pulse occurring approximately 7 microseconds after the initial excitation. For spatial points where r/a = 0.5 as in Figure 54, the responses appear to be quite similar for all three axial distances with the exception of small changes in peak amplitude. Again a small pulse, heretofore referred to as artifact "A", is noted 7 microseconds after excitation. In Figure 55 for field points along the edge of the transducer, the responses indicate pulses of similar length as for the case when r/a =

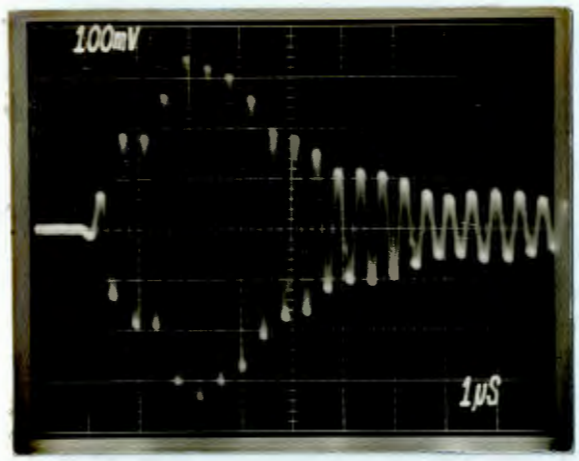

(a) Z/a = 4.

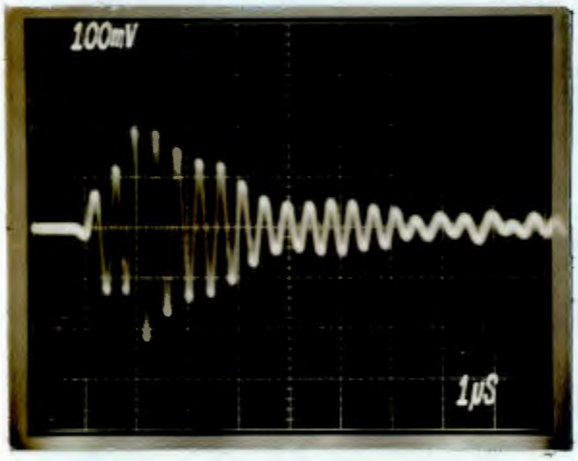

(b) Z/a = 8.

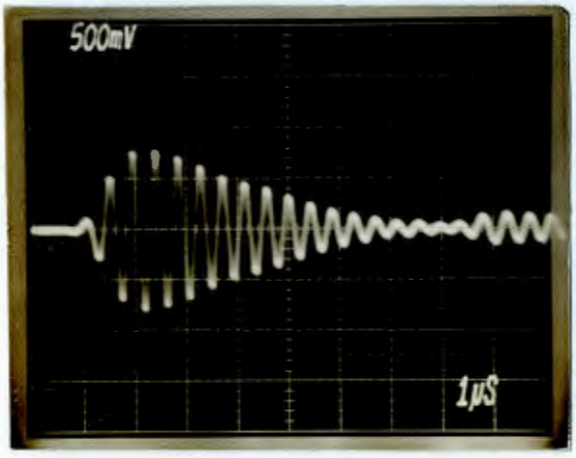

(c) Z/a = 16.

Figure 53. Acoustic transients from transducer #1 for r/a = 0.

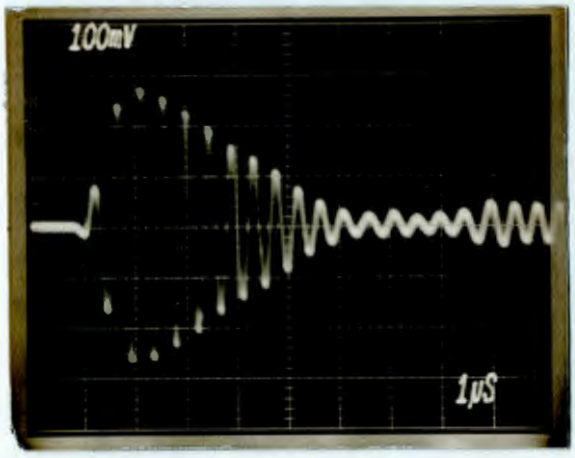

(a) Z/a = 4.

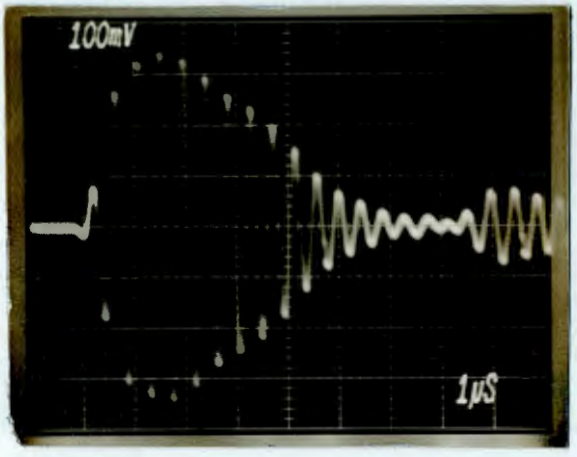

(b) Z/a = 8.

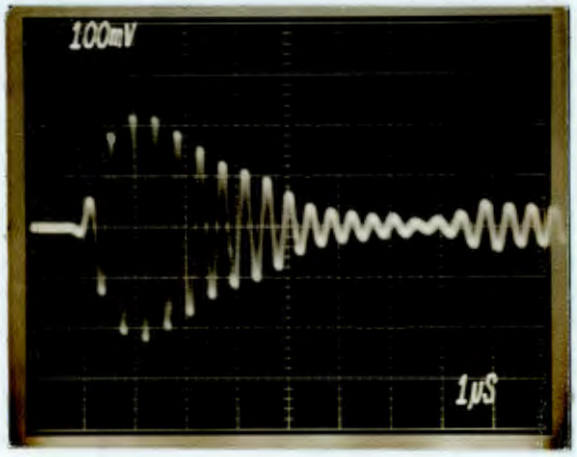

(c) Z/a = 16.

Figure 54. Acoustic transients from transducer #1 for r/a = 0.5.

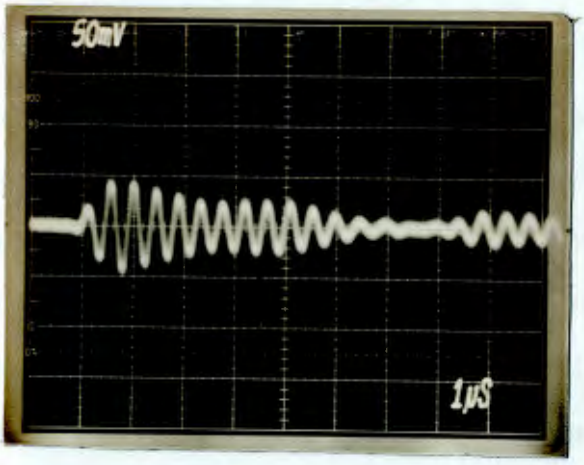

(a) Z/a = 4.

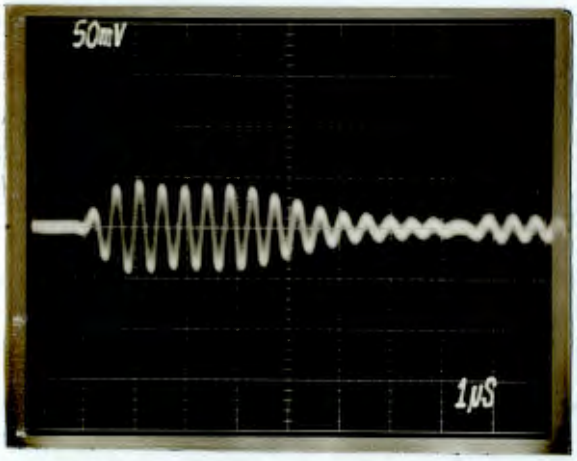

(b) Z/a = 8.

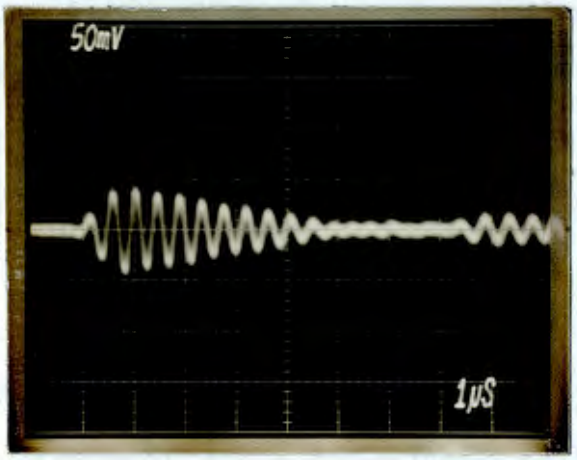

(c) Z/a =16.

Figure 55. Acoustic transients from transducer #1 for r/a = 1.0.

0.5. These pulses though have significantly decreased in amplitude.

The pulse-echo responses for transducer #2 are given in the next three figures. The matching conditions on this transducer correspond to an unbacked element with a quarter wavelength epoxy matching layer. This transducer had a pulse length 1.8 microseconds and a bandwidth of 34% from the characterization. In Figure 56 the responses from on-axis reflectors are given. When z/a equals 4 the echo consists of modulated pulse similar to the one from transducer #1; however, the length of the main pulse has decreased considerably. Again artifact A is noted. As the axial distance is increased to z/a = 8, the tail end of the main pulse trails off to zero amplitude where artifact A is encountered. Finally, when the reflector is 16 radii from the transducer, the main pulse has further decreased in length. However, another small pulse is located 3.5 microseconds after the initial excitation along with artifact A. For spatial points along r/a = 0.5 as shown in Figure 57, the responses are similar to those from transducer #1, the duration and amplitude of the main pulses are relatively constant. However, the small pulse occurring 3.5 microseconds, heretofore referred to as artifact "B", is noted along with artifact A. For field points along the edge of the transducer as shown Figure 58, the responses all have similar pulse lengths and lower amplitudes. Artifacts A and B are still present.

If the transducer is highly damped with a high impedance backing as with transducer #3, a dramatically different response is obtained. This transducer was characterized as having a pulse length of one microsecond and a 70% bandwidth. Figure 59 corresponds to the case when the reflector is placed along the axis of the transducer. It is noted

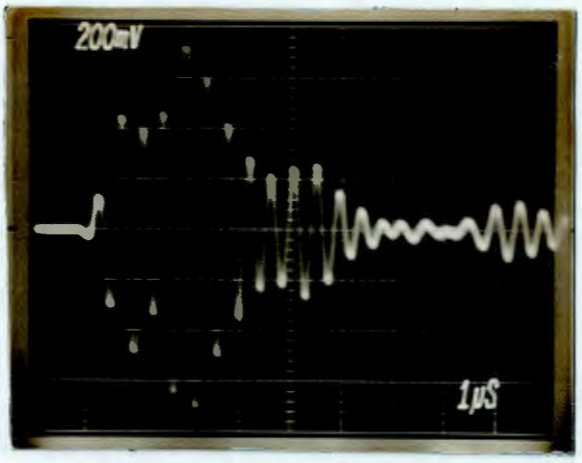

(a) Z/a = 4.

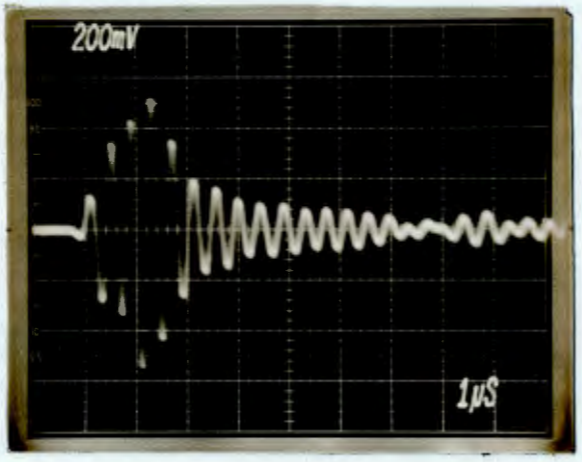

(b) Z/a = 8.

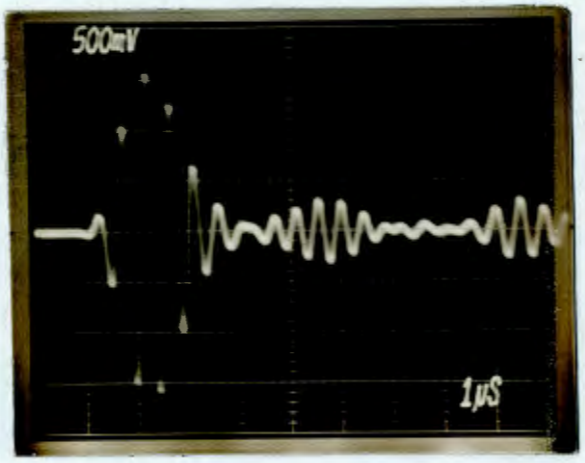

(c) Z/a = 16.

Figure 56. Acoustic transients from transducer #2 for r/a = 0.

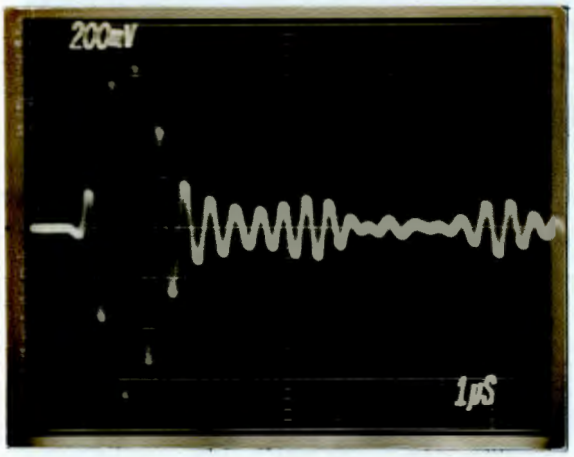

(a) Z/a = 4.

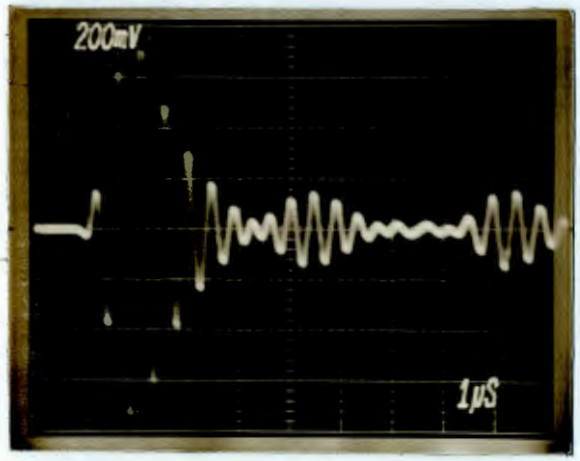

(b) Z/a = 8.

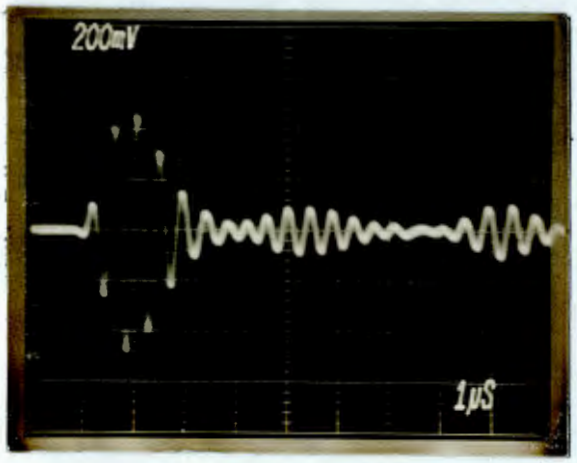

(c) Z/a = 16.

Figure 57. Acoustic transients from transducer #2 for r/a = 0.5.

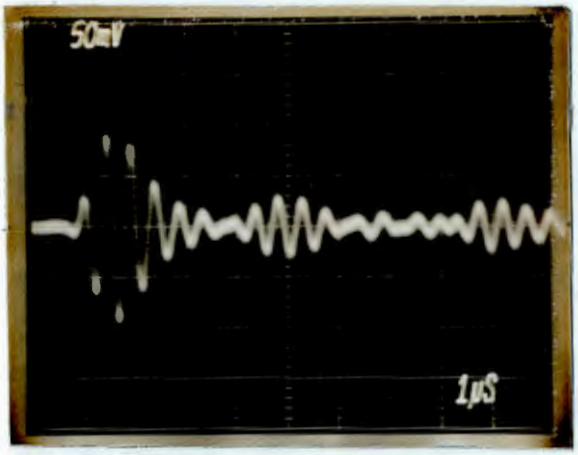

(a) Z/a = 4.

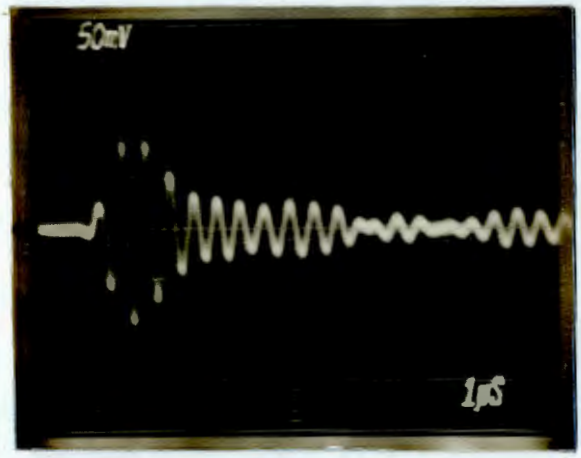

(b) Z/a = 8.

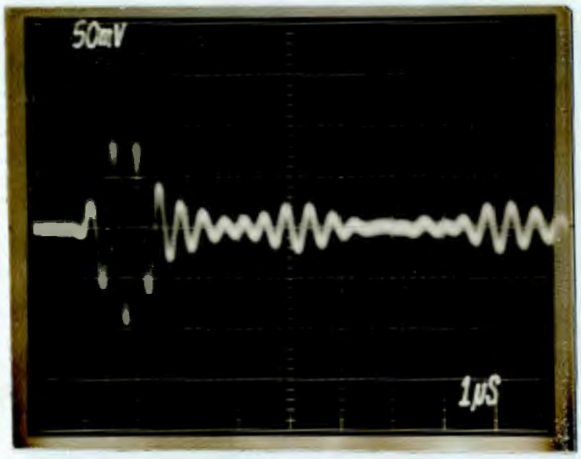

(c) Z/a = 16.

Figure 58. Acoustic transients from transducer #2 for r/a = 1.0.

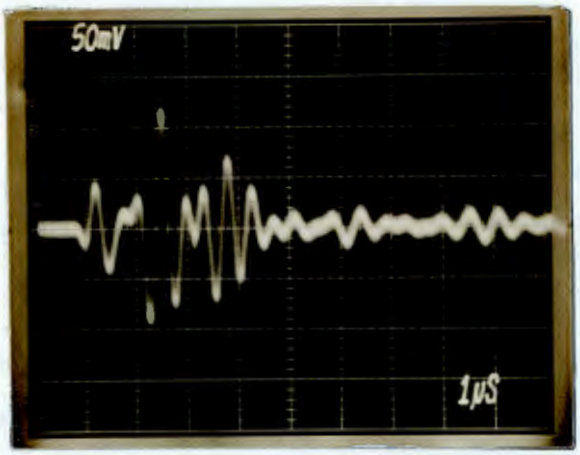

(a) Z/a = 4.

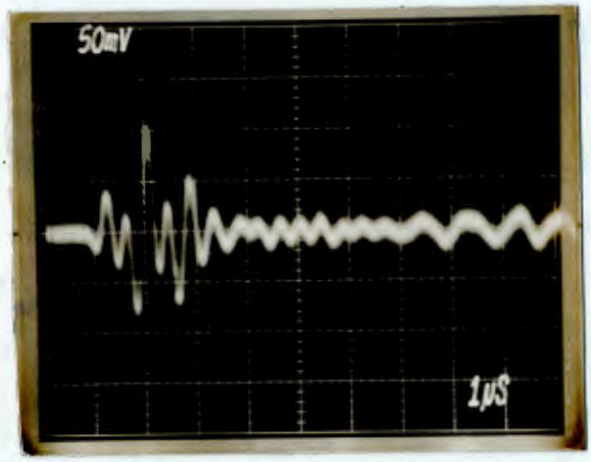

(b) Z/a = 8.

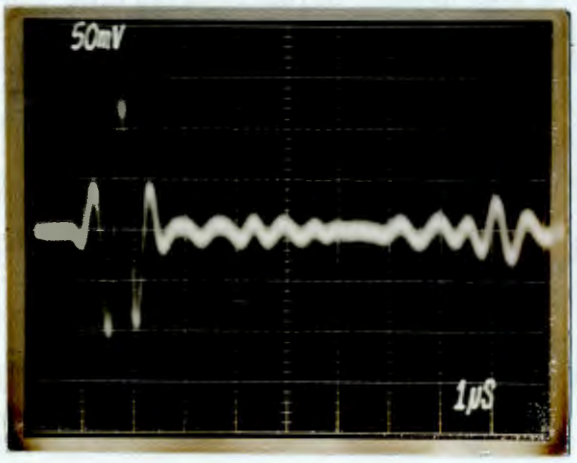

(c) Z/a = 16.

Figure 59. Acoustic transients from transducer # 3 for r/a = 0.

that the echo that was referred to as the main pulse for transducers #1 and 2 really consists of three distinct pulses for this field point. These pulse are replicas of the transmitted velocity pulse and are noted due to the highly damped nature of the transducer. As the axial distance increases, the multiple pulses merge together forming a single pulse. Again the peak signal amplitude occurs at z/a = 16 at the end of the nearfield. Artifact A is still present, while artifact B is gone. As the radial distance increases to r/a = 0.5 as in Figure 60, the initial pulse maintains a constant pulse length; however,the peak signal amplitudes for all axial distances are markedly lower. Remnants of artifact A are noted. For field points along the edge of the transducer shown in Figure 61, the signal amplitudes are very low and cannot be easily distinguished from the noise level.

Finally, consider the pulse-echo response from transducer #4. The matching conditions on this transducer correspond to a high impedance backing with a matching layer. This transducer was characterized as having a 0.9 microsecond pulse length and a 56% bandwidth. For the on-axis case shown in Figure 62, the three pulses noted in the previous transducer response for the same point are no longer distinctly separated and have a shorter composite length. As the axial distance is increased from the transducer, the pulse duration further decreases. Again note that artifact A is present in all three cases. In Figure 63 for radial distances equal to r/a = 0.5, the pulse-echo responses are all quite similar, as for the same points in transducer #3's responses, with the exception that artifact A is more pronounced. As the radial distance is increased to r/a = 1.0, the signal amplitudes shown in Figure 64 again are quite low.

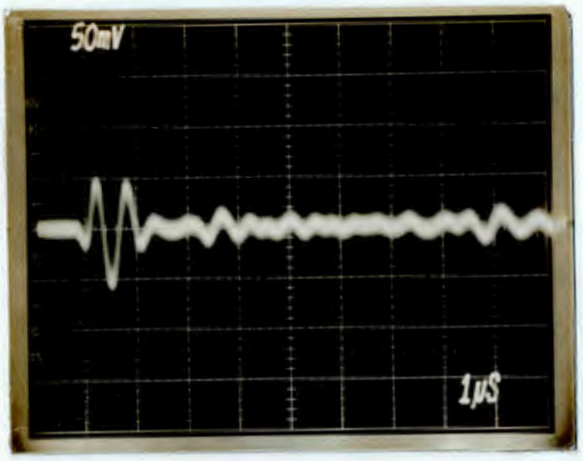

(a) Z/a = 4.

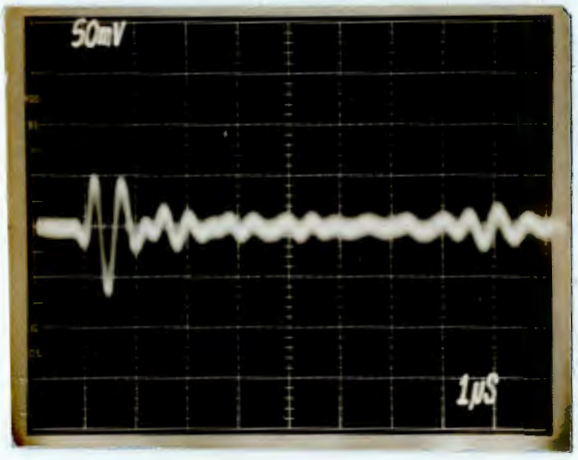

(b) Z/a = 8.

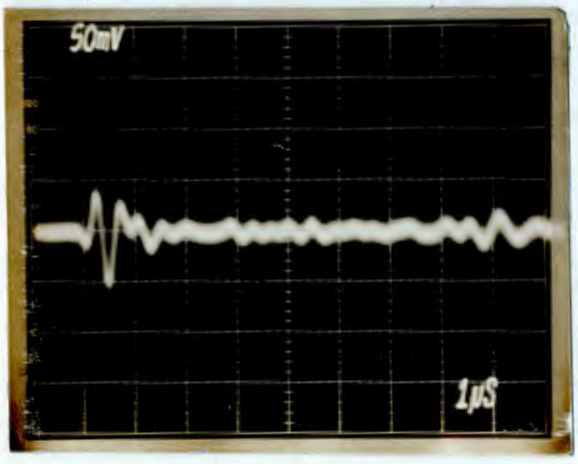

(c) Z/a = 16.

Figure 60. Acoustic transients from transducer #3 for r/a = 0.5.

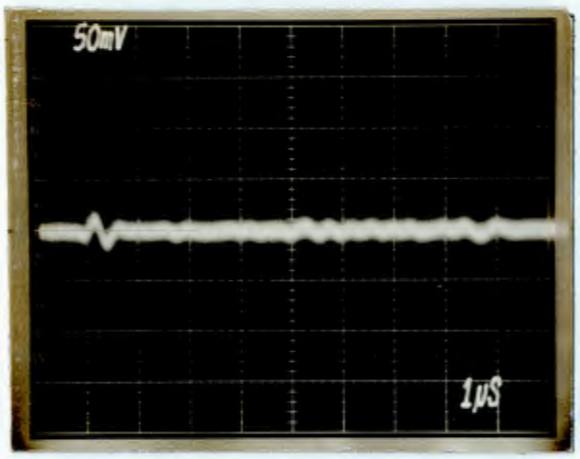

(a) Z/a = 4.

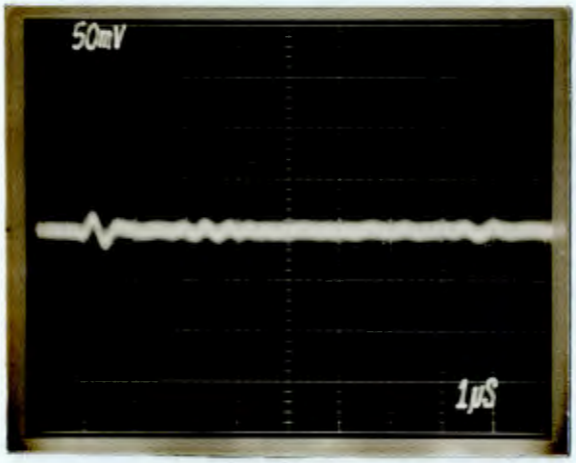

(b) Z/a = 8.

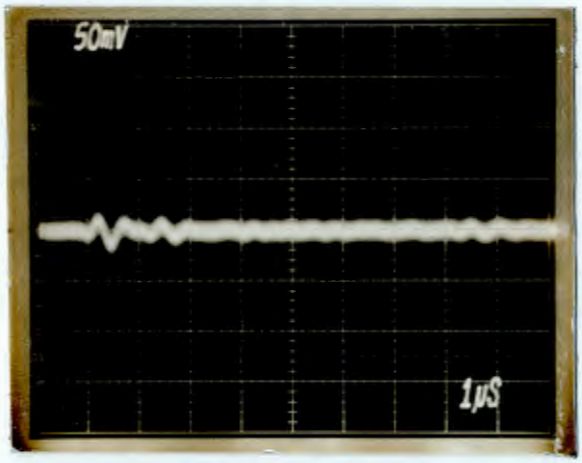

(c) Z/a =16.

Figure 61. Acoustic transients from transducer #3 for r/a = 1.0.

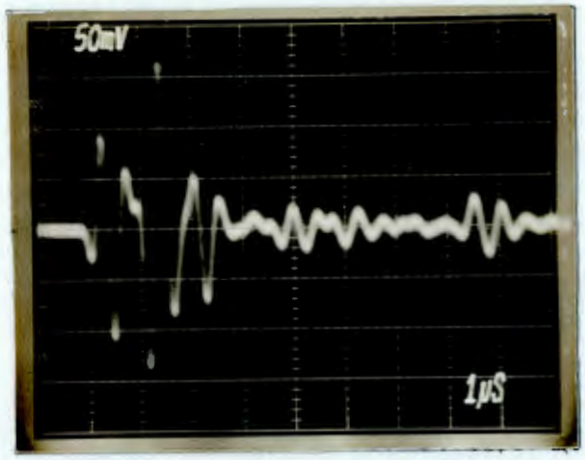

(a) Z/a = 4.

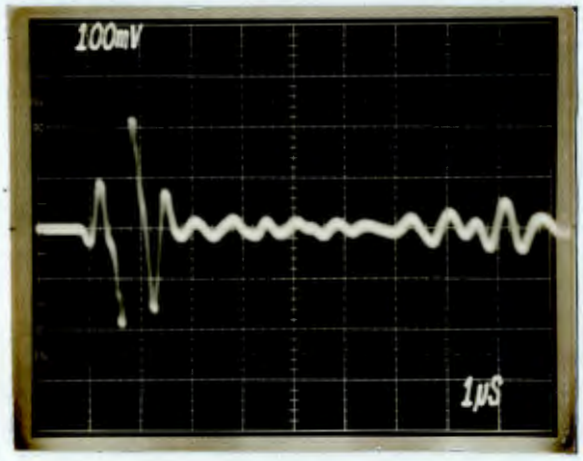

(b) Z/a = 8.

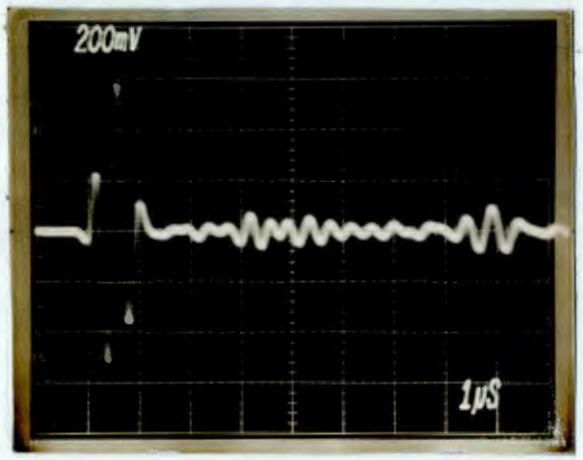

(c) Z/a = 16.

Figure 62. Acoustic transients from transducer #4 for r/a = 0.

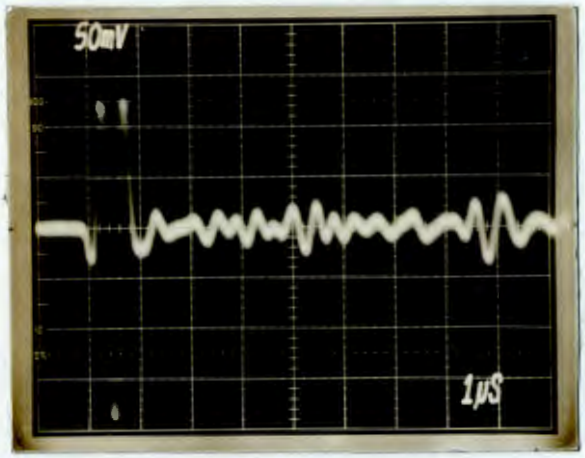

(a) Z/a = 4.

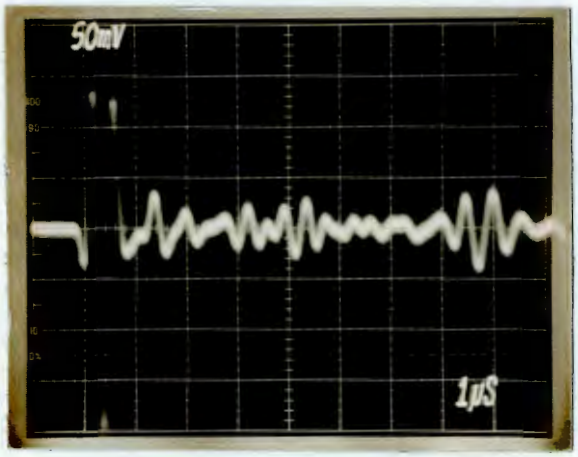

(b) Z/a = 8.

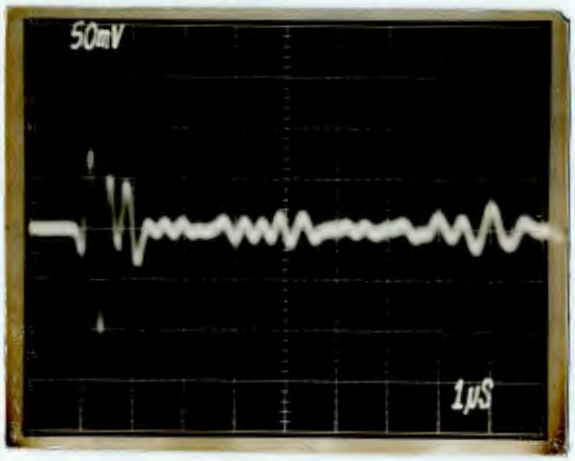

(c) Z/a = 16.

Figure 63. Acoustic transients from transducer #4 for r/a = 0.5.

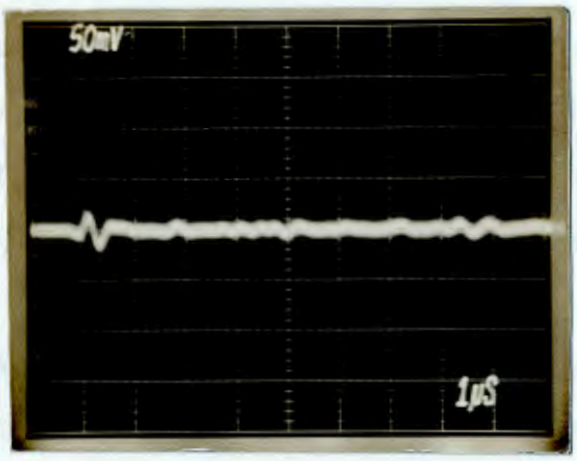

(a) Z/a = 4.

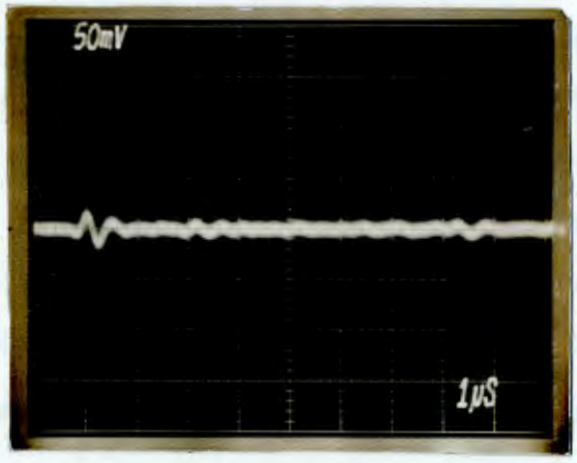

(b) Z/a = 8.

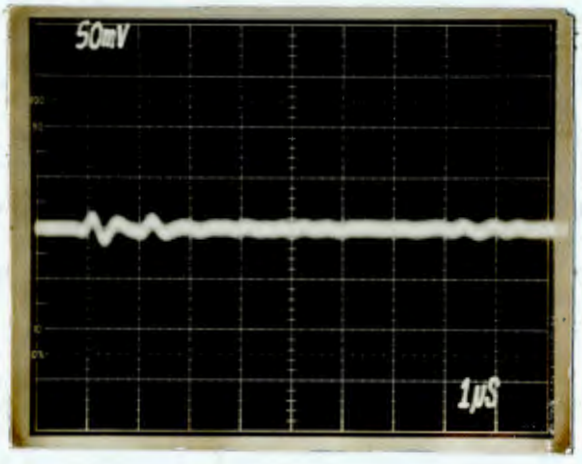

(c) Z/a = 16.

Figure 64. Acoustic transients from transducer #4 for r/a = 1.0.

A word of mention should be made on the artifacts encountered in the above responses. When the characterization of the transducers was discussed at the beginning of this chapter, several time domain artifacts were noted on the front end response just after the transducer had been pulsed. As the recover time of the pulser-transducer was quite large, many of the front end responses were masked. However, in the present case when the measurements were made well after the pulser had settled down, some heretofore unseen effects were revealed. It is thought that these artifacts arise from plate waves that are generated within the piezoelectric element. It should be recalled that the velocity in the element corresponds to 7 microseconds per inch of material, while all the transducers have diameters of one inch. Here waves could be generated at the edges of the element, propagate in the element diametrically to the opposite edge where they hit a boundary and are radiated into the water medium, hence artifact "A". For the case when the transducers are unbacked, as for transducers #1 and 2, waves are generated possibly in the center of the element, propagate radially in the element to the edge where a fixed boundary occurs and is radiated out into the medium, hence artifact "B". Where backings are employed, these waves are damped out since the backing provides some rigidity to the element.

CHAPTER V

PULSED ACOUSTIC FIELD FROM FOCUSED TRANSDUCERS

It has been shown both analytically and experimentally that acoustic transients originate from pressure waves radiating from the transducer face and edge. It has also been shown that for the case where broadband transducers are considered, these transients can manifest as individual acoustic pulses. It becomes immediately apparent that where high resolution is demanded from these ultrasonic transducers, the transient effects need to be minimized, if not eliminated. One of the ways of accomplishing this is to decrease the difference in arrival times from the transducer face and edges to the acoustic field points of interest. This can be achieved by modifying the acoustic field through transducer focusing.

Characteristics of Focused Transducers

Focused transducers have found use in medical ultrasonics and in ultrasonic testing of materials where increased lateral resolution and higher acoustic intensities are desired. Two types of focusing methods are usually considered: acoustic lenses and shaped-elements. The lenses generally are plano-concave in shape with the planar side in contact with the transducer. Commonly used materials include epoxy, acrylic and polystyrene. These lenses can be either cast or machined to the desired contour. The shaped-elements generally have coplanar surfaces, starting as a piezoelectric blank that is machined to the desired contour. The elements are then plated with electrodes and repoled to regain their piezoelectric nature.

Various aperture geometries have been considered in literature for transducer focusing. The three types that have received the most attention are spherical, conical and toroidal shapes and are illustrated in Figure 65. The spherical configuration is the most widely used one (Refs.24-27) and is defined by its radius of curvature, R. It concentrates acoustic energy to a point about the transducer axis and produces a small diameter acoustic beam over a short focal zone. The closer that the beam is focused to the transducer, the smaller the beam diameter proportionally becomes in that zone. However, before and after the focal zone, the beam rapidly diverges and exhibits large pressures flucuations, similar to those found in the nearfield of a conventional, unfocused transducer. The spherical configuration thus provides a narrow, high amplitude beam over a narrow focal range. It finds use only over a limited inspection zone.

Another type of geometry that has been considered is the conical shape (Refs.28-30) and is defined by an included cone angle, ϕ , as shown in Figure 65b. It distributes the energy along the transducer axis producing an acoustic beam having a focal zone longer than for the spherical configuration. An interesting feature of this acoustic field is that a small diameter beam is maintained over a long range. The usual rapid fluctuations of sound pressures outside of the focal zone are also suppressed. However, the energy that is spread along the axis results in the production of sidelobes.

To minimize the sidelobes resulting from the conical shape, another focusing geometry has been recently investigated (Refs.29-31), the toroidal configuration and is illustrated in Figure 65c. The shape is defined by a radius of curvature, R, whose center is offset from the

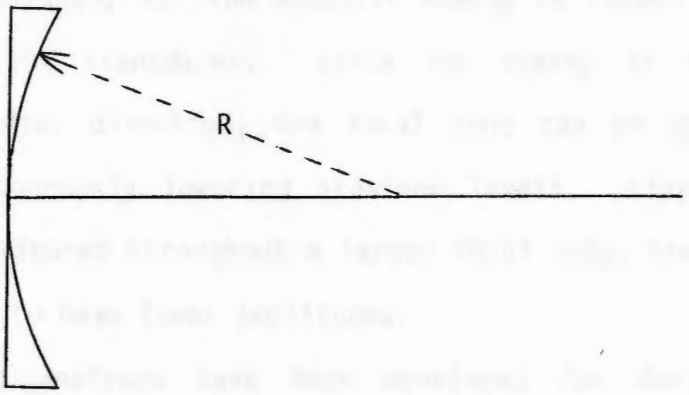

(a) Spherical

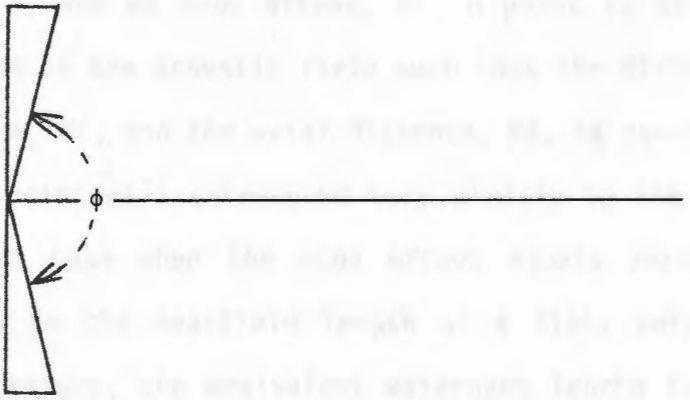

(b) Conical

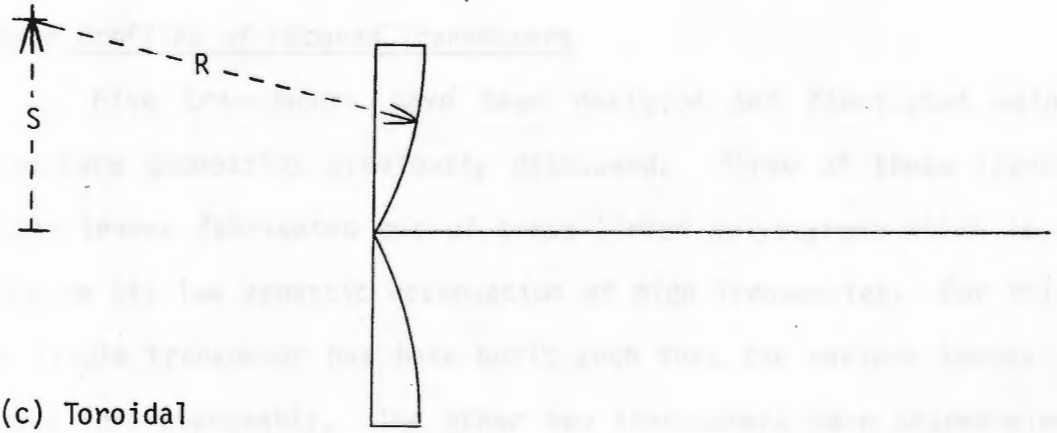

(c) Toroidal

Figure 65. Aperture Geometries For Transducer Focusing.

transducer axis by a distance, S. The acoustic energy is spread along the entire axis of the transducer. Since the energy is spread nonuniformly in the radial direction, the focal zone can be greatly increased, while simultaneously lowering sidelobe levels. Since the acoustic energy is distributed throughout a larger focal zone, the peak acoustic pressures tend to have lower amplitudes.

Although detailed analyses have been developed for designing focused transducers, an approximate diffraction approach will be utilized here. Figure 66 shows the edge view of a circular transducer surface having radius, a, and an edge offset, h. A point is selected along the transducer axis in the acoustic field such that the difference between the edge distance, P1, and the axial distance, P2, is equal to a half wavelength. This point will correspond very closely to the focal point. For the special case when the edge offset equals zero, the distance P2 corresponds to the nearfield length of a flat, unfocused transducer. For lens designs, the equivalent waterpath length for the edge offset is used in the design instead of the actual length.

Beam Profiles of Focused Transducers

Five transducers have been designed and fabricated using the aperture geometries previously discussed. Three of these transducers have lenses fabricated out of cross-linked polystyrene which is chosen due to its low acoustic attenuation of high frequencies. For this case a single transducer has been built such that the various lenses can be used interchangeably. The other two transducers have shaped-elements: spherical and conical. The toroidal shaped-element was not characterized due to difficulties encountered during manufacture. The

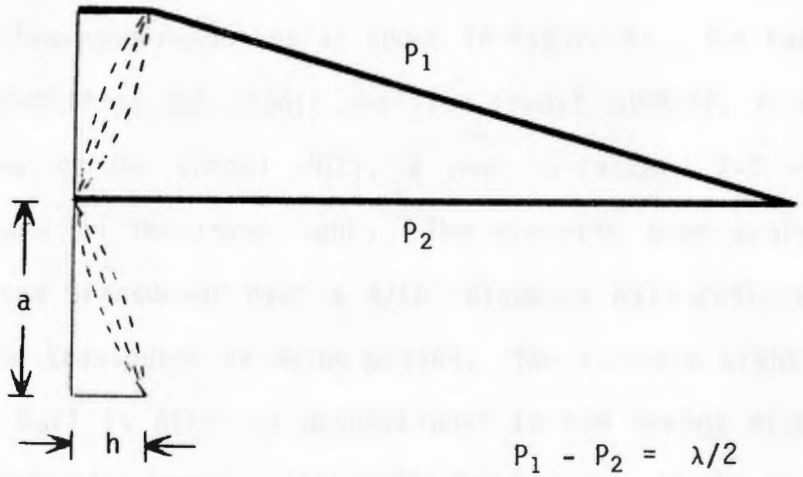

Figure 66. Configuration For Focusing Design.

transducers for this study were chosen to have diameters of 1.5" and resonant frequencies of 3.5 MHz, yielding a nearfield length of 34". Each transducer was designed to have a focal distance equal to ten percent of the nearfield length, resulting in a very sharply focused acoustic beam. A low impedance tungsten-epoxy backing was poured onto the elements due to the fragile nature of the shaped-elements, while an epoxy matching layer was used on the front.

To determine the focusing characteristics of these transducers, an apparatus was developed for profiling the acoustic beams based upon their pulse-echo responses as shown in Figure 67. The test bed consists of a Panametrics ultrasonic analyzer (Model 5052UA), Trienco transducer profiling bridge (Model 701), a Hewlett-Packard X-Y recorder (Model 7015B) and an immersion tank. The acoustic beam profile is made by moving the transducer over a 3/16" diameter ball reflector in the tank while the transducer is being pulsed. The acoustic signal that reflects off the ball is directly proportional to the energy distributed across the ultrasonic beam. The reflected signal is then received, peak detected and input to the X-Y recorder. The resulting profile yields a relative intensity plot laterally across the sound beam for a given distance from the transducer.

Utilizing the apparatus, acoustic beam profiles for the five transducers have been obtained. The parameters that are measured from the profiles include focal depth, depth-of-field and beam diameter at focus. The focal depth corresponds to the distance from the transducer where the peak amplitude response is obtained. The depth-of-field is determined by moving axially on either side of the focus until the amplitude is 6 dB down (1/2 echo amplitude) from the focal amplitude.

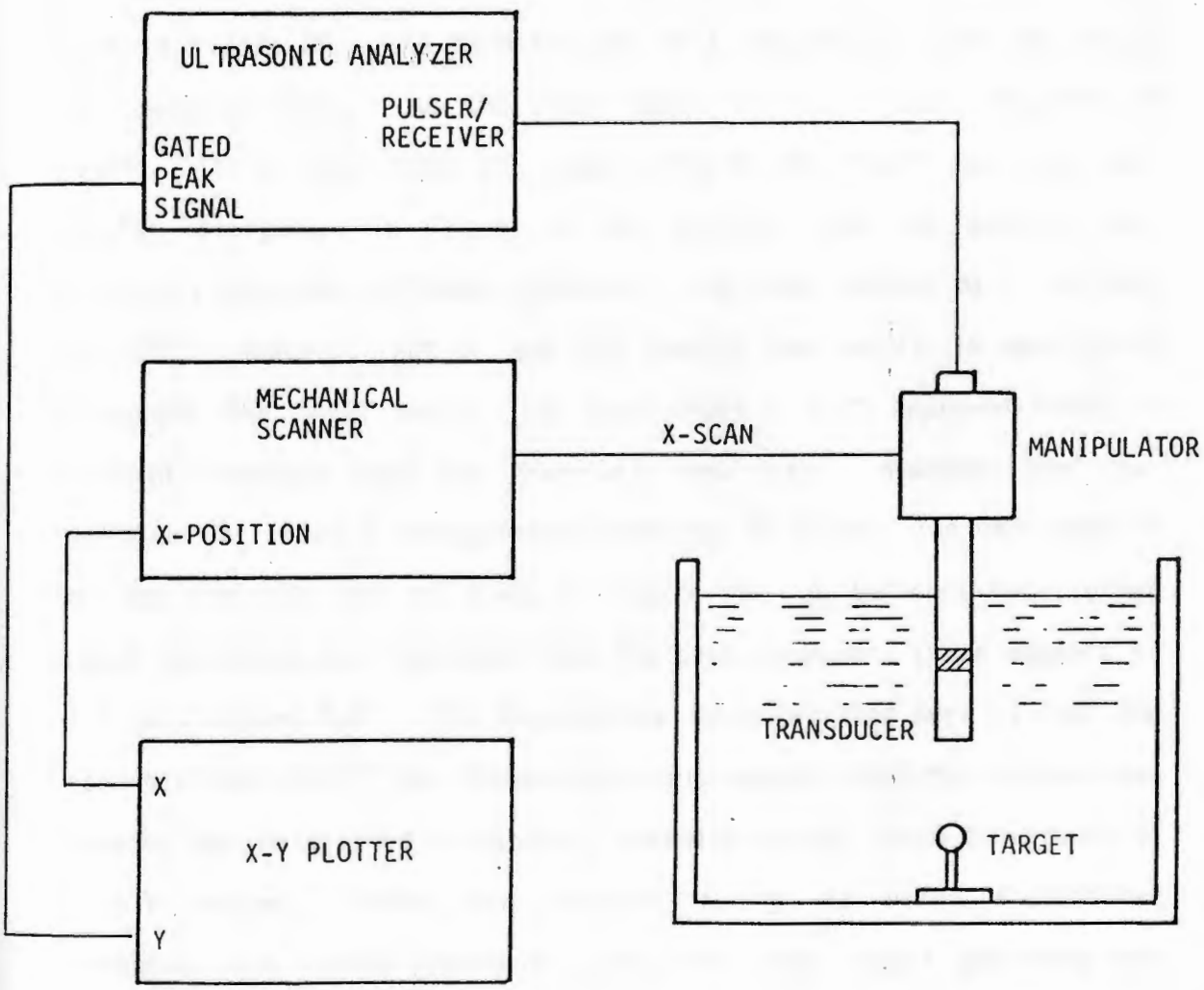

Figure 67. Sound Beam Profiling Test Bed.

The beam diameter of the focal point is defined as the width of the beam 6 dB down (1/2 echo amplitude) from the peak amplitude at focus.

Using these parameters the beams from the transducers can be characterized. The beam profile for the spherical lens transducer is given in Figure 68. The beam focuses at a distance of 3.5" and has a 5/8" depth-of-field. At the focal point it has a beam diameter of 0.045". It is noted that on either side of the focal zone the beam rapidly diverges. In Figure 69 the profile from the conical lens exhibits a somewhat different behavior. The beam focuses at 5" and has a 0.055" diameter. Notice how the narrow beam width is maintained throughout the focal zone. The beam shows a 2.5" depth-of-field, a fourfold increase from the spherical lens case. However, the peak amplitude has shown a corresponding decrease of 13 dB. The beam profile for the toroidal lens is given in Figure 70. A definite focal point cannot be easily distinguished from the plot; however, there appears to be a peak around 2.5". The interesting characteristic here is that the depth-of-field (9.4") has dramatically increased, while the narrow beam diameter has maintained throughout, yielding a total beam divergence of a half degree. Since the acoustic energy is being distributed throughout the entire transducer axis, the peak signal amplitude has decreased 24 dB from the spherical lens case.

Consider now the beam profiles from the shaped-element transducers. Figure 71 gives the profile from the spherical element. It has a focal length of 3.5" and a beam diameter of 0.050". The depth-of-field for this case (3/4") is similar to that of the spherical lens profile. The profile for the conical shaped-element shown in Figure 72 indicates a focus at 4.5" and a 0.065" beam diameter. The conical

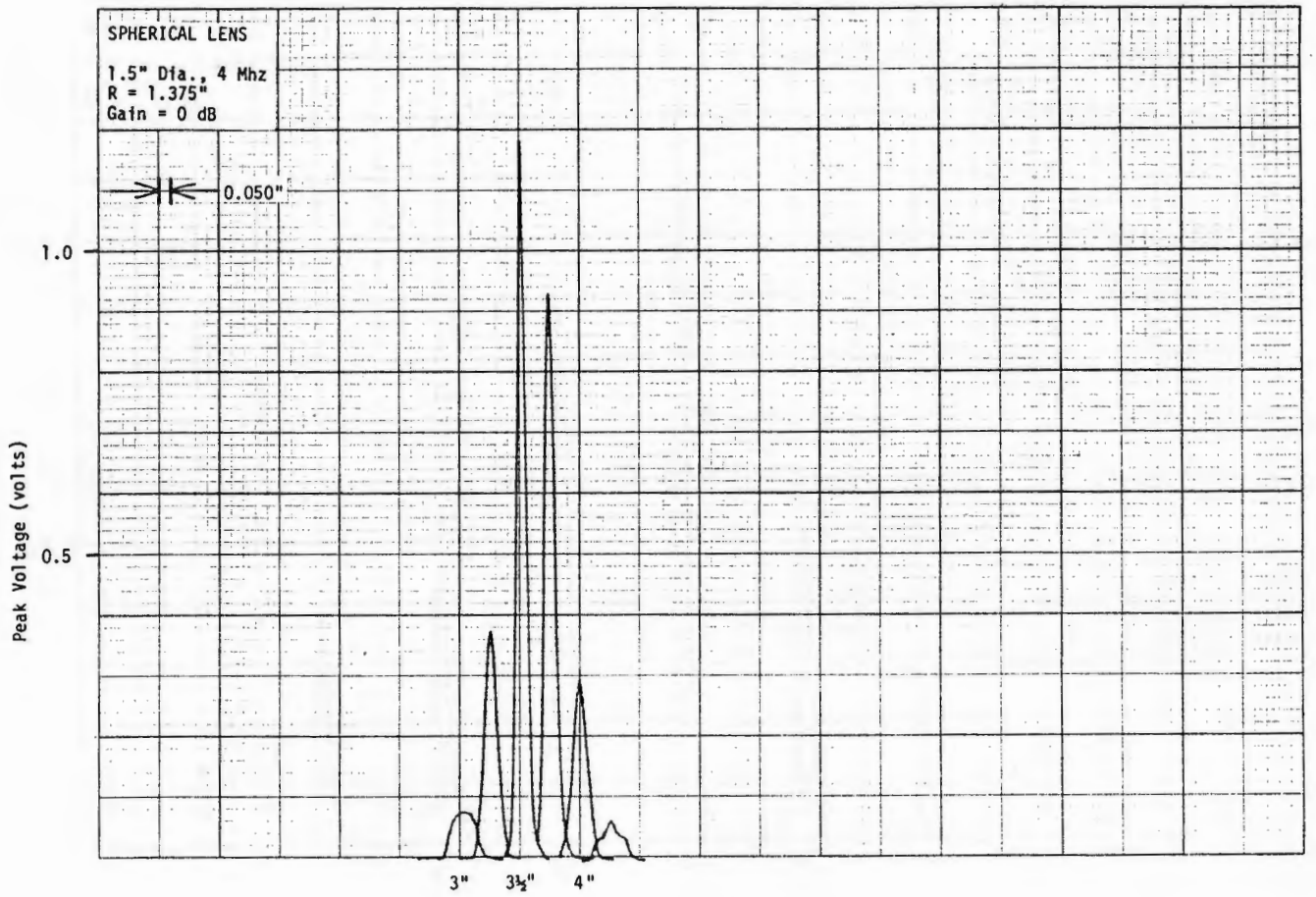

Figure 68. Beam Profile For Spherical Lens.

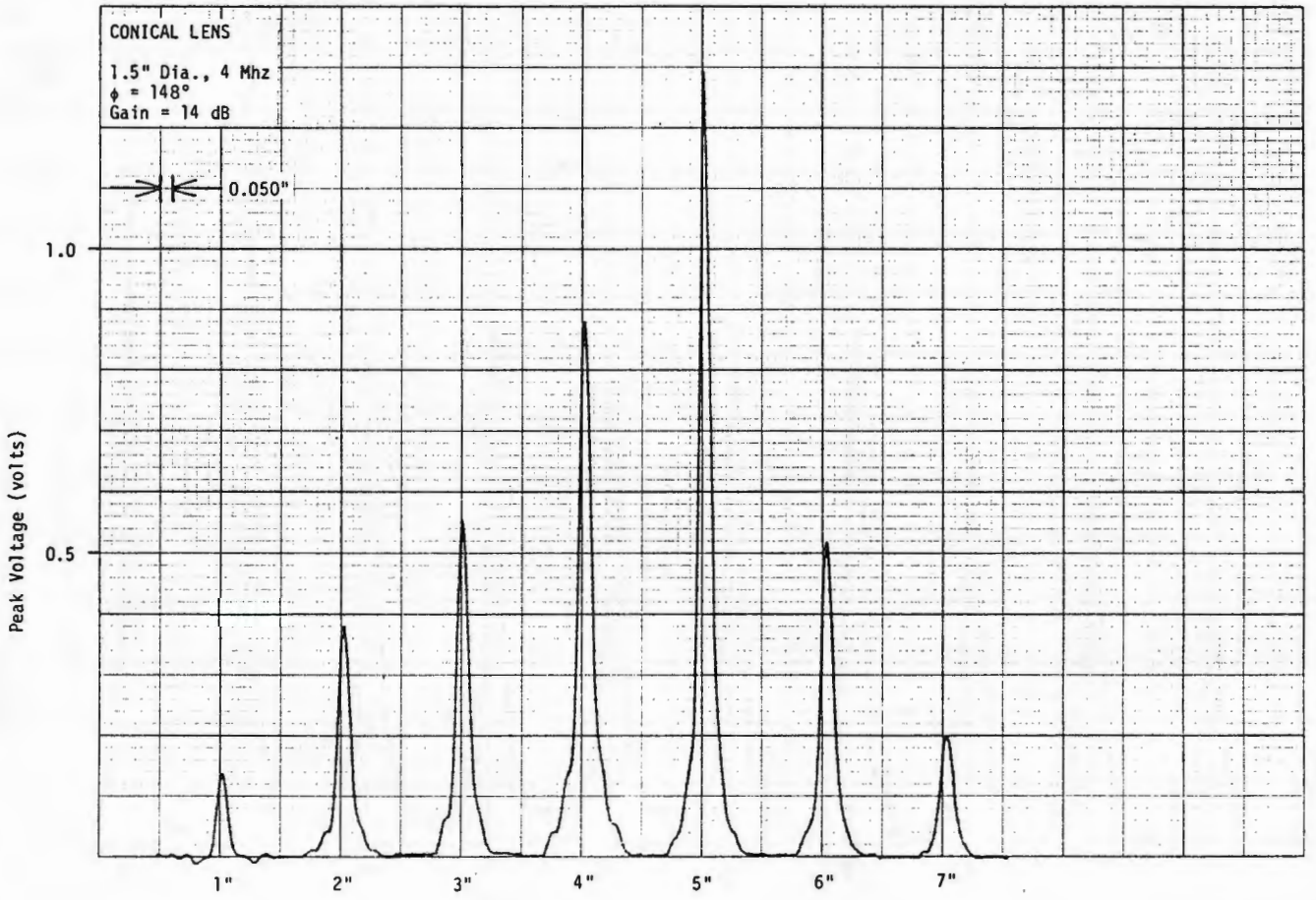

Figure 69. Beam Profile For Conical Lens.

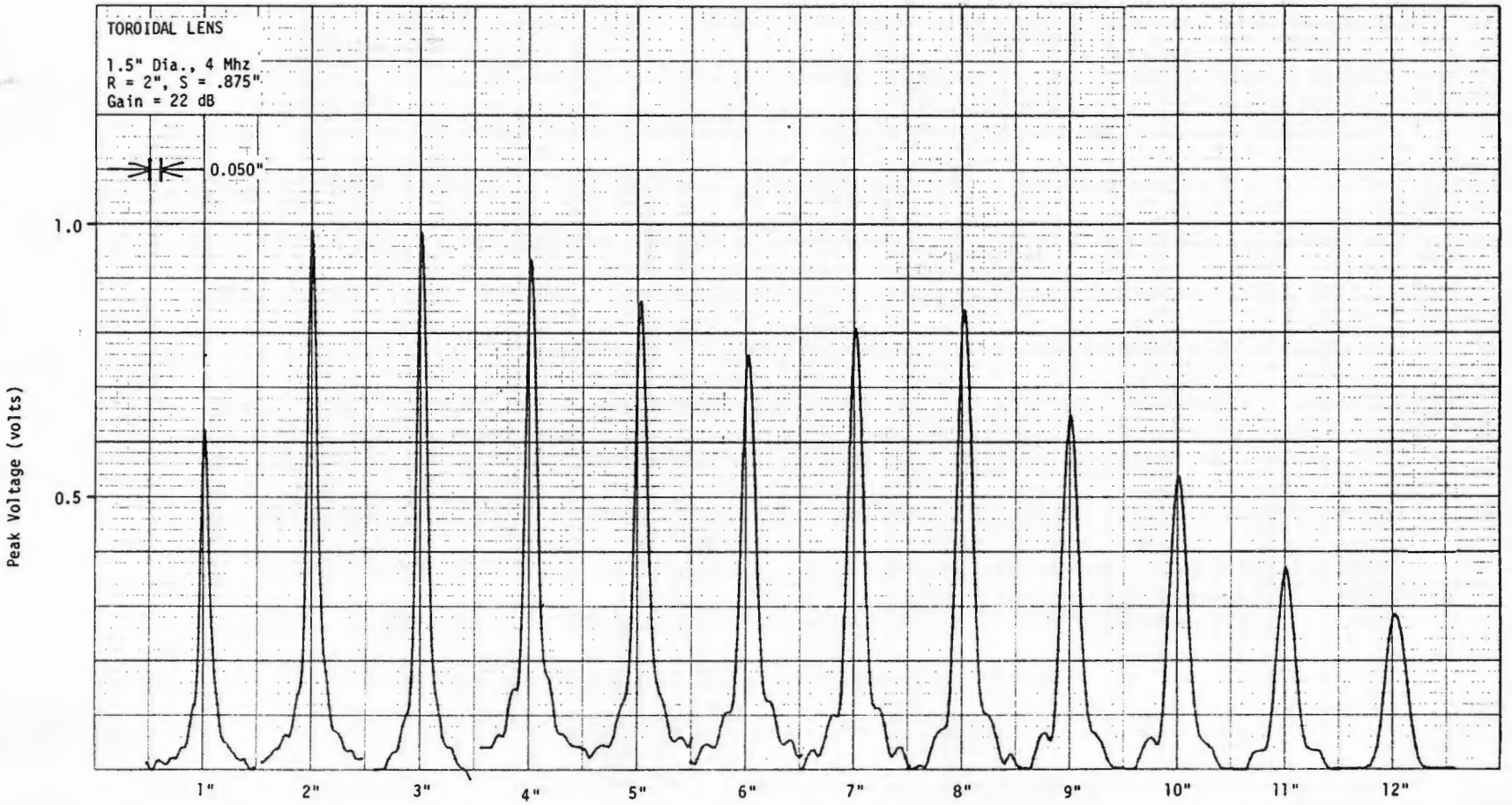

Figure 70. Beam Profile For Toroidal Lens.

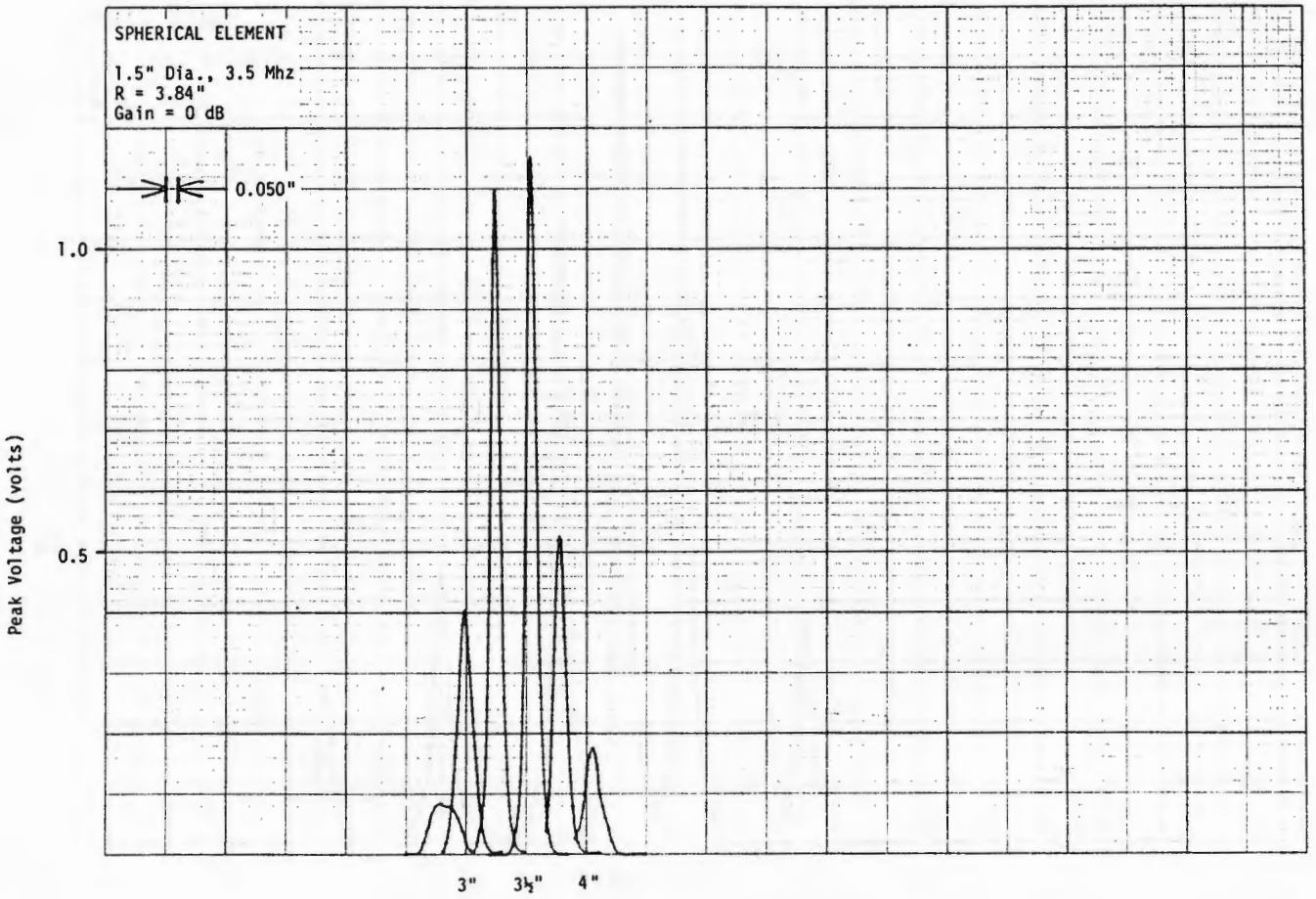

Figure 71. Beam Profile For Spherical Element.

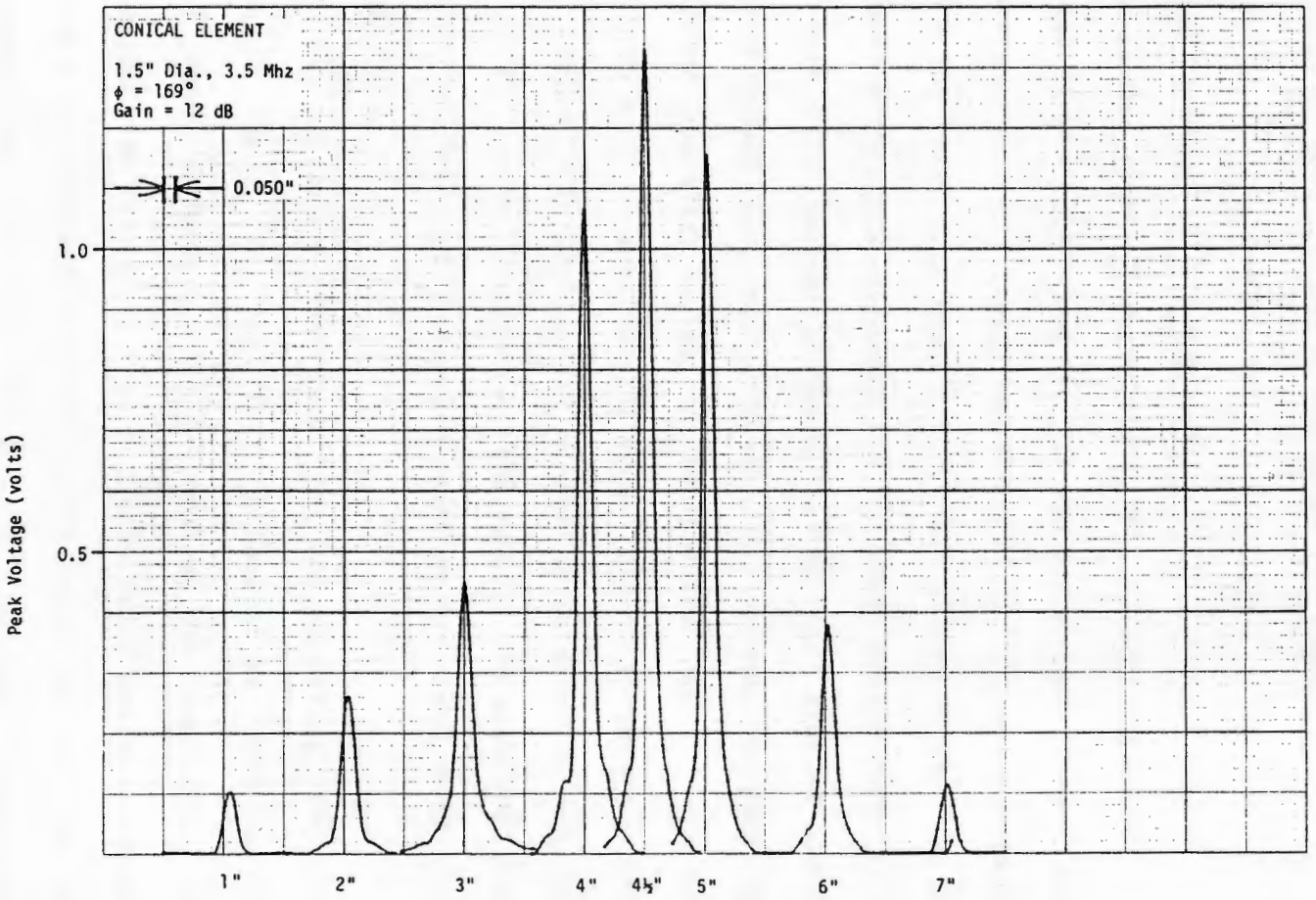

Figure 72. Beam Profile For Conical Element.

element also has a depth-of-field (2.3") that is similar to that of the conical lense. It is also noted that the peak amplitude at focus has decreased 11 dB from that of the spherical element.

Pulsed Acoustic Field Measurements

In the previous discussions the characteristics of a variety of focused fields where studied. It was noted that in all cases that the majority of acoustic energy was concentrated along the transducer's axis within the focal zone over a very narrow beam width. As the off-axis acoustic energy was extremely low for these transducers, it was decided that only axial spatial points along the focal zone be considered. The same procedure that was used in the previous chapter for sampling unfocused acoustic fields is implemented here. However the time waveforms will be spectrum analyzed yielding frequency responses. From this frequency information it will be determined if the focused field affects the center frequency of the pulse. The waveforms are sampled in an eight microsecond window beginning at the first echo arrival to the transducer.

The pulse-echo responses from the spherical lens transducer is given in Figure 73. The field is sampled at three points along the focal zone: the focus and the extremes of the focal zone.. In all three cases the time responses show a single pulse having a center frequency of 3.9 $\pm$ 0.2 MHz and a uniform pulse length of 1.4 $\pm$ 0.1 microseconds throughout the focal zone. No acoustic transient effects are noted.

In Figure 74 the responses for the conical lens transducer are indicated. It should be recalled that the depth-of-field of this transducer is much larger that the previous one and that spatial points

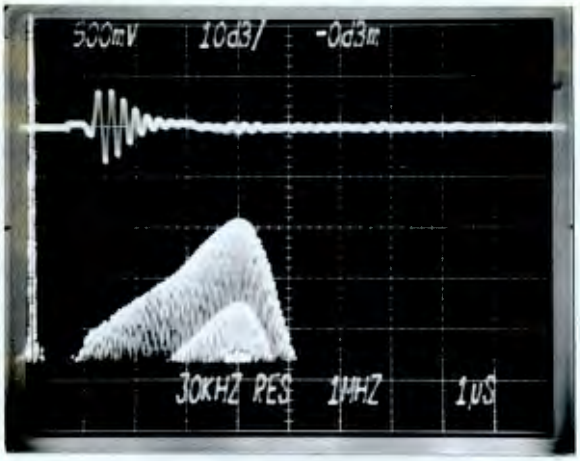

(a) Z = 3.25".

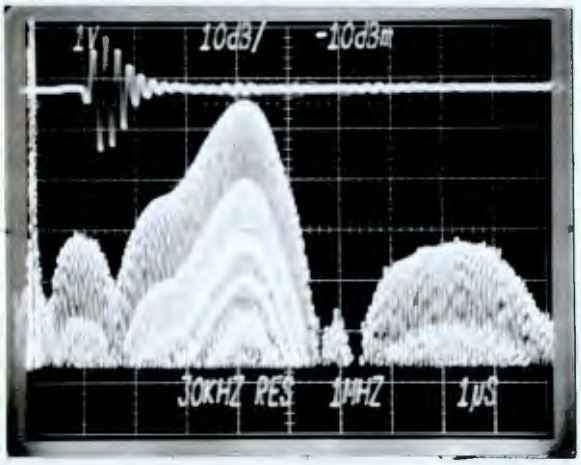

(b) Z = 3.5".

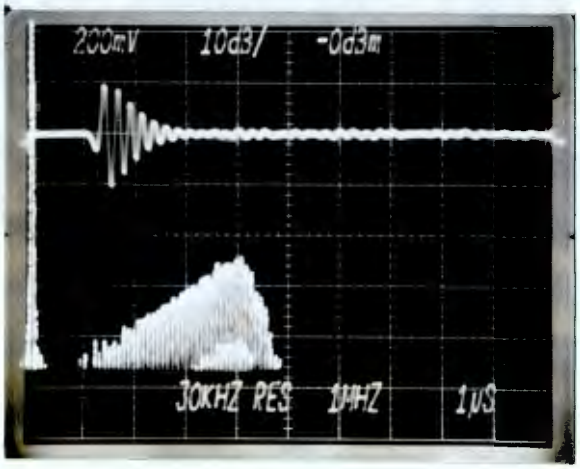

(c) Z = 4.0".

Figure 73. Axial Pressure Response From Spherical Lense Transducer.

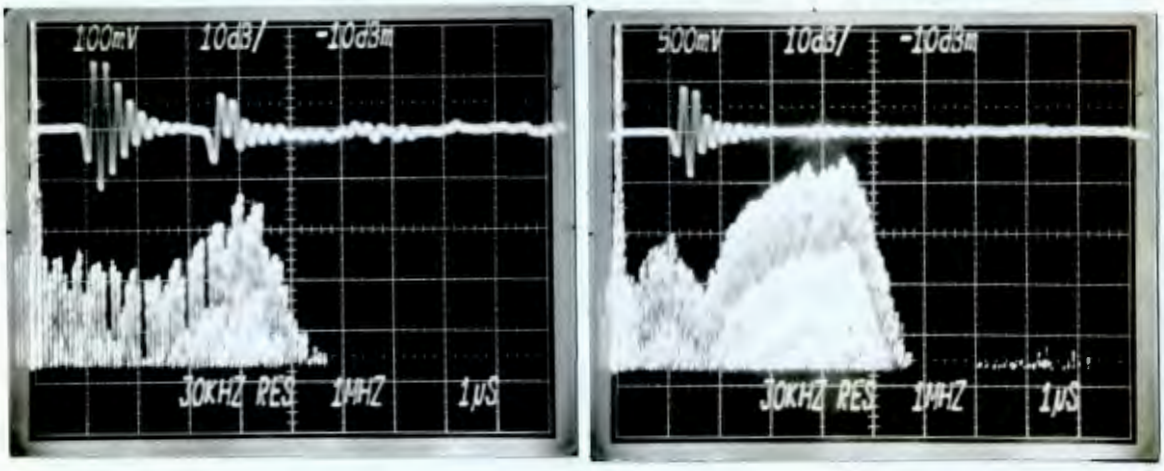

(a) Z = 1.0". (b) Z = 3.0".

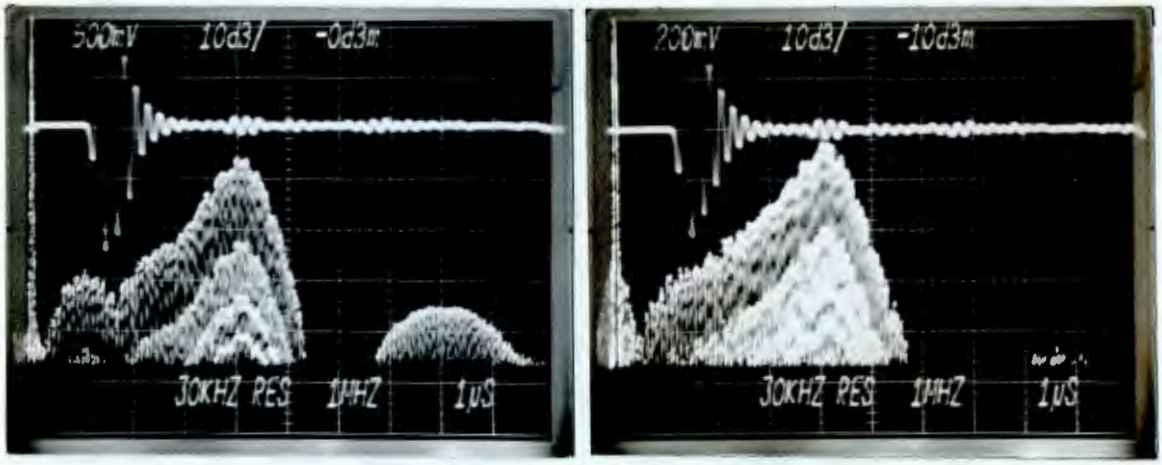

(c) Z = 5.0". (d) Z = 7.0".

Figure 74. Axial Pressure Response From Conical Lense Transducer.

much closer to the radiating face are sampled. When the ball target is one inch from the transducer, a two pulse structure is noted in the time response where a second pulse occurs 2.5 microseconds after the start of the first pulse. It should be noted that this field point is outside of the 6 dB focal zone. When the target is further out along the transducer axis, the time responses indicate a single pulse structure. The frequencies for all of the waveforms are centered at 4.0 $\pm$ 0.1 MHz and have slightly shorter pulse lengths of 1.1 $\pm$ 0.1 microseconds as compared to those from the spherical lense.

A similar pulse-echo response is noted for the toroidal lens transducer as shown in Figure 75. When the target is one inch from the transducer, the response again shows two echos. The second pulse though has a lower relative amplitude than for the same pulse in the previous case. This occurence is possibly due to the fact that the toroid configuration distributes the energy over a much larger focal zone. The time responses for the other field points in the focal zone show a single pulse waveform. Again these pulses have frequencies centered about 3.9 $\pm$ 0.1 MHz; however, the pulses near the middle of the focal zone have pulse lengths that are about 35% shorter than those near the extremes of the focal zone (about 1.1 $\pm$ 0.1 microseconds long).

The pulse-echo responses from the shaped-elements are presented in the following two figures. The spherical element response shown in Figure 76 has a very similar response as that of the spherical lens case. The waveforms all contain a single pulse having a center frequency of 3.3 $\pm$ 0.2 MHz and a pulse length approximately 1.1 $\pm$ 0.2 microseconds long, although the signals tend to be broader in bandwidth further out in the focal zone. As for the lens case, no acoustic

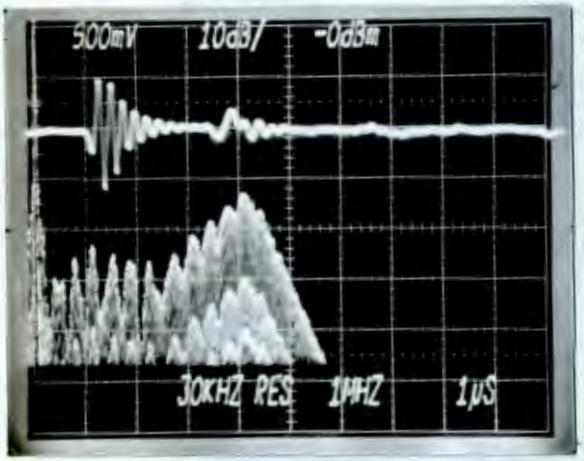

(a) Z = 1.0".

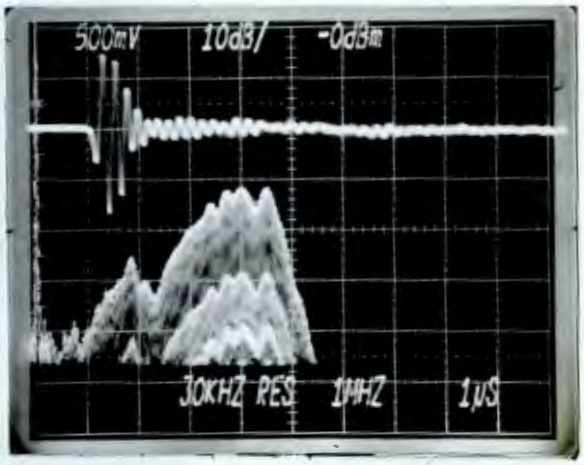

(b) Z = 3.0".

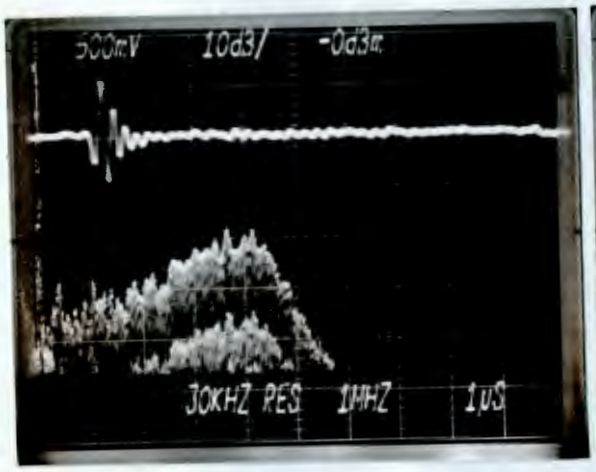

(c) Z = 6.0".

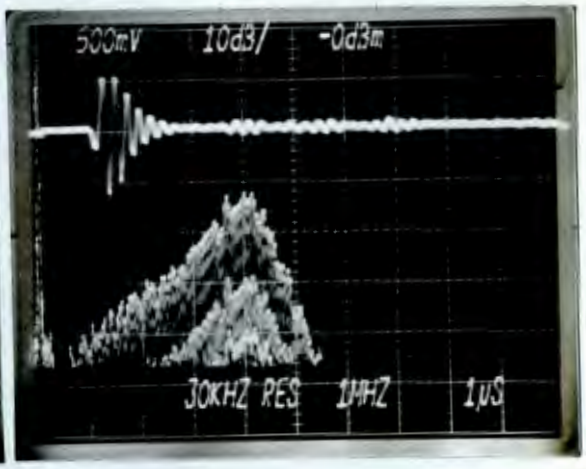

(d) Z = 9.0".

Figure 75. Axial Pressure Response From Toroidal Lense Transducer.

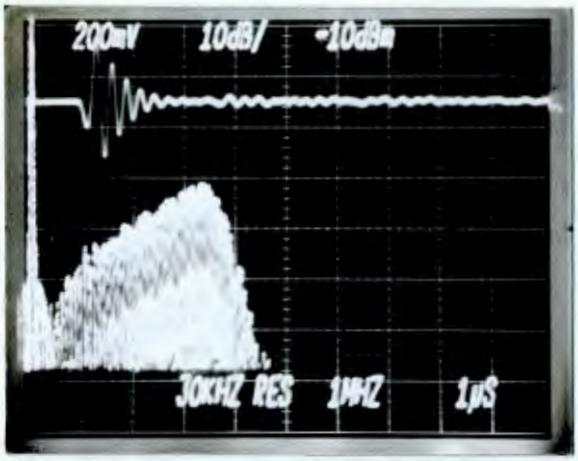

(a) Z = 3.0".

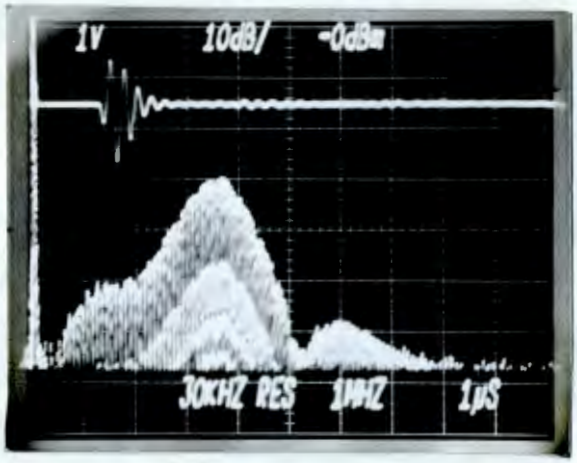

(b) Z = 3.375".

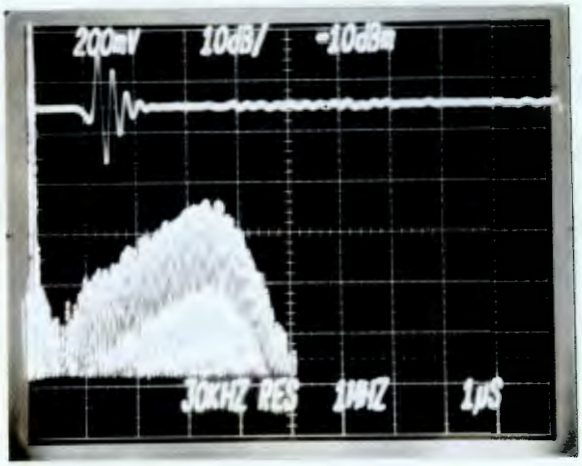

(c) Z = 3.75".

Figure 76. Axial Pressure Response From Spherical Element Transducer.

transients are noted.

In Figure 77 the responses from the conical shaped element are almost identical to that of the spherical element. The waveforms show uniform signals with frequencies centered about 3.3 $\pm$ 0.1 MHz and 1.1 $\pm$ 0.2 microseconds. It should be noted that for the conical lens case, the focal zone began closer to the transducer than for the present case and that at z = 1.0" the time response had two distinct signals. Had the amplitude for the same point for the conical element been greater, the same multiple pulse structure would have been noted. However since it was out of the focal zone of the transducer, it was not recorded.

In summary, focused ultrasonic transducers of various configurations were studied experimentally. Spherical, conical and toroidal apertures were examined for both shaped-elements and lens systems. Transducers of identical diameters, frequencies and focal distances were designed and fabricated for each of the cases. Measurements were made of the axial and lateral field intensity distributions, indicating that significant improvements could be achieved in beam width and depth-of-field. Measurements of the pulsed acoustic field indicated that for the case when sharply focused field were implemented, no acoustic transient effects were noted within the focal zone. One exception though was noted for the toroidal configuration at the very beginning of the focal zone.

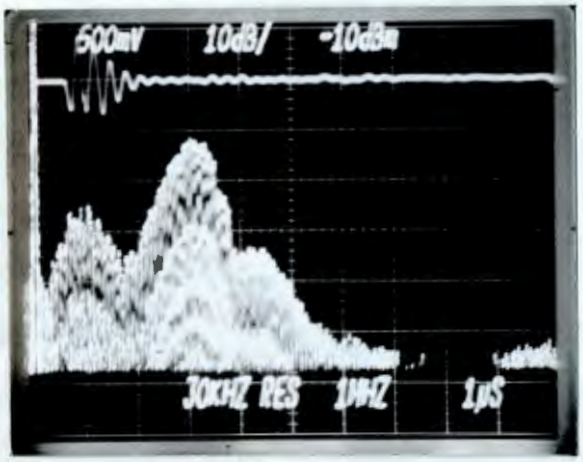

(a) Z = 3.0".

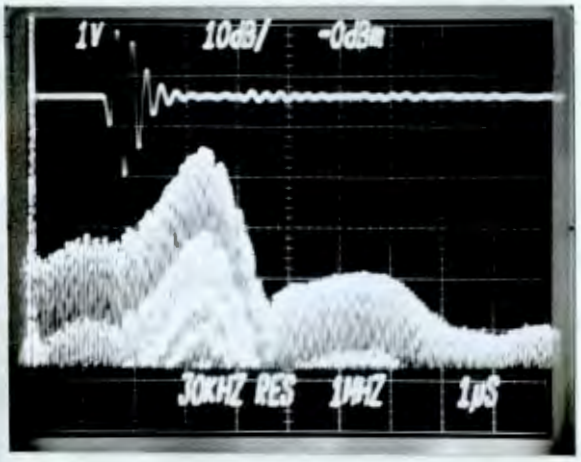

(b) Z = 4.5".

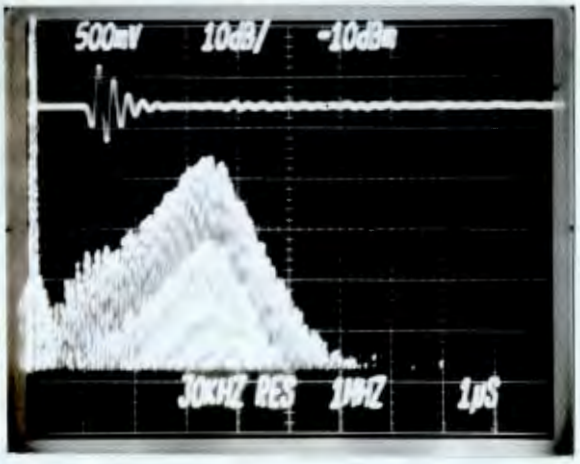

(c) Z = 6.0".

Figure 77. Axial Pressure Response From Conical Element Transducer.

SUMMARY AND CONCLUSIONS

The behavior of an ultrasonic transducer operating in a pulse-echo mode has been studied both analytically and experimentally. An investigation of the normalized harmonic pressure distribution indicates that the field exhibits an oscillatory behavior with periods corresponding to the duration of various portions of the impulse response. The magnitudes of these oscillations are related to the peak values of the impulse response function. For large "ka" values asymptotic methods can be used to accurately describe the harmonic pressure field.

A mathematical model of a pulse-echo ultrasonic system has been developed and used to investigate the pulsed acoustic field response from an ultrasonic transducer for a variety of spatial points and electrical excitations. It has been shown that the pulsed acoustic field effectively lengthens the duration of the acoustic pulses. If the time response of the transducer is short enough, a multiple pulse structure can occur.

To measure these acoustic transients, several transducers having different matching conditions were designed and fabricated. Various construction techniques were studied to determine their effect on transducer performance. Pulsed acoustic field measurements not only showed acoustic transients throughout the transducers' nearfield, but also revealed various artifacts in the transducers' response. These artifacts are thought to arise from plate waves that are generated within the piezoelectric element.

As a possible method for minimizing the acoustic transient

effects, various transducer focusing schemes were studied experimentally. Spherical, conical and toroidal geometries were examined for both shaped-element and lens systems. Measurements of the pulsed acoustic fields from these transducers indicate that for the focused fields studied, the acoustic transients were virtually eliminated from the focal zone. With proper focusing design these transient effects could be completely eliminated.

LIST OF REFERENCES

1. Hanish,S., "A Review of World Contributions from 1945 to 1965 to the Theory Radiation, Chapter III, Theory of Transient Radiation," Naval Res.Lab.Mem.Rep. 1688 (10 Mar. 1966).

2. Freedman,A., "Transient Fields of Acoustic Radiators," J.Acoust.Soc. Amer. 48, 135-138 (1970).

3. Harris,G.R., "Review of Transient Field Theory for a Baffled Planar Piston," J.Acoust.Soc.Amer. 70, 10-20 (1981).

4. Miles,J.W., "Transient Loading of a Baffled Piston," J.Acoust.Soc. Amer. 25, 200-203 (1953).

5. Stepanishen,P.R., "Transient Radiation from Pistons in an Infinite Planar Baffle," J.Acoust.Soc.Amer. 49, 1629-1638 (1970).

6. Robinson,D.E., Lees,S. and Bess,L., "Near Field Transient Radiation Patterns for Circular Pistons," IEEE Trans.Acoust.Speech Signal Proc. ASSP-22, 395-403 (1974).

7. Beaver,W., "Sonic Nearfields of a Pulsed Piston Radiator," J.Acoust, Soc.Amer. 56, 1043-1048, (1974).

8. Weight,J.P. and Hayman,A.J., "Observations of the Propagation of Very Short Ultrasonic Pulses and Their Reflections by Small Targets," J.Acoust.Soc.Amer. 63, 396-404 (1978).

9. Hayman,A.J. and Weight,J.P., "Transmission and Reception of Short Ultrasonic Pulses by Circular and Square Transducers," J.Acoust. Soc.Amer. 66, 945-951 (1979).

10. Stepanishen,P.R., "Asymptotic Behavior of the Acoustic Nearfield of a Circular Piston," J.Acoust.Soc.Amer. 59, 749-754 (1976).

11. Mason,W.P., Electromechanical Transducers and Wave Filters. Princeton,NJ: Van Nostrand, 1948.

12. McSkimin,H.J., "Transducer Design for Ultrasonic Delay Lines," J.Acoust. Soc.Amer. 27, 302-309 (1955).

13. Sittig,E.K., "Effects of Bonding and Electrode Layers on the Transmission Parameters of Piezoelectric Transducers Used in Ultrasonic Digital Delay Lines," IEEE Trans.Sonics and Ultrason. SU-16, 2-10 (1969).

14. Kossoff,G., "The Effects of Backing and Matching on the Performance of Piezoelectric Ceramic Transducers," IEEE Trans.Sonics and Ultrason. SU-13, 20-30 (1966).

15. Souquet,J., Defranould,P. and Desbois,J., "Design of Low Loss Wideband Ultrasonic Transducer for Noninvasive Medical Application," IEEE Sonics and Ultrason. SU-26, 75-81 (1979).

16. Desilets,C.S., Fraser,J.D. and Kino,G.S., 'The Design of Efficient Broadband Piezoelectric Transducers," IEEE Trans.Sonics and Ultrason. SU-25, 115-125 (1978).

17. Krimholtz,R., Reedom,D. and Matthaei,G., "New Equivalent Circuits for Elementary Piezoelectric Transducers," Electronics Letters 6, 398-399 (1970).

18. Goll,J.H., "The Design of Broadband Fluid-Loaded Ultrasonic Transducers," IEEE Trans.Sonics and Ultrason. SU-26, 385-393 (1979).

19. Stepanishen,P.R., "The Time-Dependent Force and Radiation Impedance on a Piston in a Rigid Infinite Planar Baffle," J.Acoust.Soc.Amer. 49, 841-849 (1970).

20. Lees,S., Gilmore,R.S. and Kranz,P.R., "Acoustic properties of Tungsten Vinyl Composites," IEEE Trans.Sonics and Ultrason. SU-20, 1-2 (1973).

21. Larson,J.D. and Leach,J.G., "Tungsten-Polyvinyl Composite Materials - Fabrication and Performance," 1979 Ultrasonics Symposium Proceedings, IEEE Cat. 79CH1482-9SU.

22. Rokhlin,S., Golan,S. and Gefen,Y., "Acoustic Properties of Tungsten-Tin Composites," J.Acoust.Soc.Am. 65(5), 1505-1506 (1981).

23. Kino,G.S. and Desilets,C.S., "Design of Slotted Transducer Arrays with Matched Backings," Ultrasonic Imaging I, 189-209 (1979).

24. O'Neil,H.T., "Theory of Focusing Radiators," J.Acoust.Soc.Amer. 21 516-526 (1949).

25. Kossoff,G., "Improved Techniques in Ultrasonic Cross Sectional Echography," Ultrasonics 10(5), 221-227 (1972).

26. Wustenberg,V.H., Kutzner,J. and Morhle,W., "Fokussierende Prufkopfe zur Verbesserung der Fehlergrossenabschatzung bei der Ultraschallprufung von dickwandigen Reaktorkomponenten," Materialpruf 18(5), 152-161 (1976).

27. Schlengermann,U., "The Characterization of Focussing Ultrasonic Transducers by Means of Single Frequency Analysis," Materials Evaluation 38(12), 73-79 (1980).

28. Burckhardt,C.B., Hoffman,H. and Grandchamp,P.A., "Ultrasound Axicon: A Device for Focussing Over a Large Depth," J.Acoust.Soc.Amer. 54(6), 1628-1630 (1973)

29. Murphy,R.V., "Toroidal, Conical and Spherical Lenses in Ultrasonic Inspection," Material Evaluation 39(3), 391-395 (1981).

30. Yamada,K. and Shimizu,H., "Conical and Toroidal Piezoelectric Polymer Transducers for Long Range Focusing," 1982 Ultrasonics Symposium Proceedings, IEEE Cat. 82CH1823-4.

31. Andrew,G. "Development of an Ultrasonic Imaging System," General Dynamics, Electric Boat Division, Report No. MRR-EB82-001, January,1983.

BIBLIOGRAPHY

1. Andrew,G. "Development of an Ultrasonic Imaging System," General Dynamics, Electric Boat Division, Report No. MRR-EB82-001, January,1983.

2. Beaver,W., "Sonic Nearfields of a Pulsed Piston Radiator," J.Acoust, Soc.Amer. 56, 1043-1048, (1974).

3. Burckhardt,C.B., Hoffman,H. and Grandchamp,P.A., "Ultrasound Axicon: A Device for Focussing Over a Large Depth," J.Acoust.Soc.Amer. 54(6), 1628-1630 (1973)

4. Desilets,C.S., Fraser,J.D. and Kino,G.S., 'The Design of Efficient Broadband Piezoelectric Transducers," IEEE Trans.Sonics and Ultrason. SU-25, 115-125 (1978).

5. Freedman,A., "Transient Fields of Acoustic Radiators," J.Acoust.Soc. Amer. 48, 135-138 (1970).

6. Goll,J.H., "The Design of Broadband Fluid-Loaded Ultrasonic Transducers," IEEE Trans.Sonics and Ultrason. SU-26, 385-393 (1979).

7. Hanish,S., "A Review of World Contributions from 1945 to 1965 to the Theory Radiation, Chapter III, Theory of Transient Radiation," Naval Res.Lab.Mem.Rep. 1688 (10 Mar. 1966).

8. Harris,G.R., "Review of Transient Field Theory for a Baffled Planar Piston," J.Acoust.Soc.Amer. 70, 10-20 (1981).

9. Hayman,A.J. and Weight,J.P., "Transmission and Reception of Short Ultrasonic Pulses by Circular and Square Transducers," J.Acoust. Soc.Amer. 66, 945-951 (1979).

10. Kino,G.S. and Desilets,C.S., "Design of Slotted Transducer Arrays with Matched Backings," Ultrasonic Imaging I, 189-209 (1979).

11. Kossoff,G., "The Effects of Backing and Matching on the Performance of Piezoelectric Ceramic Transducers," IEEE Trans.Sonics and Ultrason. SU-13, 20-30 (1966).

12. Kossoff,G., "Improved Techniques in Ultrasonic Cross Sectional Echography," Ultrasonics 10(5), 221-227 (1972).

13. Krimholtz,R., Reedom,D. and Matthaei,G., "New Equivalent Circuits for Elementary Piezoelectric Transducers," Electronics Letters 6, 398-399 (1970).

14. Larson,J.D. and Leach,J.G., "Tungsten-Polyvinyl Composite Materials - Fabrication and Performance," 1979 Ultrasonics Symposium Proceedings, IEEE Cat. 79CH1482-9SU.

15. Lees,S., Gilmore,R.S. and Kranz,P.R., "Acoustic properties of Tungsten Vinyl Composites," IEEE Trans.Sonics and Ultrason. SU-20, 1-2 (1973).

16. Mason,W.P., Electromechanical Transducers and Wave Filters. Princeton,NJ: Van Nostrand, 1948.

17. McSkimin,H.J., "Transducer Design for Ultrasonic Delay Lines," J.Acoust. Soc.Amer. 27, 302-309 (1955).

18. Miles,J.W., "Transient Loading of a Baffled Piston," J.Acoust.Soc. Amer. 25, 200-203 (1953).

19. Murphy,R.V., "Toroidal, Conical and Spherical Lenses in Ultrasonic Inspection," Material Evaluation 39(3), 391-395 (1981).

20. O'Neil,H.T., "Theory of Focusing Radiators," J.Acoust.Soc.Amer. 21 516-526 (1949).

21. Robinson,D.E., Lees,S. and Bess,L., "Near Field Transient Radiation Patterns for Circular Pistons," IEEE Trans.Acoust.Speech Signal Proc. ASSP-22, 395-403 (1974).

22. Rokhlin,S., Golan,S. and Gefen,Y., "Acoustic Properties of Tungsten-Tin Composites," J.Acoust.Soc.Am. 65(5), 1505-1506 (1981).

23. Schlengermann,U., "The Characterization of Focussing Ultrasonic Transducers by Means of Single Frequency Analysis," Materials Evaluation 38(12), 73-79 (1980).

24. Sittig,E.K., "Effects of Bonding and Electrode Layers on the Transmission Parameters of Piezoelectric Transducers Used in Ultrasonic Digital Delay Lines," IEEE Trans.Sonics and Ultrason. SU-16, 2-10 (1969).

25. Souquet,J., Defranould,P. and Desbois,J., "Design of Low Loss Wideband Ultrasonic Transducer for Noninvasive Medical Application," IEEE Sonics and Ultrason. SU-26, 75-81 (1979).

26. Stepanishen,P.R., "The Time-Dependent Force and Radiation Impedance on a Piston in a Rigid Infinite Planar Baffle," J.Acoust.Soc.Amer. 49, 841-849 (1970).

27. Stepanishen,P.R., "Transient Radiation from Pistons in an Infinite Planar Baffle," J.Acoust.Soc.Amer. 49, 1629-1638 (1970).

28. Stepanishen,P.R., "Asymptotic Behavior of the Acoustic Nearfield of a Circular Piston," J.Acoust.Soc.Amer. 59, 749-754 (1976).

29. Weight,J.P. and Hayman,A.J., "Observations of the Propagation of Very Short Ultrasonic Pulses and Their Reflections by Small Targets," J.Acoust.Soc.Amer. 63, 396-404 (1978).

30. Wustenberg,V.H., Kutzner,J. and Morhle,W., "Fokussierende Prufkopfe zur Verbesserung der Fehlergrossenabschatzung bei der Ultraschallprufung von dickwandigen Reaktorkomponenten," Materialpruf 18(5), 152-161 (1976).

31. Yamada,K. and Shimizu,H., "Conical and Toroidal Piezoelectric Polymer Transducers for Long Range Focusing," 1982 Ultrasonics Symposium Proceedings, IEEE Cat. 82CH1823-4.